UNIVERSITÉ DU QUÉBEC

THÈSE PRÉSENTÉE À L'UNIVERSITÉ DU QUÉBEC À CHICOUTIMI COMME EXIGENCE PARTIELLE DU DOCTORAT EN INGÉNIERIE

Par

FARANAK ARIANPOUR

ELABORATION OF COMPOSITE AND CHEMICALLY HETEROGENEOUS ICEPHOBIC COATINGS

ÉLABORATION DE REVÊTEMENTS GLACIOPHOBES COMPOSITES ET CHIMIQUEMENT HÉTÉROGÈNE

October 2015

Dedicated to my director ***Prof. M. FARZANEH***

ABSTRACT

Atmospheric icing happens when the surfaces of exposed structures are subjected to contact with super-cooled water droplets or snow particles. Ice build-up on overhead transmission and distribution lines may lead to mechanical failure or insulator flashover, sometimes resulting in power outages with major socioeconomic consequences.

The present study focused on the preparation of heterogeneous coatings (HCs) with hydro- and icephobic properties presenting a number of advantages, such as easy application, time-saving and low cost. The homo- and HCs were prepared by using different methods such as self-assembly, nanoparticles-based and Plasma-based techniques.

Super-hydrophobic coatings with very low wetting hysteresis are also considered to be icephobic. However, even super-hydrophobic coatings can deteriorate during successive icing/de-icing cycles, and this can lead to ice mechanical anchoring since liquid water penetrates the porous surface. Additionally, the cost and complexity involved in the fabrication of such coatings as micro and nano roughness is created, constitute other hurdles.

In this study HCs are considered as a coating including hydrocarbons and fluorocarbons, while purely hydrocarbons or fluorocarbons coatings are considered as the homogeneous coatings. It was shown by applying different functions (both C-F and C-H) the surface energy is decreased more compared to applying only one function (C-F or C-H alone). It should be noted that the water molecule orientations at the surfaces of the

fluorocarbon and hydrocarbon groups were completely different. As a result, by inducing or creating various disparities (hydrocarbons and fluorocarbons) in terms of energy bonding, and water molecule orientation at the molecular level, the ice-solid interface is weakened.

The wettability measurement of the HCs showed higher water contact angle (CA) values and smaller water contact angle hysteresis (CAH) values compared to homogeneous coatings. The most important consequence of HCs preparation, via different methods, was observed in low contact angle hysteresis (CAH) values. The prepared HCs by self assembled monolayers (*SAM*s), nanoparticles and "masked" plasma sputtering methods resulted in reducing the ice adhesion strength by factors of ~ 3, ~ 1.7 and ~ 1.3 times, respectively, compared to a polished aluminum sample.

The durability of coatings was studied under accelerated aging conditions such as UV degradation, several icing/de-icing cycles and immersion in distilled water and different pH solutions. Consequently, based on results obtained it was observed that the HCs are more stable under accelerated aging conditions compared to homogeneous coatings.

RÉSUMÉ

L'adhésion et l'accumulation de la glace atmosphérique sur une structure se produisent lorsque celle-ci entre en contact avec des gouttelettes d'eau surfondues ou des flocons de neige. Une accumulation importante de glace ou de neige collante sur les lignes de transport et de distribution de l'énergie électrique peut parfois conduire à des bris mécaniques des équipements de ces lignes ou au contournement d'isolateurs, entraînant parfois des coupures de courant ayant des conséquences socio-économiques désastreuses.

Les revêtements superhydrophobes à très faible hystérésis de mouillage sont considérés comme glaciophobes. Toutefois, les revêtements superhydrophobes sont susceptibles de se dégrader à la suite de cycles de glaçage/déglaçage successifs. Ceci peut conduire à l'ancrage mécanique de la glace à la surface, causé par la pénétration et la solidification de l'eau liquide dans la surface poreuse. De plus, le coût et la complexité de la création de micro- et nano-rugosités constituent d'autres obstacles pour la fabrication de ces revêtements.

Ce travail porte sur la préparation de revêtements hétérogènes avec des propriétés hydrophobes et glaciophobes qui présentent certains avantages, notamment la facilité d'application, des gains de temps et de plus faibles coûts de fabrication. Dans cette étude, les revêtements hétérogènes sont considérés comme des revêtements contenant à la fois des hydrocarbures et des fluorocarbures tandis que les revêtements, incluant une seule/ de ces substances sont considérés comme des revêtements homogènes. Les revêtements

homogènes et hétérogènes ont été préparés en utilisant différentes techniques. Il a été démontré que l'application de deux couches successives d'hydrocarbures puis fluorocarbures diminue l'énergie de surface comparativement à l'application d'une seule couche hydrocarbures ou bien fluorocarbures. Il convient de noter que l'orientation de la molécule d'eau à la surface des groupes hydrocarbures et fluorocarbures est complètement différente. En conséquence, en facilitant et en créant certaines disparités impliquant les hydrocarbures et les fluorocarbures en terme de force de liaison et d'orientation des molécules d'eau, il se produit un affaiblissement de l'adhésion à l'interface glace-solide.

Les propriétés hydrophobes des revêtements hétérogènes ont montré un angle de contact statique plus élevé et un angle de contact d'hystérésis plus faible comparativement à ceux observés avec des revêtements homogènes. Les revêtements hétérogènes préparés par les monocouches auto-assemblées, les nanoparticules et les méthodes de pulvérisation de plasma "masqué" ont permis de réduire la force d'adhérence de la glace sur une surface d'aluminium revêtue de ~ 3, ~ 1.7 et ~ 1.3 fois, respectivement, comparativement à un échantillon d'aluminium poli non protégé. La stabilité des revêtements a été étudiée dans des conditions de vieillissement accéléré incluant l'exposition aux UV, la succession de cycles de givrage / dégivrage ainsi que l'immersion dans l'eau distillée et dans des solutions avec différentes valeurs de pH. Il a été observé que les revêtements hétérogènes sont plus stables par rapport aux revêtements homogènes lorsqu'ils sont soumis à des conditions de vieillissement accéléré similaires.

ACKNOWLEDGMENTS

This research work was carried out within the framework of the Industrial Chair on Atmospheric Icing of Power Network Equipment (CIGELE) and the Canada Research Chair on Engineering of Power Network Atmospheric Icing (INGIVRE) at University of Quebec in Chicoutimi (UQAC).

I would like to use this window of occasion to thank those who helped me to complete this thesis. In the first place, I would like to thank wholeheartedly, my Director, **Prof. Masoud FARZANEH,** for his support, supervision, guidance, encouragement and patience, as well as deepest appreciation to Prof. Farzaneh's family for their warm welcome and kind hospitality in Chicoutimi. It is an honor for me to earn my graduation under his supervision. I would also like to express my gratitude to my co-director, Dr. Reza Jafari, for his guidance and help during my project.

I am extremely grateful to Dr. Stephen Whitney for accepting the English proof-reading of my thesis. Dr. Whitney's accuracy and attention during the proof-reading of my thesis was admirable and commendable.

I would like to appreciate Dr. Sarkissian and Dr. Ghalmi for providing useful comments in this study.

Thank you to my colleagues, technicians and professionals, Pierre Camirand, Denis Masson, Claude D'Amours in CIGELE for their constant companionship and

assistance. Mr. Pierre helped me with his smart solutions to technical problems in laboratory. He was a friend and a counselor at all times.

I would like to express my warmest and deepest appreciation to my dear parents (*Farough & Pari*), sister (*Flora*) and brothers (*Gholamreza & Hamidreza*) who helped and encouraged me during in my studies, especially my father and my brother (*Dr. Gholamreza Aryanpour)* for teaching me determination. They have always stood by me and showed me how to reach my aims. I owe them everything. Last but not least, I would like to express my profound gratitude to my beloved husband, *Shahram*, for his true love and kind help. I wish the best you and look forward to more great moments in the future with you.

TABLE OF CONTENTS

LIST OF FIGURES

LIST OF TABLES

CHAPTER I

INTRODUCTION

1. Introduction
   1.1 The icing problem
   1.2 Ice accumulation prevention
   1.3 Originality of the research work
   1.4 Objectives
   1.5 Outline of the thesis

1. Introduction

1.1 The icing problem

Cold countries subjected to extreme weather conditions are often victims of winter disasters. Atmospheric icing happens when the surfaces of exposed structures are subjected to contact with super-cooled water drops or snow particles. For instance, overhead transmission lines and their substations can be subjected to ice accumulations for an extended period of time each year [1]. This may cause mechanical damage to power network equipment, while ice and wet snow accumulation can considerably reduce the electrical performance of outdoor insulators [2]. Flashover on ice-covered insulators is a very complex phenomenon which causes damage to insulators and reduces their lifetime [3-5]. Ice can be formed in dry or wet atmospheric conditions, accumulating on insulator surfaces from freezing rain, freezing drizzles, in-cloud icing, icing fog, wet snow or frost, and strongly adhering to any surface [6].

Ice and wet snow can cause severe trouble due to their high adherence to both metallic and insulating surfaces. Prevention of ice accretion on surfaces requires reduction of adhesion strength between ice and subjected surface. Over the past decades, researchers have tried to improve on so-called de-icing methods such as thermal, mechanical and chemical methods to remove the ice/snow build-ups that are currently in use.

1.2 Ice accumulation prevention

Currently, de-icing techniques such as chemical, mechanical and thermal de-icing are applied extensively without fully preventing ice-accumulation. Among these techniques one can cite freezing-point depressants for highways (salt, chemical sprays, etc.) [7] and de-icing fluids for aircraft (ethylene and propylene glycols) [8]. Although very efficient, the main disadvantage of the de-icing methods is that they must be used after ice build-up and thus during a period when damage can still occur on accumulated ice structures. The other disadvantages of de-icing methods are: frequency of application, significant negative environmental impacts (toxicity) and cost. Other methods, specifically applicable to transmission lines, such as mechanical vibration of cables, Joule heating of the conductors [7] and electrolysis [9], are effective but consume a considerable amount of energy and require surveillance of the lines and on-site intervention. Moreover, mechanical de-icing can lead to surface damage resulting in the gradual degradation of the system itself. None of the above-mentioned techniques prevents ice from creating or accumulating in the first place. Preventing ice accumulation or reducing significantly its adhesion force may be accomplished by producing anti-icing or icephobic coatings and therefore by using an anti-icing approach [10-13]. Recently, several coatings for such applications have been tested and reported. Polymers with low critical surface tension such as organopolysiloxane and polytetrafluoroethylene (Teflon®) were examined. These coatings produced very low run-off water contamination and demonstrated a significant reduction of ice adhesion [14].

Super-hydrophobic coatings with a small value of contact angle hysteresis showed a remarkable reduction of ice adhesion strength [15]. Reduced ice adhesion on the super-hydrophobic surfaces developed by the CIGELE research group using different techniques was reported [16-23]. To prepare the super-hydrophobic coatings, generally a common two-step (and therefore disadvantageous) processes were used: surface roughening followed by applying a low surface energy material. Also, the rough structures created on the coating can be damaged and removed during icing/de-icing tests [24]. This can be considered as another important disadvantage for super-hydrophobic coatings.

1.3 Originality of the research work

Chapter 2 describes in more detail, a number of studies (some of them were cited in the previous section) that were focused on the preparation of hydro- and super-hydrophobic coatings and thin films, in order to reduce ice adhesion and thus facilitate ice removal. Much research has been conducted so far on these coatings' characteristics, properties, performance, etc. However, the super-hydrophobic coatings have disadvantages related to preparation, cost, application and rough structure damage during icing/de-icing. The originality of this research is that it is focused on the preparation of heterogeneous coatings (HCs) with icephobic properties. The low surface energy HCs on a metallic substrate such as aluminum have not yet been systematically studied and well characterized. Indeed, the literature available in this field is very rare [25-27]. These studies in addition focused on heterogeneous polymer coatings or copolymers including

hydrocarbons and fluorocarbons. Therefore, the purpose of this research work is preparation of HCs by using different techniques other than those applied and reported in literatures. More precisely, the fabrication of HC by different methods such as self-assembly, nanoparticles-based and Plasma-based techniques, as well as their hydro- and icephobic properties and performance in different conditions, have not been studied so far. This study would help to further understand the heterogeneity effect on icephobic properties of coatings. The HCs introduced in this study, indeed, were cheap, simple to prepare and easy-to-apply when compared to those applied and reported in literatures [25-28]. These types of coatings are attractive alternative for the currently well-studied homogeneous coatings, as they show lower values of ice adhesion as compared to homogeneous ones (detailed in the following chapters). Basically, by using heterogeneous coating, the ice structure directly in contact with the surface is disrupted, because water molecule orientation depends upon the material's nature, and consequently the ice adhesion force can be drastically reduced [26, 28]. Compared to the common two-step preparation process to fabricate SH coatings (surface roughening followed by applying low surface energy material), HCs have a number of advantages, such as simple preparation, easy application and low cost [28]. The other important advantage which can be considered for HCs is that the rough structures on homogeneous coatings created to prepare super-hydrophobic can be damaged and removed during icing-de-icing tests. However, in the case of HCs, by disrupting hydrogen binding between ice and the coated surface, the ability of the ice to adhere to the surface will be reduced [26].

1.4 Objectives

The present research proposes the use of chemically heterogeneous and low surface-energy coatings having higher icephobic properties than those of homogeneous coatings. Homogeneous coatings are considered here to include either hydrocarbons or fluorocarbons. The literature available on heterogeneous polymer coatings or copolymers including hydrocarbons and fluorocarbons is rare [25-27]. The main goals of this research work are the first preparation of HCs by using techniques other than those reported in the literature and the second in studying the icephobic properties of HCs. Three different methods and strategies to study the effect of heterogeneity were adopted to prepare HCs on aluminum surfaces as follows:

(i) Deposition of homo- and heterogeneous self assembled monolayers (*SAM*s) on the aluminum alloy surfaces;

(ii) Preparation of homo- and heterogeneous nanoparticles coatings on the aluminum alloy surfaces;

(iii) Fabrication of homo- and heterogeneous plasma sputtering coatings through masks on the aluminum alloy surfaces.

Finally, the durability and stability of homo- and HCs prepared by the three different methods mentioned above are studied against several extreme environmental conditions such as: several icing/de-icing cycles, immersion in various pH solutions and UV-degradation.

In order to assess such coatings, their hydrophobic and icephobic behavior will be studied using contact angle (CA) and contact angle hysteresis (CAH) measurements and centrifugal adhesion tests (CAT). Morphological, chemical, stability and durability characterizations will be performed on the different samples.

1.5 Outline of the Thesis

The thesis is ordered in eight chapters as follows:

• Chapter 1 presents a summary of icing problems and a short introduction to the prevention of ice accumulation in addition to a general introduction of this research work including the motivation for this work and objectives.

• Chapter 2 presents a review of the available literature and background studies on hydrophobicity, superhydrophobicity and icephobicity. This chapter also provides a summary of previous studies on heterogeneity, which should be of help to the reader.

• Chapter 3 explains the experimental procedures for preparing the homo- and HC characterization methods. It furthermore describes the facilities and techniques used for characterizing the prepared coatings, e.g. Contact Angle Goniometer, Atomic Force Microscope (AFM), profilometry, Centrifuge Adhesion Test Machine, Scanning Electron Microscope (SEM), Energy-Dispersive X-ray Spectroscopy (EDS), X-ray photoelectron spectroscopy (XPS), and so on.

• Chapter 4 describes the experimental results obtained on the prepared homo- and heterogeneous *SAM*s coatings in terms of hydrophobic properties and surface characterizations, e.g. morphological and chemical analysis.

• Chapter 5 presents the results of the wettability behavior study on homo- and heterogeneous nanoparticles coatings on aluminum substrates as well as surface characterizations.

• Chapter 6 provides the results obtained concerning the hydrophobic properties and surface characterizations on coated sample of homo- and heterogeneous plasma coatings through a mask.

• Chapter 7 provides the results obtained on the homo- and HCs prepared by three methods in terms of icephobicity. In the meantime, the durability of homo- and HCs are discussed in terms of several icing/de-icing cycles, immersion in various pH solutions and UV degradation. The contact angle values as a function of icing/de-icing number after each icing/de-icing cycle on the coated samples are also discussed in detail in this chapter.

• Chapter 8 includes general conclusions and recommendations for future studies based on this research work including the obtained results and their discussion.

Finally, the references cited in this thesis are presented at the end.

CHAPTER II

BACKGROUND AND LITERATURE REVIEW

2. Introduction

2.1 A brief review of hydrophobic and super-hydrophobic properties

2.1.1 Hydrophobicity and contact angle

2.1.2 Superhydrophobicity and roughness

2.2 Ice accumulation and types of ice

2.3 Review of the literature on hydro- and icephobic coatings

2.3.1 Hydro- and icephobic *SAM*s coatings

2.3.2 Hydro- and icephobic nanoparticles coatings

2.3.3 Hydro- and icephobic plasma coatings

2.4 Hydro- and icephobic heterogeneous coatings (HCs)

2.5 Conclusion

2. Introduction

Atmospheric icing on equipment may impact its operation, diminishing safety and productivity. A number of new technologies and modern versions of old technologies have been used successfully to minimize icing in the electric power industry and ground transportation systems. In this chapter, we will briefly review hydrophobicity and superhydrophobicity, showing the anti-icing properties developed with different techniques. After that, preparation of HCs with hydrophobic properties will be introduced and their hydrophobicity and icephobicity will be compared to homogeneous coatings. In addition, a review of the research on the influence of HCs in the improvement of hydrophobic and icephobic surfaces will be presented.

2.1 A brief review of hydrophobic and super-hydrophobic properties

2.1.1 Hydrophobicity and contact angle

A hydrophobic surface is the water repellent surface, in contrast with a hydrophilic surface that is easily wetted [29]. The tendency to wet the surface can be determined by way of contact angle measurements that the surface of a liquid drop makes with the solid surface [30]. Young and Laplace found out that each surface has a specific energy because the surface atoms or molecules of liquids or solids have fewer bonds with neighboring atoms. Therefore, they have higher energy than similar atoms and molecules in the interior [31]. This additional energy is characterized quantitatively by the surface tension or free surface energy γ . The unit of γ is J m^{-2} or N m^{-1} and it can be

interpreted either as energy per unit surface area or as tension force per unit length of a line at the surface.

When a liquid droplet is placed on a solid surface, the liquid and solid surfaces come together under equilibrium at a characteristic angle called the static contact angle θ_0 (Fig.2.1).

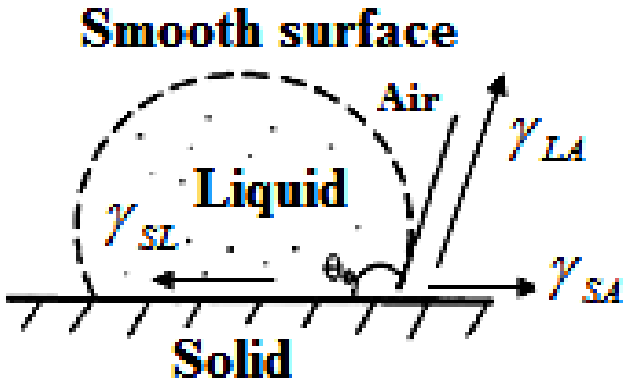

Fig.2. 1. Schematic of liquid droplet in contact with a smooth solid surface (contact angle, θ_0).

These surface energies come from the solid, liquid, and solid/liquid interfaces [31]. The well-known Young equation for the contact angle is obtained:

$$Cos\theta_0 = \frac{(\gamma_{SV} - \gamma_{SL})}{\gamma_{LV}} \qquad \textbf{(2.1)}$$

Where,

- γ_{sv} : Surface energy of solid/vapor (N/m)

- γ_{sl} : Surface energy of solid/liquid (N/m)

- γ_{lv} : Surface energy of liquid/vapor (N/m)

- θ_0 : Contact angle between solid/liquid (°)

The contact angle (CA, θ_0) is the macroscopic indicator of the surface energy balance and the equilibrium of surface energy can determine the entire shape of a droplet on a solid. The wetting phenomenon is normally described as a contact angle (θ_0) of the specific surface, i.e., $\theta_0 > 90^o$ as hydrophobic surface; $\theta_0 < 90^o$ as hydrophilic surface. Greater contact angles, preferably $\theta_0 > 150^o$, indicate super-hydrophobicity and self-cleaning abilities (Fig. 2.2) [32].

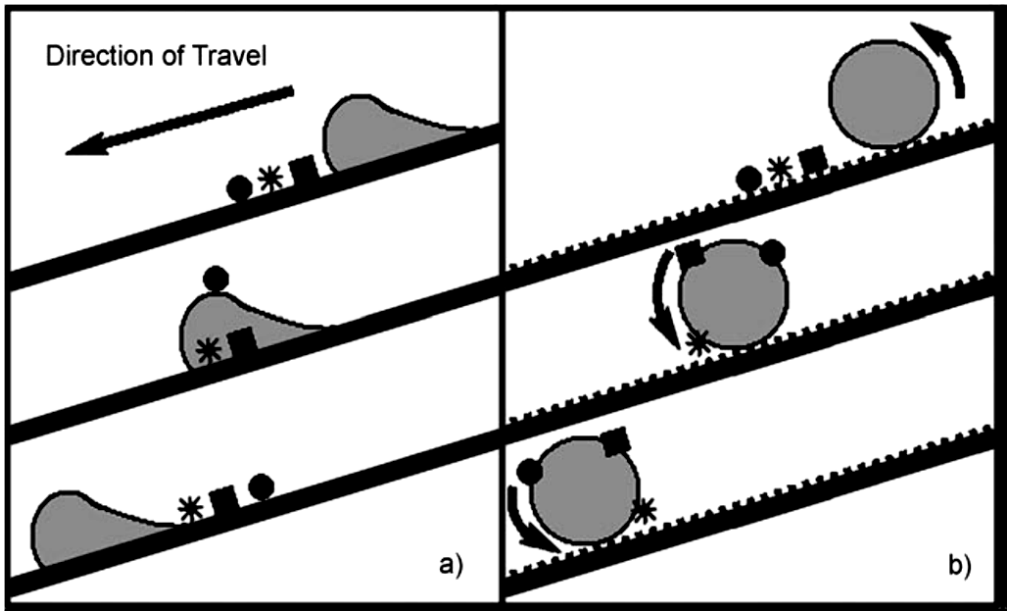

Fig.2. 2. The cleaning mechanism on hydrophobic (a) and super-hydrophobic surfaces (b).

2.1.2 Superhydrophobicity and roughness

A super-hydrophobic surface is one that repels water to such an extent that the contact angles obtained are extremely high; they are generally defined as surfaces with water contact angles above 150^{o} [33]. Several example of super-hydrophobic surfaces are observed in nature, for instance, the lotus plant (or *Nelumbo nucifera*), which also demonstrates the self-cleaning properties [34]. Figure 2.3 shows some examples of super-hydrophobic surfaces in nature [35]. The leaf of the lotus plant with properties is known to be super-hydrophobic and self-cleaning due to hierarchical roughness and the presence of a hydrophobic wax coating. The static contact angle value of a Lotus leaf is about 164^{o} [36]. The water droplets on the leaves remove any contaminant particles from their surfaces when they roll off, leading to self-cleaning [35, 37-42]. (Fig. 2.3a).

Pond skaters (*Gerris remigis*) have the ability to stand and walk upon a water surface without getting wet (Fig. 2.3b). Gao and Jiang [43] showed that the special hierarchical structure of the pond skater's legs, covered with cuticle wax, makes the leg surfaces super-hydrophobic. It is responsible for the water resistance, and enables them to stand and walk quickly on the water surface (Fig. 2.3b).

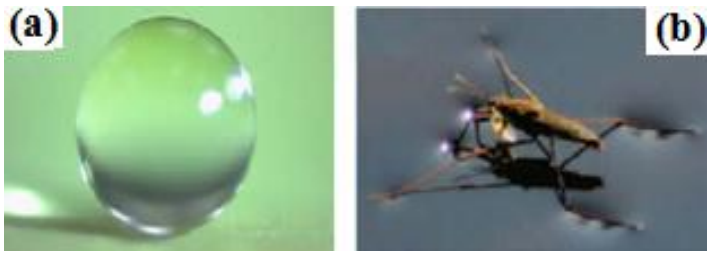

Fig.2. 3. Montage of some examples from nature: (a) Lotus leaf surface, and (b) pond skater walking on water [35].

One of the ways to increase the hydrophobic or hydrophilic properties of a surface

is to increase surface roughness, so roughness-induced hydrophobicity or hydrophilicity has become the subject of extensive investigations [44]. Wenzel [45] suggested a simple model predicting that the contact angle of a liquid with a rough surface is different from that with a smooth surface. The Wenzel regime is defined by equation (2.2) for the contact angle on a rough surface:

$$Cos\theta' = bCos\theta \qquad \textbf{(2.2)}$$

where:

- θ' : Apparent contact angle (°)
- b : Roughness factor
- θ : Contact angle of flat surface (°)

The Wenzel model describes that a hydrophobic surface with increasing roughness becomes even more hydrophobic, while a hydrophilic surface with increasing roughness becomes more hydrophilic [46].

Cassie and Baxter [47] showed that a gaseous phase including water vapor or air may be trapped in the cavities of a rough surface, resulting in a composite solid-liquid-air interface, as opposed to the solid-liquid interface. These two models describe two possible wetting regimes or states on rough surfaces: Wenzel and Cassie-Baxter regimes (Fig. 2.4). The Cassie-Baxter model is characterized by a large contact angle and a very small contact angle hysteresis.

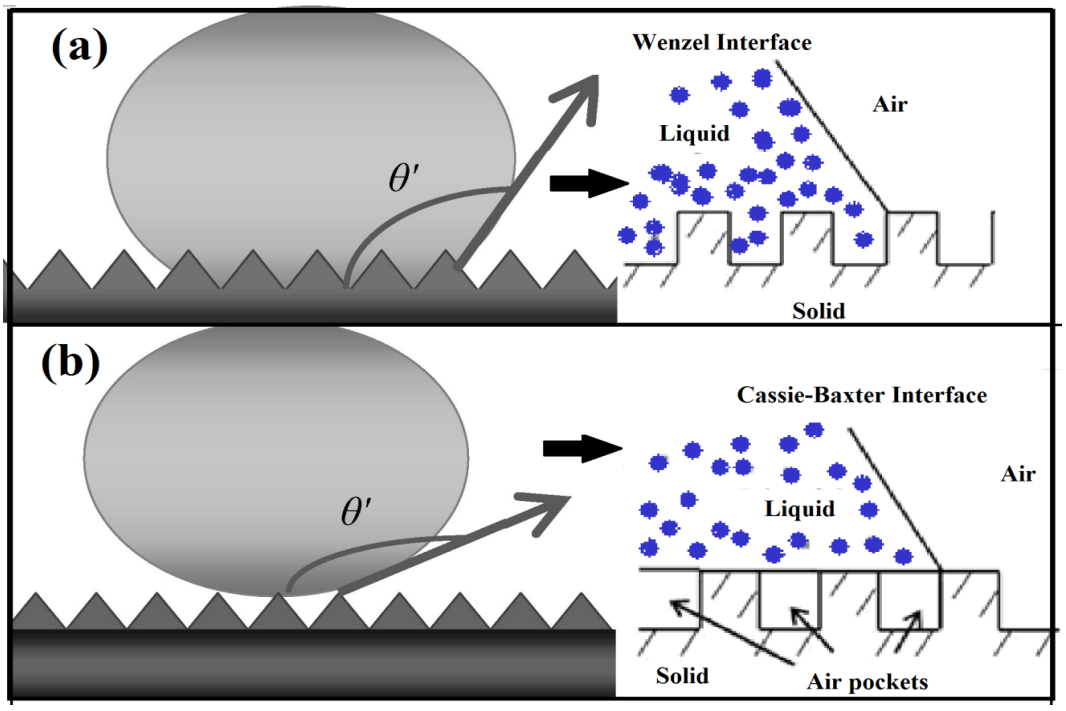

Fig.2. 4. Schematics of configurations described by the (a) Wenzel regime and Cassie–Baxter regime with air pockets [47].

In the Cassie-Baxter model [47], the contact angle values are determined by the fractions of solid and air facing the drop. Equation (2.3) describes the Cassie-Baxter model:

$$Cos\theta' = f.(Cos\theta + 1) - 1 \qquad \textbf{(2.3)}$$

where:

- θ' : Apparent contact angle (°)
- f : Surface fraction (the ratio of surface top-post to projected surface)
- θ : Contact angle of flat surface (°)

Numerous super-hydrophobic materials have been produced using a range of chemical and physical methods on rough surfaces. For example, a contact angle value of 160° was found using PECVD of fluoroalkylsilanes on an aluminum surface [49]. The combination of high surface roughness with the low-energy surface of FAS molecules (CF_3-$(CF_2)_7CH_2CH_2Si(OCH_3)_3$) gives a contact angle value of 158° [50]. A contact angle value of 162° (with CA hysteresis less than 2°) was obtained after being modified with octadecyltrichlorosilane (ODTS) [51].

2.2 Ice accumulation and types of ice

Ice accretion can be defined as any process of ice build-up and snow accretion on the surface of an object exposed to the atmosphere. For power transmission and distribution lines, the built-up ice causes the mechanical and electrical damage or flashover on the insulators. Types of accreted ice depend on wind speed, super-cooled water droplet size, compressive strength, air temperature and properties of the objects being hit by droplets [52]. The freezing process of a water droplet may be accelerated by presence of any substance that can act as a freezing nucleus, which makes possible the growth of an ice crystal on itself. Two sources of atmospheric ice accretion are recognized, according to their methods of deposition:

(1) In-cloud icing happens where super-cooled water droplets are sufficiently small to remain suspended and contact with the surface results from air movement. This usually is the case with aircraft flying through clouds or on equipment installed at high altitudes [52]. The ice formed could be hard rime, soft rime, but sometimes glazes. The

ice growth in different types of rime is called dry icing. When the water flux increases, the droplets do not have the required time to freeze before the next impinge, hence the ice growth will tend to be wet. Dry icing usually results in different types of rime containing air bubbles, while wet icing always forms glaze ice which is solid and clear (Fig. 2.5c). The maximum amount of accreted ice on an object depends on several factors. The most important factors are air temperature, relative humidity, and the duration of ice accretion. However, major preconditions for significant ice accretion are the dimensions of the object exposed and its orientation to the direction of the icing wind.

(2) Precipitation icing occurs when the droplets are massive enough to fall from the atmosphere onto an accreting surface. In other words, precipitation icing may happen when a warm layer of air (temperature > 0 °C) is trapped between two layers of cold air (temperature < 0 °C) during freezing rain. Precipitation icing can occur anywhere regardless of altitude. This type includes freezing precipitation and wet snow. Precipitation icing generally gives rise to glaze ice accumulations.

Glaze ice forms when droplets striking a surface have sufficient time prior to freezing to flow in a continuous film (Fig. 2.5c). Glaze is caused by freezing rain, freezing drizzle or wet in-cloud icing and usually causes smooth evenly distributed ice accretion. Glaze often forms a hard, nearly homogeneous ice layer having the highest density approaching 0.917 g cm^{-3}, that of bubble-free ice [53]. As well, it conducts electricity more easily, and therefore is more risky for the performance of electric networks.

Rime forms tiny coatings on snow crystals or enormous accumulations up to several meters thick on terrestrial objects and is the most common type of in-cloud icing. The lower temperatures usually create hard rime or soft rime (Fig. 2.5 a and b). Depending on meteorological conditions, rime accretions can be dense, compact masses, feathery surfaces, or slender, needle-like spikes. Rime grows into the prevailing wind and is a reliable indicator of wind direction during icing events [54]. The accretion rate for rime varies on dimensions of the exposed object, wind speed, liquid water content in the air, water drop size and air temperature.

Soft rime forms when the super-cooled droplets freeze quickly upon deposition (Fig. 2.5a). The deposit often has an opaque white, porous, and fluffy appearance. Soft rime has a density of less than 0.6 g cm^{-3} [55].

Hard rime forms when the rate of latent heat loss is relatively low, allowing "wet growth" whereby some flow of the droplets occurs before complete freezing (Fig. 2.1b). Hard rime is generally milky or translucent in appearance, depending upon the amount of air trapped within the ice structure. Its density ranges from 0.6 to 0.9 g cm^{-3}.

Although meteorological conditions associated with the formation of glaze and rime have been investigated, due to the complexity of the phenomenon, geographic differences and monitoring disparities, a wide range in conditions has been reported in table 2.1.

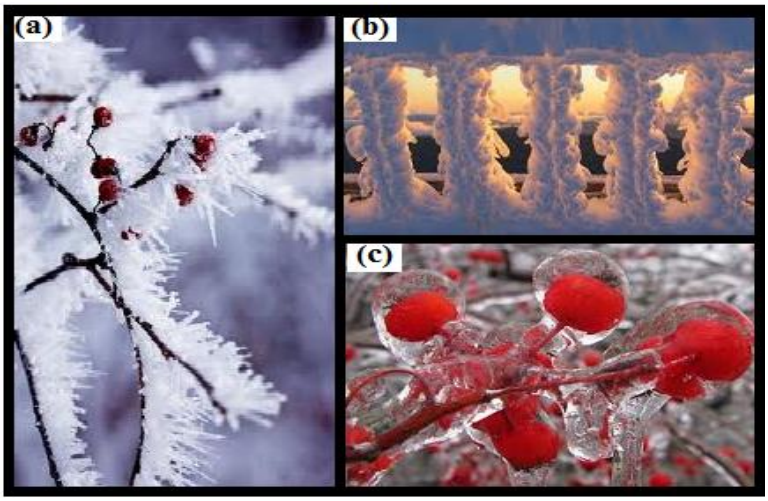

Fig.2. 5. (a) Soft rime, (b) hard rime ice and (c), glaze ice.

Table 2. 1. Summary of some field observations of natural icing [56-58].

Meteorological variable and/or range	Ice condition
Air temperature -5 to -14 ^{o}C	Rime most frequent
Air temperature 0 to -4 ^{o}C	Observer-reported icing most frequent
Air temperature blow 1^{o}C with low wind	Hard rime common
Air temperature < -5 ^{o}C and wind > 5 ms	Soft rime common
Wind speed and event duration	Positively correlated with amount of ice
Air temperature -2 to -3 ^{o}C	Optimum for hard rime
Air temperature -14 to -15 ^{o}C	Optimum for soft rime
Air temperature 0 to -6 ^{o}C	Accretion rates greatest
Air temperature -2 to -3 ^{o}C	Intensity of accretion greatest
Air temperature -3 to -6 ^{o}C	Frequency of rime events greatest
Wind speed increases	Rime growth intensity increases
Wind speed 1 to 10 ms^{-1} , air temperature -1 to 10 ^{o}C	Soft rime
Wind speed 3 to 15 ms^{-1} , air temperature -2 to -8 ^{o}C	Hard rime
Wind speed 2 to 20 ms^{-1} , air temperature 0 to -3 ^{o}C	Glaze

2.3 Review of the literature on hydro- and icephobic coatings

2.3.1 Hydro- and icephobic *SAM*s coatings

In order to develop icephobic coatings, various groups of materials or surface treatments can be considered. In this section we focus on the introduction of self-assembled monolayers (*SAMs*) and their hydro- and icephobic properties. It is possible to alter the surface energy of surfaces by an appropriate surface coating as thin as a few layers of *SAM*s molecules with $-CH_3$ or $-CF_3$ groups oriented outward to the ice surface. Deposition of self-assembled monolayers is one of the most successful approaches to hydrophobization of hydrophilic surfaces [59-61]. Such molecules usually have a polar unit at one end (head) and a non-polar long saturated hydrocarbon chain on the other end (tail) such as $-CH_3$ or $-CF_3$ groups oriented outward from the coating surface. A typical example is stearic acid (see Fig. 2.6). The performance of this treatment has been tested on a number of metal and alloy substrates including aluminum and aluminum alloys, various steels, copper and copper alloys, brass, zinc, and several automotive and aircraft alloys. A widely used class of *SAMs* is based on n-alkyltrichlorosilane or n-alkyltrialkoxysilane molecules which through a combined process of adsorption, hydrolysis and polymerization can lead to spontaneously assembled and organized alkylsiloxane monolayers at oxide surfaces such as Al_2O_3, SiO_2, SnO_2, etc. [62, 28, 64-65].

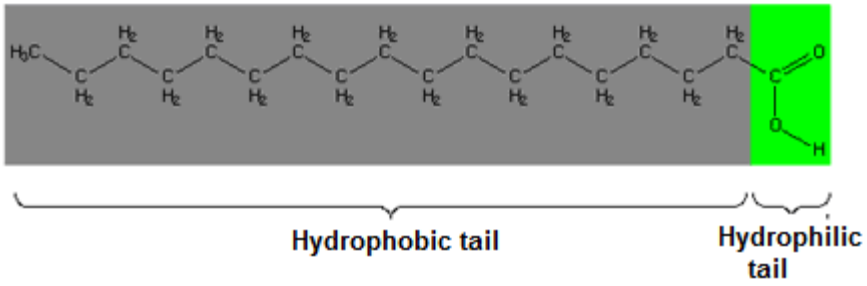

Fig.2. 6. Chemical structure of stearic acid molecule.

Figure 2.7 shows an organosilicon type of anchoring group where $-CH_3$ or $-CF_3$ groups are oriented outward from the surface. Silane groups are covalently bonded to the oxygen of the Al_2O_3 surface layer present at the aluminum surface. By its covalent nature this bonding makes the anchoring of the alkyl chain very strong and the overall deposition technique is easy to apply and reasonably priced [62]. Both static and dynamic contact angles of *SAM*s coated surfaces are strongly affected by the well ordered of self assembly of fluoroalkylsilane or alkylsilane molecules [59, 64, 66]. Fabrication of self-assembled monolayers (*SAM*s) coatings is one of the most successful approaches to chemical modification and hydrophobization of many hydrophilic surfaces [59]. Dimethyl-n-octadecilcholorosilane (DMOCS) provided a hydrophobic surface to a 6061 aluminum alloy. The tensile strength of the ice\DMOCS interface at -10 ^oC was found to be 131MPa which is lower than for as-received Al surfaces (274 MPa) and surfaces prepared with chemical and mechanical polishing (181 MPa) [66]. The contact angles of the substrates modified with self-assembled monolayers are 107^o for dodecanethiol and 110^o for octadecyltrichlorosilane (OT), respectively [67]. The formation of Octadecylphosphonic acid (OPA) *SAM*s on a titanium substrate showed the water

wettability of 110^{o} which suggests that the well ordered homogeneous OPA layers are present on the titanium substrate [68]. The contact angle values of water droplet on monolayers of Octadecanehydroxamic acid, Stearic acid, Octadecanephosphonic acid, 16-Hydroxyhexadecanehydroxamic acid, and Octadecanethiol on Al substrates showed contact angles of 111.93^{o}, 110.83^{o}, 113.83^{o} and 72.36^{o}, respectively [69]. Water contact angle values of untreated Si (no coating) and Si treated using OD, FAS-3, and FAS-17 were, respectively, 68^{o}, 101^{o}, 77^{o}, and 106^{o}. Freezing temperatures of super-cooled droplets were -16.3 ^{o}C, -19.9 ^{o}C, -22.4 ^{o}C, and -22.7 ^{o}C for the respective surfaces [70].

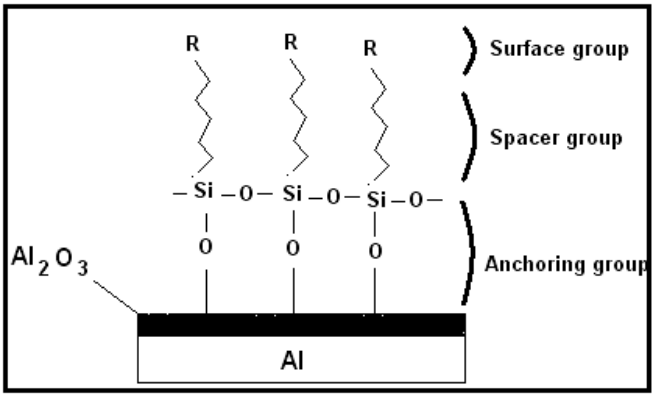

Fig.2. 7. Schematic presentation of *SAM*s grafted onto an aluminum substrate.

2.3.2 Hydro- and icephobic nanoparticles coatings

In this section the hydro- and icephobic properties of various nanoparticles incorporated in polymer coatings are reviewed. There is extensive research on nanoparticles incorporated in polymers such as RTV silicon rubber coatings with TiO_2, CeO_2 and carbon black, respectively [16, 71]. The adhesion reduction factor *(ARF)* value of 1 wt. % of CeO_2 nanoparticles incorporated in RTV silicon rubber coatings was 7

times lower on this coating than with bare aluminum [72]. A preparation of nanoparticles incorporation (SiO_2 and $CaCO_3$) in stearic acid coatings by spraying gave contact angle and CAH values of 160^o and 3^o, respectively [73]. For the meantime, the results showed that the super-hydrophobic surface became rather hydrophobic at super-cooled temperatures (-10 ^oC). Super-hydrophobic micro-patterned aluminum surfaces were created by chemical etching that it was shown a water contact angle as high as $164 \pm 3^\circ$ with a contact angle hysteresis as low as $2.5 \pm 1.5^\circ$ on rf-sputtered Teflon-coated etched aluminum substrates [74]. A thin nanostructured silver film with stearic acid demonstrated water contact angle as high as 156^o and contact angle hysteresis as low as 5^o [75]. A simple method to elaborate fluoro-alkyl-terminated nanostructured superhydrophobic surfaces was provided by depositing a layer of FAS-17 on etched AA2024 surfaces in hot water, which showed good superhydrophobic and self-cleaning properties [76].

2.3.3 Hydro- and icephobic plasma coatings

Plasma-assisted deposition of thin fluorocarbon, organosilicon and hydrocarbon coatings have also resulted in hydro- and icephobic surfaces [77-79]. A hydrophobic layer was coated on the nanotextured surfaces by means of either the low-temperature CVD or the PECVD [80]. The surface-modified showed ultra water-repellency with water contact angles greater than 150° [80]. The created nanostructured patterns on aluminum alloy surfaces by immersion in boiling water, coated with RF-sputtered polytetrafluoroetylene demonstrated a high static CA (164°) and low CAH (~4°) [81]. A treated Teflon film with oxygen plasma became a super-hydrophobic surface with a

contact angle value of ~ 168^{o} [82]. A poly (ethylene terephthalate) (PET) substrate with selective oxygen plasma etching followed by plasma-enhanced chemical vapor deposition using tetramethylsilane (TMS) as a precursor produced a transparent super-hydrophobic surface [83].

2.4 Hydro- and icephobic heterogeneous coatings (HCs)

In the previous sections the hydro- and icephobic coatings prepared via *SAM*s, incorporated nanoparticles in polymers, and plasma methods, were reviewed. It was observed that the prepared coatings by the three methods mentioned above included hydrocarbon or fluorocarbon functions named as homogeneous coatings. However, the low surface energy of HCs or surfaces including both hydrocarbons and fluorocarbons have drawn less attention. These types of coatings are a very attractive alternative because they show lower ice adhesion as compared to homogeneous coatings. Basically, using HC the ice structure directly in contact with the surface is disrupted, because the orientation of water molecules depends upon the nature of the material, and consequently ice adhesion force can be reduced. Three important articles close to this work have been published in the field of heterogeneous polymer coatings, where the authors tried to decrease ice adhesion by applying a HC [25-27]. For instance, two different heterogeneous polymers, polyperfluoroalkylmethacrylate combined with hydrophobic silicon dioxide (A), and also an organopolysiloxane modified with lithium compound (B), have been studied. The ice adhesion values of heterogeneous polymers A and B compared to PTFE were reduced two fold and 25 times, respectively. To explain such behavior, the authors evaluated the lengths of the hydrogen bond to oxygen and fluorine

(O---H and F---H) as well as the different interaction energies [26-28] (see Fig. 2.8). They found that there is a slight repulsion between a water molecule and a siloxane group, while a strong attraction was observed between a fluorocarbon group and a water molecule. It should be noted that the water molecule orientations at the surface of fluorocarbon group and at the polysiloxane one were completely different. Consequently, by inducing and creating various disparities (hydrocarbons and fluorocarbons) in terms of energy bonding and water molecule orientation at the molecular level, the ice-solid interface is weakened by the possible creation of a wide range of dislocations and slips in the accumulated ice structure immediately adjacent to the solid surface (ice-solid interface line). The principle is the same as already proposed by Murase *et. al* and Byrd [26-28]. They have indicated the presence of a synergistic effect caused by the heterogeneity of the polymer coating leading to lower values of ice adhesion strength [26-28].

In theory, their calculation of the enthalpy of the F---H bond gives -50.89 KJ/mol with a bond length of 0.189 nm. For the O---H bond, the enthalpy is equal to -15.65 KJ/mol with a bond length of 0.329 nm. However, by applying heterogeneous surface coatings i.e. F---H and O---H bondings at the same time, the enthalpy and bond length change to -10.28 KJ/mol and 0.307 nm respectively for F---H and to -9.60 KJ/mol and 0.267 nm respectively for the O---H bond [26]. Therefore, it may be concluded that in the case of heterogeneous surfaces, due to the significant increase in the bond length of F---H and eventually the increase in the enthalpy, the overall interaction energy will be greater [26]. It must be mentioned that few studies and uses of such HCs were found in the literature.

2.5 Conclusion

In this chapter a literature review on hydrophobic, super-hydrophobic and icephobic properties of the coatings were presented. Three different methods, namely, *SAM*s, nanoparticles and plasma, for preparing homo- and HCs with hydro-, super- and icephobic properties, were studied. The definitions of HCs as well as the review of the scant pertinent literature were summarized. The effect of heterogeneity, empirically and theoretically, on the hydro- and icephobic characteristic of the coatings was discussed.

CHAPTER III

EXPERIMENTS AND TEST PROCEDURE

3. Introduction

3.1 Substrate preparation and cleaning

3.2 Preparation of homogeneous and heterogeneous of *SAM*s coatings

3.3 Preparation of homo- and heterogeneous nanoparticles coatings

3.4 Preparation of homo- and heterogeneous plasma coatings through masks

3.5 Sample analysis and characterization

3.5.1 Atomic force microscope (AFM)

3.5.2 Optical profilometry analysis

3.5.3 X-ray photoelectron spectroscopy (XPS)

3.5.4 QUV tester

3.6 Wettability Tests

3.6.1 Contact angle hysteresis

3.6.2 Sliding angle

3.7 Ice adhesion test

3. Introduction

In order to achieve the objectives of this study, a set of experiments is systematically carried out on the hydro- and icephobic properties of prepared coated aluminum surfaces. The objective of this chapter is to describe in detail the methods for preparing and characterizing the homo- and HCs on aluminum alloy 6061 surfaces. The coating morphology and anti-ice performance are also analyzed by applying a set of surface analysis and characterization techniques explained in this chapter.

3.1 Substrate preparation and cleaning

Aluminum alloy 6061 (Al 97.9 wt.%, Mg 1.0 wt.%, Si 0.60 wt.%, Cu 0.28 wt.%, Cr 0.20 wt.%), with plate dimensions 1×1 cm^2 and 5.1 × 3.2 cm^2, were used as the substrate. Prior to coating, the plates were mechanically polished, first using different grit sand papers, then finer SiC abrasive papers lubricated with water, and finally aqueous 1.0 μm alumina slurry, in order to obtain mirror-polished surfaces. The polished aluminum plates were then cleaned and degreased in a soap solution, and finally ultrasonically rinsed in acetone (99.5%, EMD), methanol (99.8%, MAT) and distilled water, respectively, each for 5 minutes.

3.2 Preparation of homogeneous and heterogeneous of *SAM*s coatings

The cleaned and polished aluminum surfaces were coated with a number of organic molecules providing low surface energy, namely Trichloro(octadecyl)silane

($C_{18}H_{37}Cl_3Si$), Trichloro(octyl)silane ($C_8H_{17}C_{l3}Si$) and Trichloro (1H,1H, 2H, 2H-perfluorooctyl)silane ($C_8H_4Cl_3F_{13}Si$), abbreviated here as OD, OT and PF, respectively. All three organic molecules were purchased from the Sigma-Aldrich Company and used as-received, without any further purification. Based on their chemical structures, these organic coatings would be potentially good candidates for *SAM*s deposition. The molecular structures of OD, OT and PF can be observed schematically in Figure 3.1.

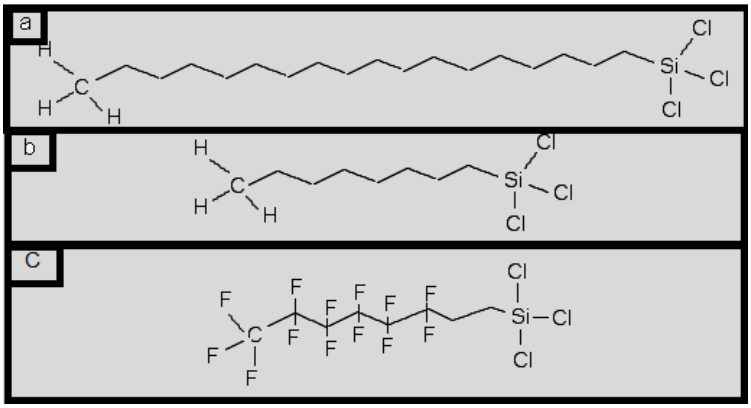

Fig.3. 1. Image of molecular structure of trichloro (octadecyl) silane (a), trichloro (octyl) silane (b) and trichloro (1H,1H,2H,2H-perfluorooctyl) silane (c).

These coatings were prepared on the aluminum surface by a simple dip-coating process followed by air drying in a conventional oven. The polished aluminum substrates (AA6061) were coated with four different prepared solutions of well stirred diluted OD (at 1 mM); OT (1mM) and OT (6mM), in toluene, and a solution of diluted PF in methanol (6 mM) stirred for 15 minutes before dip-coating. The detail of preparation of homogeneous and HCs of OD, OT and PF (6 mM) on the aluminum surface can be observed in Table 3.1.

Table 3. 1. The preparation procedure of homogeneous and HCs.

Homogeneous Coatings	Sample	Immersion time (h, first layer)	Drying time (h) at 70 °C (interval steps)	Immersion time (h, Second layer)	Drying time (h) at 70 °C (Final step)
	OD-OD OT-OT PF-PF	2, 6, 12	1 h	2, 6, 12	2
HCs	OD-PF OT-PF	2, 6, 12	1 h	2, 6, 12	2
	PF-OD PF-OT	2, 6, 12	1 h	2, 6, 12	2
	PF\OD	2, 6, 12	2 h	-	-

3.3 Preparation of homo- and heterogeneous nanoparticles coatings

Solutions of one gram (1 g) of various polymers such as polyethylene (PE), polyethylene (PS) and polymethylmethacrylate (PMMA) in 50 ml of toluene, and a solution of diluted stearic acid (STA) in acetone (1g/50 ml), were prepared as a first layer for homogeneous coatings. For HCs, suspensions of 1 g of dispersed nanoparticles with different surface energy such as polytetrafluoroethylene (PTFE), Al_2O_3 and ZnO in 50 ml of methanol were prepared. These suspensions were oscillated by ultrasonic waves for 5 minutes followed by magnetic stirring during 20 minutes. The suspensions were used to fabricate several series of HCs on polished aluminum surface, in order to study the effect of different surface energies and surface roughness. Due to the effect of the diameter of nanoparticles on surface roughness and consequently on surface wettability, in this step, two different sizes of nanoparticles were used. More precisely, two dissimilar

nanoparticles, e.g. ZnO (molecular diameter 100 nm) and Al_2O_3 (200 nm), were used to trace and compare any possible effect of nanoparticles size on sample wetting properties, compared to the PTFE nanoparticles (200 nm).

The homogeneous and heterogeneous nanoparticles coatings were prepared using a spin-coater from Laurel (WS-400B-6NPP). Spin coating is a commonly used technique for preparing uniform thin films on flat substrates which involves the controlled precipitation from solution of a compound on a suitable substrate while spinning with specific parameters. The spinning rate was set at 500 rpm (15 s) (Fig. 3.2). Upon coating, all samples were heat-treated at 70 °C in oven for 2 hours to remove residual solvents.

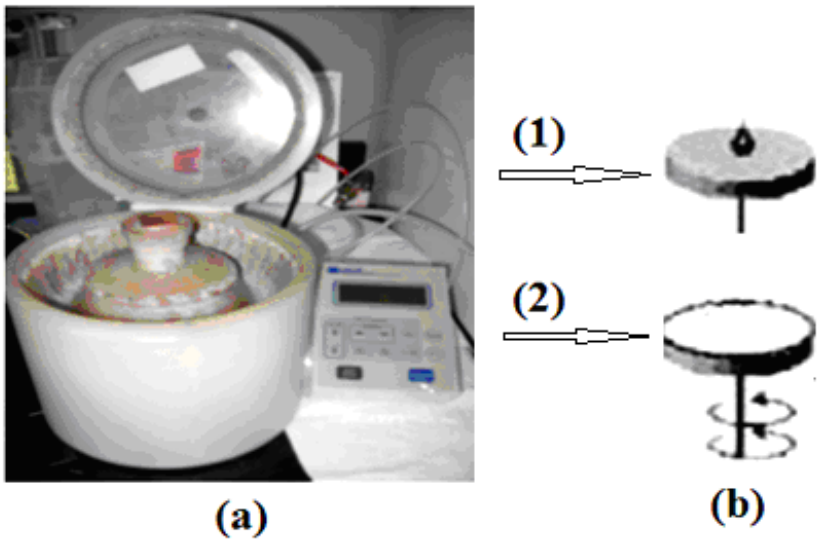

Fig.3. 2. (a) Spin-coater (model WS-400B-6NPP, Laurell Technologies Corporation), (b) steps of coating preparation, (1) deposit solution, (2) spreading.

Table 3.2 and 3.3 present the procedure for preparing of homogenous and heterogeneous nanoparticles coatings.

Table 3. 2. Detail information for the preparation of homogeneous coatings.

One step					
Material	**Quantity**	**Solvent**	**Method**	**Company**	**Abbreviate**
PE	1 g	50 ml Toluene (at 110^{o} cc)	Spin coating	Good-fellow	PE-spin
PS	1 g	50 ml Toluene	Spin coating	Sigma-Aldrich	PS-spin
PMMA	1 g	50 ml Toluene	Spin coating	Sigma-Aldrich	PMMA-spin
STA	1 g	50 ml Acetone	Spin coating	Sigma-Aldrich	STA-spin
PTFE	1 g	50 ml Methanol	Spin coating	Sigma-Aldrich	PTFE-spin
Al_2O_3	1 g	50 ml Methanol	Spin coating and Immersion	Nano-Amor	Al_2O_3-spin Al_2O_3 _immersion
ZnO	1 g	50 ml Methanol	Spin coating and Immersion	Sigma-Aldrich	ZnO-spin, ZnO-immersion
PE / PTFE	1g / 1g	100 ml Toluene	Spin coating	Goodfellow / Sigma	PE+PTFE
PE / ZnO	1g / 1g	100 ml Toluene	Spin coating	Sigma / Sigma	PE+ZnO

Table 3. 3. The details information for preparation of heterogeneous nanoparticles coatings.

First step						Second step					
Material	**Quantity**	**Solvent**	**Method**	**Company**	**Abbreviate**	**Material**	**Quantity**	**Solvent**	**Method**	**Company**	**Abbreviate**
PE	1 g	50 ml Toluene (at 110^{o} cc)	spin coating	Good-fellow	–	PTFE	1 g	50 ml Methanol	spin coating	Sigma-Aldrich	PE-PTFE
PE	1 g	50 ml Toluene (at 110^{o} cc)	spin coating	Good-fellow	–	ZnO	1 g	50 ml Methanol	spin coating	Sigma-Aldrich	PE-ZnO
PE	1 g	50 ml Toluene (at 110^{o} cc)	spin coating	Good-fellow	–	Al_2O_3	1 g	50 ml Methanol	Spin coating	Nano-Amor	PE- Al_2O_3
PS	1 g	50 ml Toluene	spin coating	Sigma-Aldrich	–	PTFE	1 g	50 ml Methanol	spin coating	Sigma-Aldrich	PS-PTFE
PS	1 g	50 ml Toluene	spin coating	Sigma-Aldrich	–	Al_2O_3	1 g	50 ml Methanol	Spin coating	Nano-Amor	PS- Al_2O_3
PMMA	1 g	50 ml Toluene	spin coating	Sigma-Aldrich	–	PTFE	1 g	50 ml Methanol	Spin coating	Sigma-Aldrich	PMMA-PTFE
PMMA	1 g	50 ml Toluene	spin coating	Sigma-Aldrich	–	Al_2O_3	1 g	50 ml Methanol	Spin coating	Nano-Amor	PMMA-Al_2O_3
STA	1 g	50 ml Acetone	spin coating	Sigma-Aldrich	–	PTFE	1 g	50 ml Methanol	Spin coating	Sigma-Aldrich	STA-PTFE
STA	1 g	50 ml Acetone	spin coating	Sigma-Aldrich	–	Al_2O_3	1 g	50 ml Methanol	Spin coating	Nano-Amor	STA - Al_2O_3
PE / PTFE	1g / 1g	100 ml Toluene	spin coating	Good fellow / Sigma	PE+ PTFE	–	–	–	–	–	–
PE / ZnO	1g / 1g	100 ml Toluene	spin coating	Sigma / Sigma	PE+ ZnO	–	–	–	–	–	–

3.4 Preparation of homo- and heterogeneous plasma coatings through masks

To prepare homogeneous and heterogeneous plasma coatings, various copper masks were placed on the aluminum substrates (for homogeneous coating) and aluminum substrates coated with polyethylene (PE) and polystyrene (PS). The used masks of the copper gauze were 20 and 60 mesh, corresponding to 0.41 and 0.19 mm in wire width, respectively. Then, to apply the plasma sputtering, polytetrafluoroethylene (PTFE) was used as a target, and it was deposited on polished aluminum surface, polyethylene (PE) and polystyrene (PS) coated aluminum surfaces through a different mask.

The HCs prepared in these ways by the plasma method were called PE-PTFE (0.41 mm), PE-PTFE (0.19 mm), PS-PTFE (0.41 mm) and PE-PTFE (0.19 mm). The RF plasma-sputtering process was carried out in an HICP-600SB PECVD system, manufactured by Plasmionique Inc. The distance between the target (Teflon®) and the substrates (aluminum) was set at 30 cm. After being evacuated to a base pressure of 2.0×10^{-6} Torr, argon gases were admitted into the chamber. The flow rate of the sputtering gas was controlled by an MKS mass flow controller (MFC) and set at 50 standard cubic centimeters per minute (sccm). The aluminum surface was pre-cleaned and pre-activated in 75W plasma argon for 5 min. The sputtering deposition process was carried out under 75W RF power for 20 min at 20mTorr. Figure 3.3 shows the plasma reactor available at CIGELE and PE samples without and with different copper gauzes as a mask (0.19 mm and 0.41 mm).

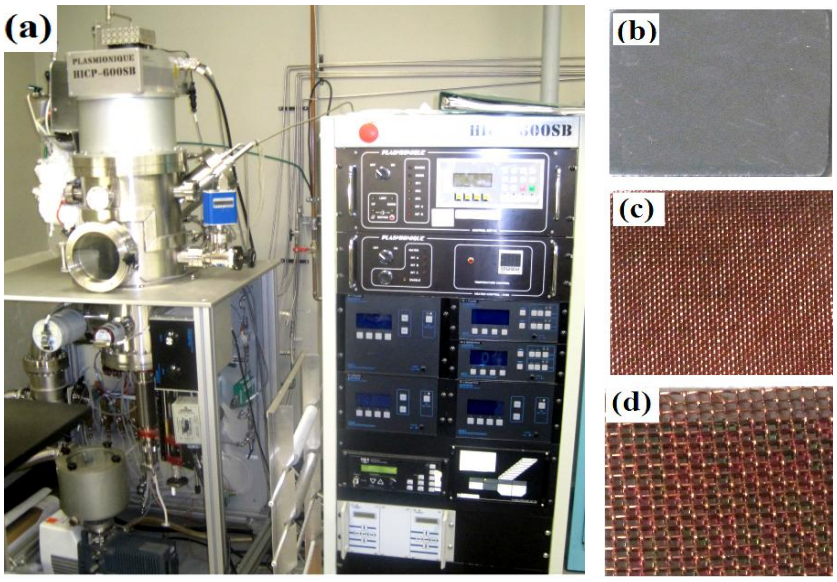

Fig.3. 3. (a) Plasma reactor (CIGELE), (b) PE coated Al sample, (c) PE sample covered with copper gauze of with 0.19 mm and (d) PE sample covered with copper gauze of with 0.41 mm.

3.5 Sample analysis and characterization

In this research, surface characterizations and analysis were carried out to study the morphology, chemical composition and durability of the prepared coatings. This section discusses various techniques for analyzing and characterizing the homo- and HCs prepared by three different methods.

3.5.1 Atomic Force Microscope (AFM)

An atomic force microscope (AFM, Escope, Veeco) was used to characterize and analyze the surface morphologies of the coated samples (Fig. 3.4). To generate the AFM images, the tapping mode method was used. Conditions were at room temperature under

normal air pressure. In this mode, a swing silicon probe (Nanosensors™) designed an image in the topography of the surface. A surface topography was mapped by lightly tapping the surface with an oscillating probe. Atomic force microscopy provides us with information on the surface features, for instance, measurements of the nanoscale features of the surfaces including the z-height and surface roughness. The tip radius is less than 10-15 nm and the height 10-15 µm set on a cantilever of length 220-230 µm and width 35-45 µm, respectively.

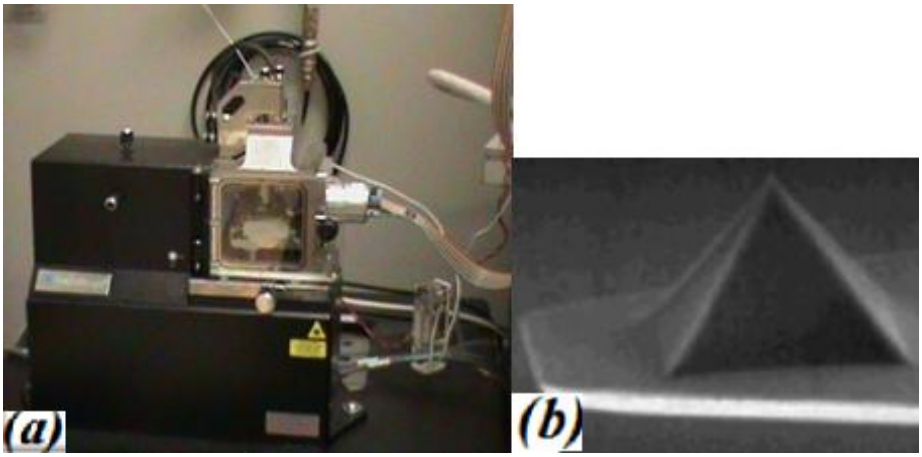

Fig.3. 4. *(a)* Atomic force microscope (AFM), CIGELE and *(b)* Silicon nitride probe fixed on cantilever.

3.5.2 Optical profilometry analysis

The AFM technique is an efficient and useful approach to investigate substrate surfaces with nano-scale roughness features. However, it should be noted that it is complicated to have an appropriate image in the case of a micro textured surface In this case, therefore, other surface assessment techniques and methods should be used, *e.g.*

optical profilometry. Therefore, the surface morphology of coatings was carried out using an optical profilometer machine (micro XAM100 in CURAL and Confocal CHR 150-L in CTA laboratory) (Fig. 3.5). The optical profilometer uses a high resolution non-contact sensor and facilitates the examination of opaque and/or highly reflective surface finishes.

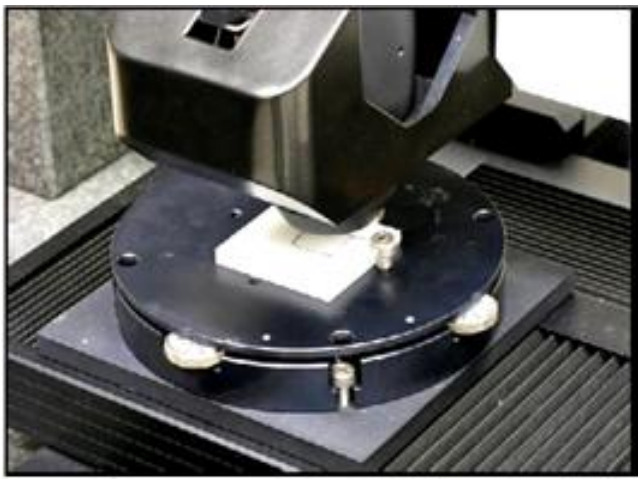

Fig.3. 5. : Photo of profilometer device, CTA laboratory.

3.5.3 Scanning Electron Microscopy (SEM/EDX)

SEM measurements produce a two dimensional image of the morphological features of the surface in addition to providing the atomic composition of the material by means of energy dispersive X-ray spectroscopy (Hitachi S-4700 Field-Emission SEM with accelerating voltages from 500 V to 25 kV) (Fig. 3.6). Before each measurement, samples with low surface conductivity were covered with a very thin film of platinum or carbon to lessen charge build-up during the scanning.

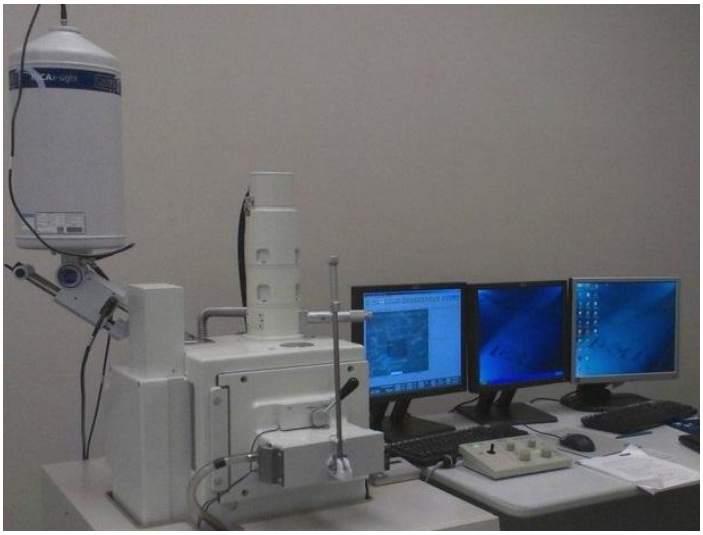

Fig.3. 6. SEM machine, CURAL laboratory.

3.5.4 X-ray photoelectron spectroscopy (XPS)

Various chemical compositions on coated aluminum surfaces were identified and analyzed by X-ray photoelectron spectroscopy (XPS, manufactured by Staib Instruments GmbH (Germany) and Plasmionique (Quebec, Canada)) (Fig. 3.7). X-ray photoelectron spectroscopy is a quantitative and semi-qualitative spectroscopic technique that analyzes surface chemical composition for a thickness as low as a few nanometers. The X-ray source was polychromatic Mg lines which operated at 15 kV and P = 300W.

Fig.3. 7. XPS instruments, CIGELE laboratory.

3.5.5 QUV tester

Several tests were performed to determine the durability and ageing behavior of the different coatings. Degradation due to UV illumination was assessed using accelerated tests with the QUV/Accelerated Weathering Tester (ASTM G154), which was among the equipment acquired by CIGELE (Fig. 3.8). The QUV tester irradiance is 75 % higher than noon summer sunlight [84]. The test cycle was 8 hours at the conditions 0.89 W/m^2 irradiance, temperature 60 ºC in the QUV tester. Its programmable methods meet the standard of ASTM G154. The annual mean of UV radiant exposure (295-385 nm) in a site north of Ottawa in Canada was estimated at 172 MJ/m^2 for one year, based on several years of data gathering [84,85]. The irradiance from a narrow wavelength band (340 nm) to a wider wavelength range (295-385nm) can also be converted as follows [84,85]:

$10\ kJ/m^2$ (at 340 nm) $\cong 1\ MJ/m^2$ (at 295-385 nm) **(3.1)**

Thus, the required number of hours of UV exposure in the mentioned apparatus

equal to one year of natural exposure can be calculated as follows [84]:

$$1720000\ J/m^2\ (at\ 340nm) = 0.89\ W/m^2\ (at\ 340nm) \times Time\ (sec) \quad \textbf{(3.2)}$$

$$Time\ (sec) \approx 1933200\ sec \approx 537\ hr \quad \textbf{(3.3)}$$

Then, 537 hours of exposure to the artificial UV instrument is equal to one year of sunlight exposure.

Fig.3. 8. QUV tester apparatus, CIGELE laboratory.

3.6 Wettability Tests

The wetting behavior of the prepared coatings was assessed on a contact angle goniometer following standard procedures by measuring the water contact angle (Fig. 3.9). The system used for contact angle measurements is a drop shape analyzer system (DSA 100 from Kruss GmbH). Contact angles and surface energy were measured using the sessile-drop method: small water droplets (4 µL in volume) were placed on the surface by an injection mechanism with several convenient syringes. Then their shape was evaluated with the goniometer optics and software using a light source to light the

sample surface and a camera connected to a computer where the drop shape can be recorded and analyzed. Another important advantage of the software is to calculate the contact angles by using appropriate techniques. To investigate changes in surface energy upon a prepared coating, water and formamide were used as probe liquids. Surface energy parameters of the probe liquids are the total, dispersive and polar components of the probe liquid surface free energy. The symbols γ_l , γ_l^d and γ_l^p represent the total, dispersive and polar components of the probe liquid surface free energy, respectively. The subscripts *s* and *l* represent solid and liquid, respectively. The components of the total surface free energy for the prepared coatings were determined from the Owens and Wendt equation [20]. This is a linear equation, $Y = mX + b$, where the slope *m* and intercept *b* are given by the square root of the polar and dispersive components of the solid surface free energy. Therefore, the polar and dispersive components of the total surface free energy are determined from the slope and the intercept of the linear fit. The total surface free energy can be obtained from according to equation [20] (3.1):

$$Y = \frac{\gamma_l(1+\cos\theta)}{2\sqrt{\gamma_l^d}} = \sqrt{\gamma_s^p}\,X + \sqrt{\gamma_s^d} \qquad \textbf{(3.4)}$$

$$\text{where } X = \left(\gamma_l^p\right)^{1/2} \Big/ \left(\gamma_l^d\right)^{1/2}$$

From to equation (3.1), the surface free energy components of the three surfaces were calculated from contact angle measurements. The static contact angle data were obtained by fitting the symmetric water drops using the Laplace-Young equation.

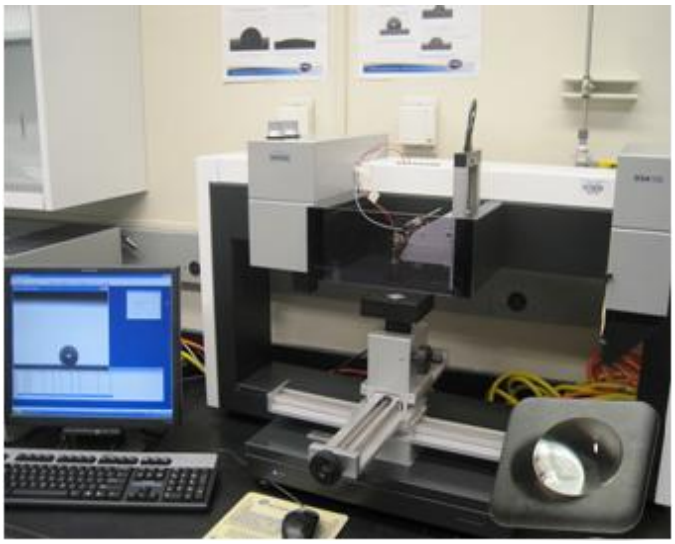

Fig.3. 9. Kruss DSA100 contact angle goniometer, CIGELE laboratory.

3.6.1 Contact angle hysteresis (CAH)

The method of measuring contact angle hysteresis (CAH) is to slowly move the substrate from right to left or *vice versa*, allowing for a visualization of the advancing (θ_A) and receding (θ_R) contact angles (Fig. 3.10). After injecting a water droplet on the sample, the droplet was held in contact with the sample surface with a stationary needle. Then the advancing and receding contact angles were measured while moving the sample in one direction [63]. After settling the water droplet on the sample surface, it is necessary to wait for 10 s prior to each measurement to be sure that the droplet is stabilized. The contact angle values reported here were the averages of at least five measurements on various parts of each sample.

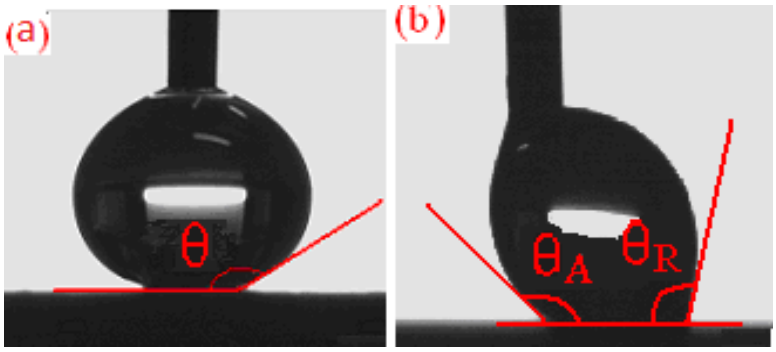

Fig.3. 10. Advancing and receding contact angles on a sample with (a) a low hysteresis (static CA), and (b) a high hysteresis (advancing (θ_A) and receding (θ_R) CAs.

3.6.2 Sliding angle

The sliding angle is the angle at which a water droplet of a certain mass starts to slide down an inclined plate. This can be obtained by measuring the angle of the sample surface and the horizontal plane at which the water or liquid droplet begins to slide off the surface due to gravity [86, 87]. In this study, the Groz instrument was used to measure the sliding angle (Fig. 3.11).

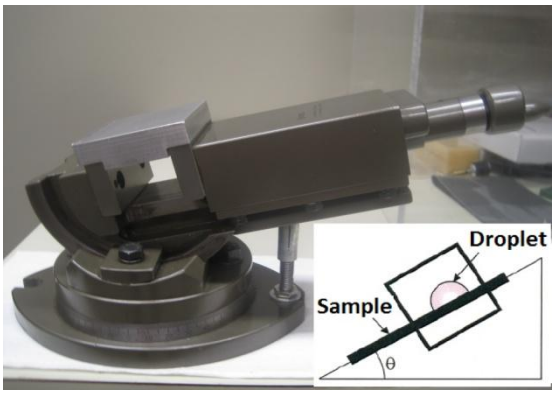

Fig.3. 11. Sliding angle instrument and schematic illustration of water droplet on a tilted surface.

3.7 Ice Adhesion Test

Different methods have been developed to measure ice adhesion, but some of them are not applicable for the atmospheric ice formed by the freezing of the super-cooled water drops in contact with structures. Shear stress of ice detachment depends on the techniques used to measure ice adhesion. In this series of experiments, the ice accumulation conditions were generated in the CIGELE laboratories. The ice-adhesion evaluation tests were conducted on aluminum beams with samples spun in a homemade centrifuge device (Fig. 3.12). The ice was accumulated on coated samples in a wind tunnel at subzero temperature (-10 ^{o}C) and with adjusted wind velocity, water pressure and air pressure values to l0 m/s, 325 kPa, 100 kPa, respectively, to simulate the atmospheric glaze ice created on surfaces in nature. The samples were first placed in a wind tunnel to build up a given thickness of glaze ice accretion by spraying super-cooled micrometer-sized water droplets (63.7 μm). To balance the beam in the centrifuge, a counter-weight was used on the opposite side (Fig. 3.12 b and c). The glaze ice of ~ 1 cm thick was prepared over the area of ~ 5.1 $\times$ 3.2 cm^2. This ice geometry was found to be optimal to provide adhesive failure of the ice and well reproducible results during de-icing. The samples were placed in a wind tunnel at subzero temperature to accumulate glaze ice because the subzero tests need to be performed in a cold environment in order to study how ice grows on prepared coated surfaces. The wind tunnel used was adjusted thoroughly under conditions similar to those in nature leading to accretion of glaze ice during freezing rain. The effect of controllable wind tunnel parameters such as temperature, air speed and liquid water content were considered. The atmospheric icing wind tunnel used was based on room temperature water injection through warm nozzles

into a cold air stream provided by three nozzles on the spray line. Figure 3.13 shows the samples during ice accumulation in a wind tunnel. The distance between the nozzles and the samples was chosen to be long enough to reach thermodynamic equilibrium for all sprayed droplets in the wind tunnel [88-90]. After ice accumulation was completed, the samples were removed, weighed and kept in a climatic chamber at -10 °C. Ice mass and area were carefully evaluated both after icing and de-icing. The centrifuge test machine can increase rotation speed of the beam from 0 to 5500 rpm with an acceleration of approximately 300 rpm s^{-1}. Rotation generates a centrifugal force and when this force is larger than adhesion force of ice, the ice detaches from the sample. At the moment of detachment (detected with sensors embedded into the centrifuge wall), the adhesion strength of ice is assumed to be equal to the centrifugal force, $F = mr\omega^2$, where m is the ice mass in g, r is the beam radius in cm and ω is the rotational speed in rad s^{-1}. The corresponding shear stress was calculated as $\tau = F/A$, where A is the de-iced area in cm^2.

Fig.3. 12. (a) Sample covered with artificial glaze ice, (b) centrifuge adhesion test machine, and (c) sample with coating in centrifuge set-up measuring ice adhesion where (1) sample, (2) aluminum beam, (3) counter-weight.

It should be noted that all samples were placed in the tunnel for roughly about 8 to 15 min to be cooled down prior to each icing test. The time period needed to have about 4-6 g (up to ~ 1 cm thick) of ice on each sample was traced as well.

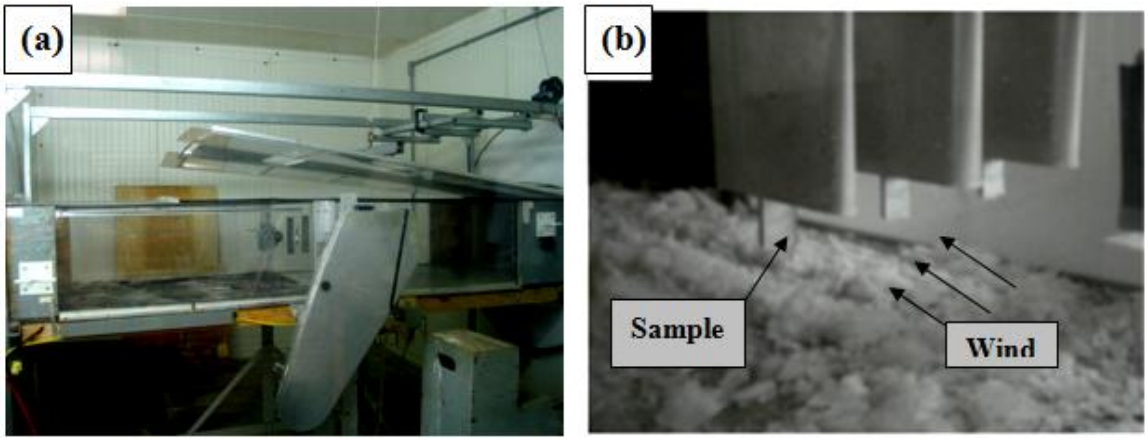

Fig.3. 13. Photo of (a) Atmospheric icing wind tunnel, and (b) ice accumulation on coated samples in wind tunnel.

3.8 Conclusion

In this chapter, different methods and techniques for preparation and characterization of homo- and HCs on aluminum alloy 6061 surfaces were presented in detail. The hydrophobic property and icephobicity of the prepared homo- and HCs samples were evaluated and measured via contact angle goniometer, sliding angle Groz instrument and centrifuge adhesion test machine, respectiveley. Meanwhile, the chemical composition of the prepared coatings was studied by XPS analysis. To study the morphology and topography of such prepared homo- and HCs, the SEM, AFM and profilometer techniques were used. Finally, the durability of the homo- and HCs was studied by using the QUV tester apparatus.

CHAPTER IV

HYDROPHOBIC PROPERTIES OF HOMO- AND HETEROGENEOUS *SAMS* COATING

4. Introduction

According to our research objectives, the first step in studying the heterogeneity effect is the preparation of homo- and HCs using the *SAM*s method. In this step, three different organic molecules, Trichloro(octadecyl)silane ($C_{18}H_{37}Cl_3Si$), Trichloro(octyl)silane ($C_8H_{17}Cl_3Si$) Trichloro (1H,1H,2H,2H-perfluorooctyl)silane ($C_8H_4Cl_3F_{13}Si$), abbreviated here as OD, OT and PF respectively, are applied. Our literature review showed that several parameters such as immersion time (IT) and Alkyl length and etc. could affect on the formation of *SAM*s coating. Here, the effects of immersion time and Alkyl length on the heterogeneous *SAM*s coatings were studied. The SEM, XPS and profilometry analyses are used to characterize the surface of such coatings.

4.1 Immersion time (IT) effect

A review of the literature indicates that by increasing the immersion time (IT), the efficiency of *SAMs* formation on a surface can be described in terms of order degree of self assemble monolayer and thus the surface coverage. Therefore, the IT parameter plays a very important role in the self-assembly process [91-93]. Figures 4.1 and 4.2 illustrate the contact angle (CA) and contact angle hysteresis (CAH) values of sample surfaces coated with a) OD-OD; b) PF-PF; c) PF-OD; and d) a mixed solution of PF (6mM)/OD (1mM). The procedures to prepare coatings were shown in detail in chapter 3. The homogeneous OD-OD and PF-PF coated samples were also prepared and used as a reference. Figure 4.1 demonstrates how increasing IT influences the wetting

characteristics of different prepared coatings. When the IT was increased from 2 to 12 hours, the CA values of all homo- and heterogeneous dip coated samples increased. More precisely, the contact angle values for homogeneous coatings of OD-OD and PF-PF after 12 hours of IT were ~ 140^{o} and ~ 120^{o}, respectively. However, a remarkable enhancement of contact angle values was observed for HCs of PF-OD and OD-PF, *i.e.* ~ 150 ^{o} and ~ 160^{o} respectively, after 12 hours. This corresponds to a super-hydrophobic characteristic. Thus, the observed results concerning the wetting properties of both homo- and HCs are probably due to well-ordered *SAM* fabrications on a well-immersed aluminum oxide layer [91-93, 95].

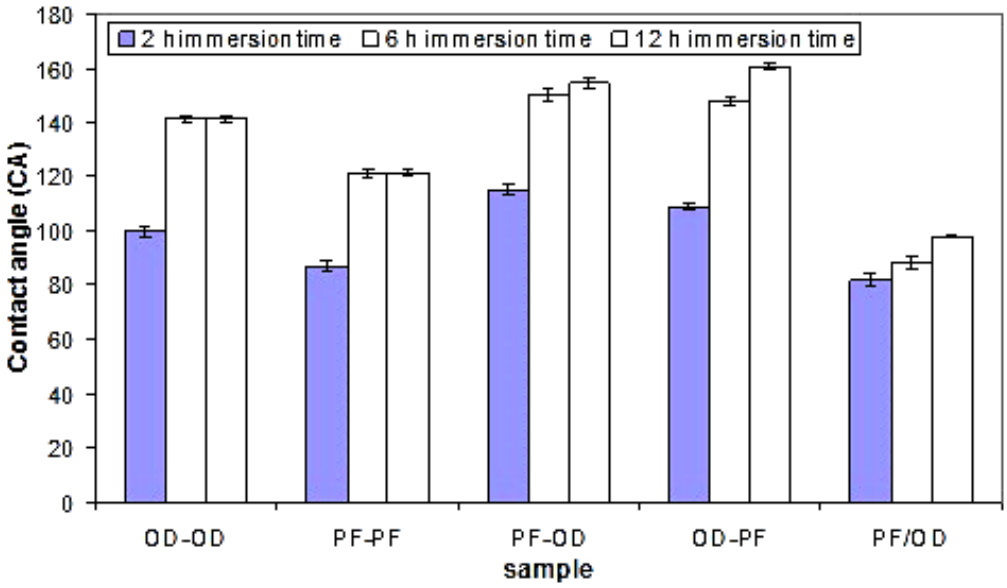

Fig.4. 1. CA values (deg.) of different prepared samples with 2, 6 and 12 h ITs.

Figure 4.2 presents the CAH values for homo- and HCs. We can see that the CAH values decreased when the IT increased from 2 to 12 hours. A significant decrease in CAH values was also obtained in the case of HCs coatings of PF-OD and OD-PF, as it was only ~ 7^{o} (after 12 h of IT), while the CAH values for homogeneous coatings were ~

40-70^{o} (for 2, 6 and 12 h). The CAH value of a homogeneous PF-PF sample after a 2h immersion time was larger than ~ 70^{o}. The super-hydrophobic coatings with very low wetting hysteresis (CAH) are considered to be truly icephobic coated samples [15]. It is also important to highlight the fact that the CAH value for a mixed solution of PF (6 mM) and OD (1mM), abbreviated here as PF/OD and immersed for 2 and 6h immersion was very large (CAH > 60^{o}). The results obtained from the mixed solution of OD/PF showed that the molecules of OD and PF do not probably order well on aluminum oxide layer surfaces. In other words, they were randomly distributed on the aluminum substrate [94]. For an in-depth study of prepared coatings that can suitably interpret the obtained results, we used other characterization techniques, including surface energy calculation and SEM, profilometry and XPS analyses of these coatings. This will be presented in the following sections.

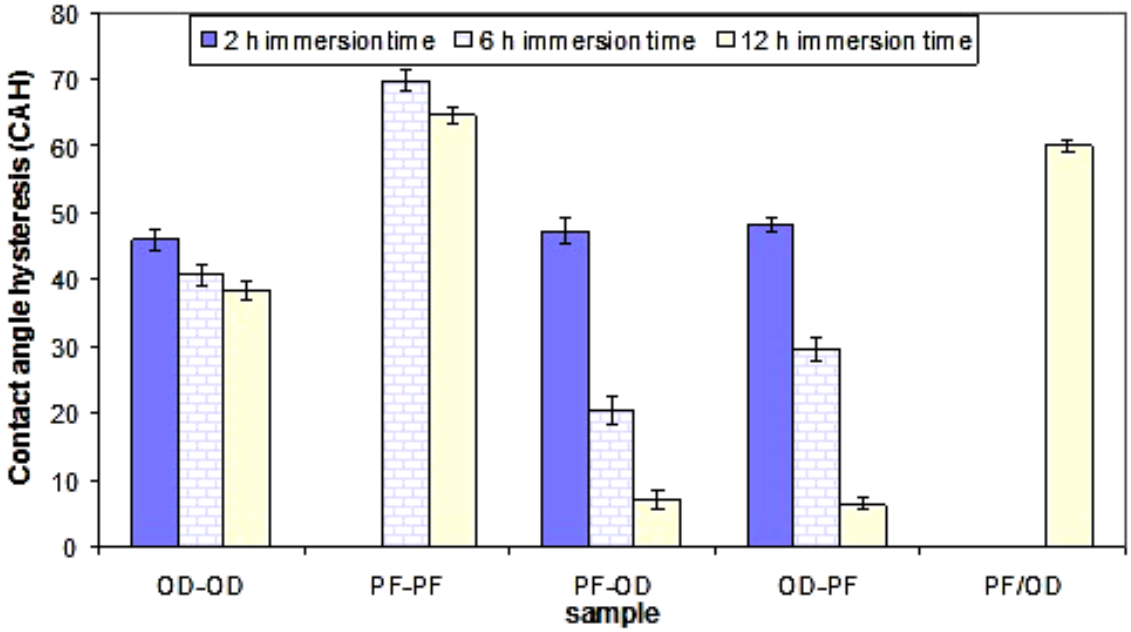

Fig.4. 2. CAH values (deg.) of different prepared samples with 2, 6 and 12 h ITs.

4.1.1 Surface energy calculation

Another important investigation technique for the hydrophobic properties of homo- and heterogeneous *SAM*s coatings is the determination of surface energy values. It is well known that when the surface energy is lowered, the water repellency is enhanced [94]. The surface energy of a solid surface is a characteristic relevant to surface chemistry, depending on its chemical composition and atomic arrangements near the surface [20]. Table 4.1 presents the surface energy values of prepared coatings obtained from contact angle measurements [20]. For the immersion times of 2, 6 and 12 hours, the table shows smaller values for the HCs than for homogeneous samples. Moreover, the smallest values were obtained for HCs coatings of OD-PF and PF-OD with 12 hours of immersion time, i.e. 0.04 ± 0.03 mNm^{-1} and 0.23 ± 0.05 mNm^{-1}, respectively. It can be concluded that by applying dissimilar functions of C-F and C-H on an aluminum surface, the wetting characteristics of samples were affected seriously as the surface energy values decreased. This is known as the heterogeneity effect.

Table 4. 1. Surface energy values (mNm^{-1}) of homo- and heterogeneous *SAM*s coatings.

Immersion time (IT) (h)	Sample	Surface energy (mNm^{-1})
2	OD-OD	15.6 ± 0.57
	PF-PF	21.10 ±0.51
	PF-OD	9.41±0.50
	OD-PF	6.63±0.42
	PF/OD	23.27±0.83
6	OD-OD	1.23±0.99
	PF-PF	4.32±0.88
	PF-OD	0.60±0.16
	OD-PF	0.74±0.28
	PF/OD	20.22±0.60
12	OD-OD	1.23±0.27
	PF-PF	4.36±0.29
	PF-OD	0.23±0.05
	OD-PF	0.04±0.03
	PF/OD	15.62±0.47

4.1.2 Scanning Electron Microscopy (SEM) analysis

Figures 4.3 to 4.5 show the scanning electron microscopy (SEM) images of samples coated with OD-OD, PF-PF and OD-PF (12 h immersion time) at 2000 and 11000 magnifications. These series of experiments were conducted to investigate surface morphology. The SEM images of coated surfaces show a rough structure at the micro-/nano-meter scale on a polished aluminum surface. This micro/nano scale roughness is obtained following sample immersion in chemical solutions where in the hydrolysis step of the *SAM*s configuration process, the chloride ions (Cl^-) are released to form hydrochloric acid (HCl), which in turn causes the erosion of the aluminum substrate spontaneously by increasing the immersion time. This reaction can be expressed by the following general scheme [95]:

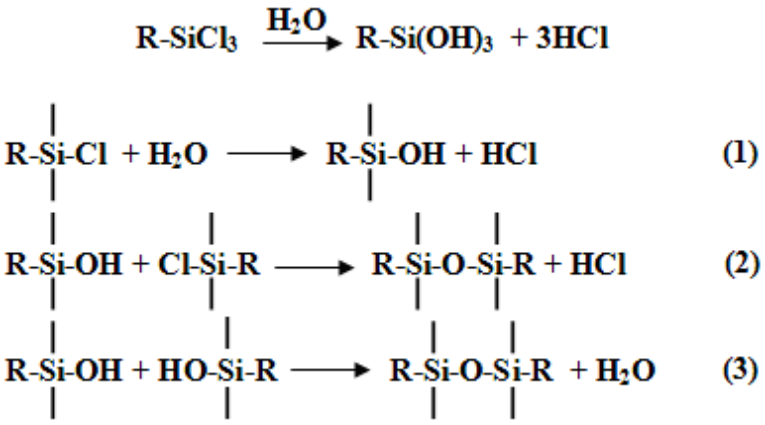

This hypothesis was furthermore confirmed by measuring the pH values of prepared PF and OD solutions, i.e. ~ 2 and ~ 3, respectively. This rough structure on a polished aluminum surface combined with the application of a low surface energy

material, as is the case for the OD-PF coating by 12 h of immersion, leads to superhydrophobicity. Therefore, using the HCs (e.g. OD-PF) is the main reason to switch surfaces from hydrophobic to super-hydrophobic ones. In section 4.1, it was shown that the increase of immersion time has an effect on the wetting properties of samples [91-93], as it causes the increase of contact angle and decrease of CAH values. Figure 4.5 confirms the presence of micro/nano-scale surface roughness which can effect on wetting properties after a 12 h IT, as the contact angle values go as high as ~ 160^{o} and the CAH values go as low as ~ 7^{o}. In other words, based on these new results, it is therefore possible to conclude that by increasing the immersion time the surface roughness as well as the effect of heterogeneity were increased; this resulted in higher values of contact angle and lower values of CAH, characteristic of superhydrophobicity.

As it is evident in this series of SEM images, the surface topography of both OD-OD and OD-PF samples are similar. This can be attributed to the dominant effect of an OD self-assembled layer on surface asperities and topography in the heterogeneous OD-PF coating, as this layer exists in both homo- and HCs.

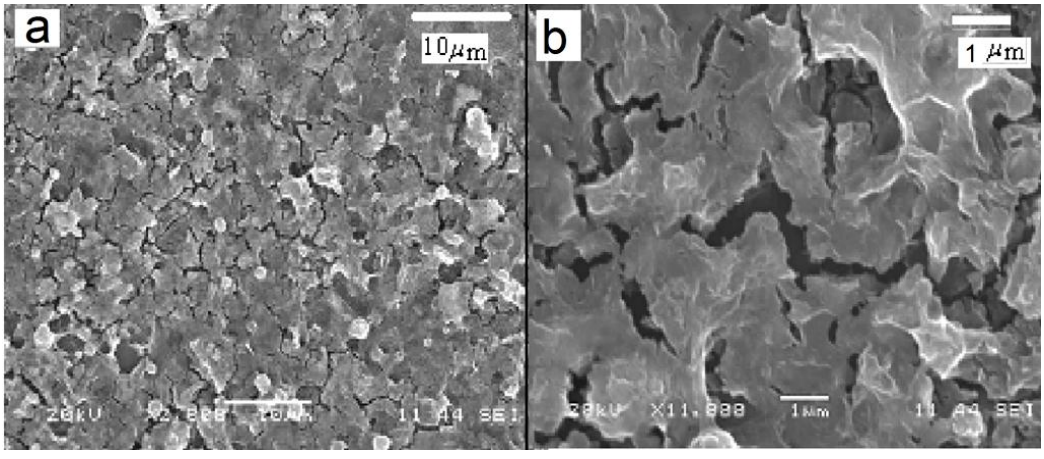

Fig.4. 3. Scanning electron microscopy (SEM) images of sample coated with OD-OD (12 h). Magnification is (a) 2,000 and (b) 11,000.

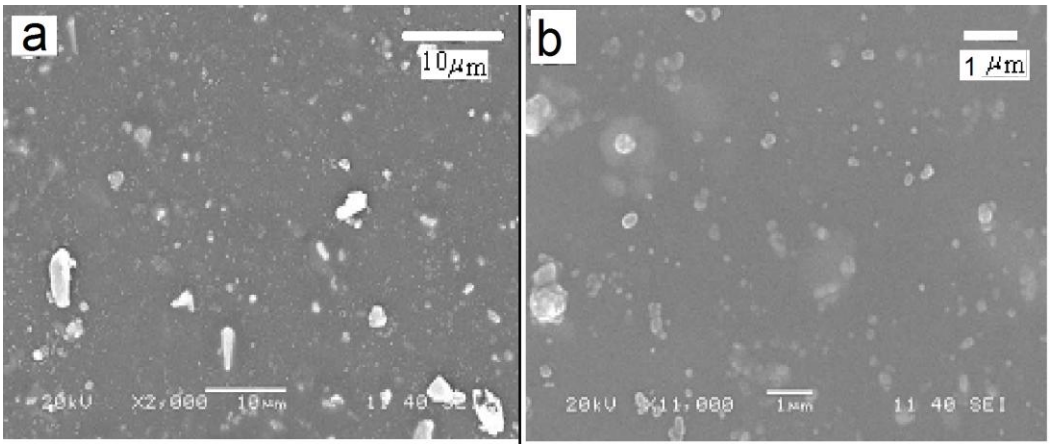

Fig.4. 4. Scanning electron microscopy (SEM) images of sample coated with PF-PF (12 h). Magnification is (a) 2,000 and (b) 11,000.

Figures 4.3 and 4.5 show that the SEM image of an OD-OD sample has the similar rough structure as an OD-PF sample. However, on OD-OD coating it does not result in higher values of contact angle and lower values of CAH compared to an OD-PF sample. This observation is another proof of the heterogeneity effect on heterogeneous samples.

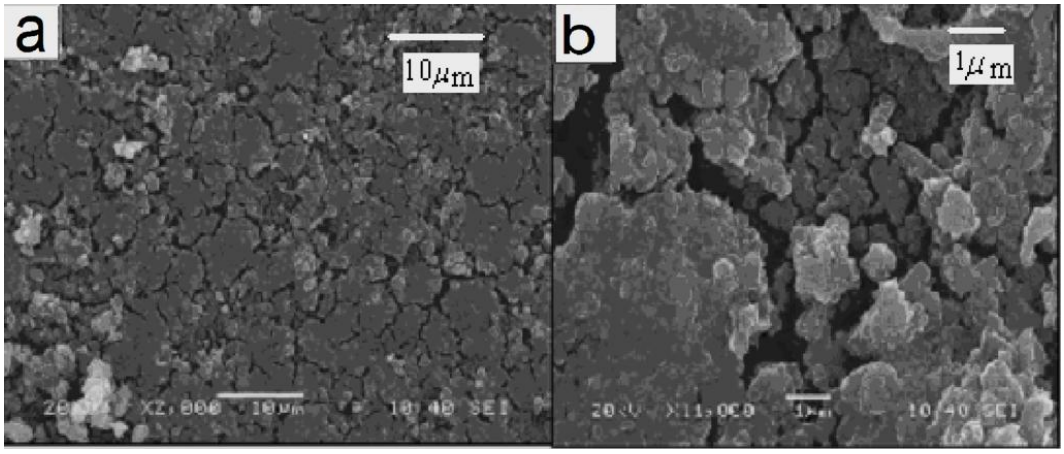

Fig.4. 5. Scanning electron microscopy (SEM) images of sample coated with OD-PF (12 h). Magnification is (a) 2,000 and (b) 11,000.

4.1.3 Profilometry analysis

The SEM analysis results obtained in previous sections can be validated by various surface roughness values obtained for these homo- and heterogeneous *SAM*s samples which were measured using root-mean-square roughness (Sq) values. These Sq values of prepared *SAM*s coatings on aluminum surfaces were measured by profilometry analysis. Figure 4.6 illustrates the surface roughness values (Sq) of different treated surfaces. As it is evident in this figure, the maximum value of Sq corresponds to the homogeneous OD-OD coated Al sample. In contrast, the HCs have smaller values of surface roughness (Sq). It should be noted that while more rough structure can be observed on homogeneous OD-OD coating compared to HCs (OD-PF and PF-OD), nevertheless higher contact angle value was observed in the case of HCs. These observations, thus, affirm again the effect of heterogeneity of coatings on wetting properties.

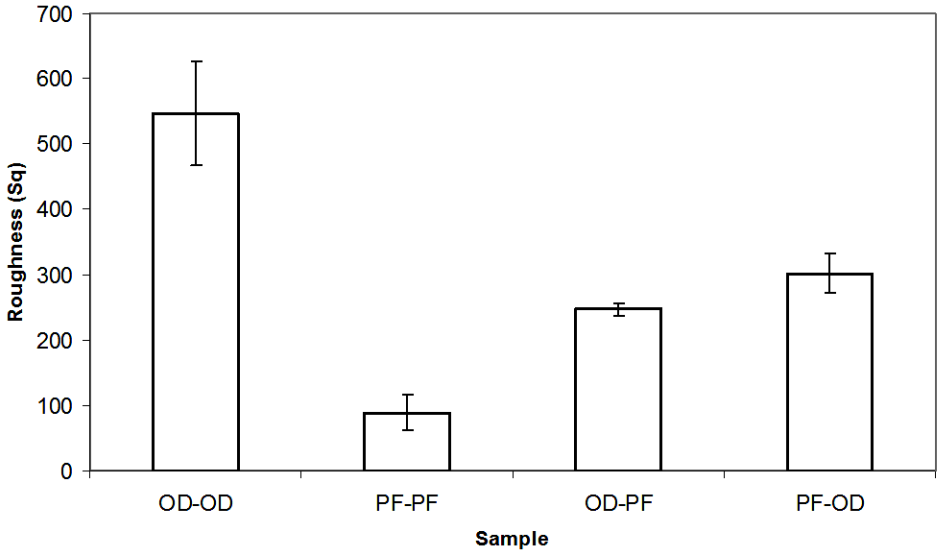

Fig.4. 6. Surface roughness (root-mean square) (nm) of prepared *SAM*s coatings.

4.1.4 X-ray photoelectron spectroscopy (XPS) analysis

The surface chemical composition of prepared coatings was examined via X-ray photoelectron spectroscopy (XPS). Figure 4.7 illustrates XPS analysis results of samples immersed in the OD-OD, PF-PF and PF-OD solution for 12 hours. As it is obvious from XPS spectra in Figure 4.7 (a), the high-binding-energy peak at ~ 284 (eV) indicates the existence of C-H/C-C bonds with high concentration, implying the presence of a homogeneous coating of OD molecules on polished aluminum substrates.

The peak at ~ 281 (eV) corresponds to C–Si bond. Figure 4.7 (b) shows the observed peaks at ~ 290, ~ 291 and ~ 293 (eV) corresponding to the CHF, CF_2 and CF_3 groups, respectively, which confirm the presence of PF molecules on polished aluminum substrates. Figure 4.7 (c) presents the peaks of XPS analysis of coated OD-OD and PF-PF samples. This observation confirms the presence of OD and PF on HC coating. Meanwhile, these XPS results show that the aluminum surfaces were covered with alkylsilane (OD) or fluoroalkylsilane (PF) molecules.

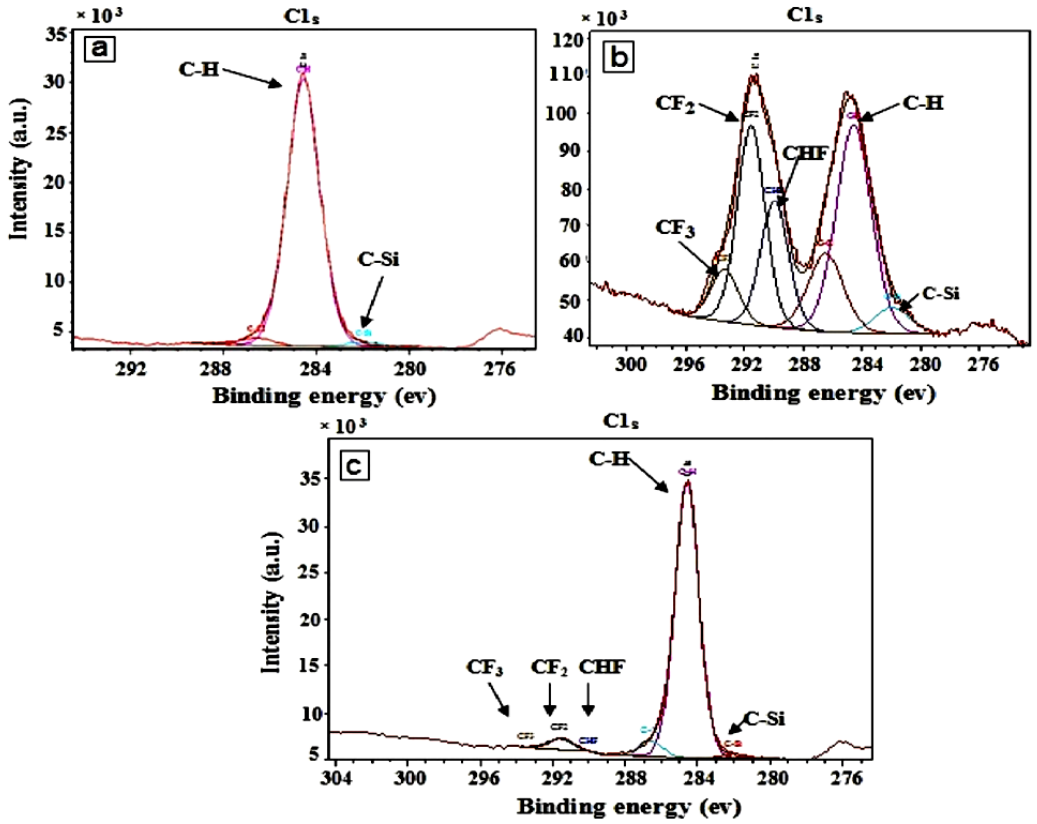

Fig.4. 7. XPS high resolution spectra of Al samples coated with OD-OD (a), PF-PF (b) and OD-PF (c), after 12 h ITs.

4.2 *SAM*s coatings on glass substrate

To better understand the observed results and establish the effect of heterogeneity, another set of experiments, including the replacement of an Al sample by a glass substrate, was conducted to avoid any possible effect of surface roughening. Since the glass substrate does not react with hydrochloric acid (HCl). Figure 4.8 shows contact angle and CAH values of different coated glass samples for 12 h IT. The contact angle values of homogeneous coatings of OD-OD and PF-PF on glass substrate were ~ 106 ^{o}

and ~ 108 ^{o}, respectively. However, for HCs coatings of PF-OD and OD-PF on a glass substrate the values were ~ 115 ^{o} and ~ 114 ^{o}, respectively. As it is clear, a low variation of CA values was found on this series of samples compared to those observed on aluminum surfaces which are probably due to created surface roughness on aluminum surfaces. However, the most important consequence of the heterogeneity effect is the low contact angle hysteresis values [26]. Indeed, the CAH of homogeneous coatings of OD-OD and PF-PF on a glass substrate were ~ 45 ^{o} and ~ 50 ^{o}, respectively. However, for HCs coatings of PF-OD and OD-PF, the CAH values were ~ 22 ^{o} and ~ 17 ^{o}, respectively.

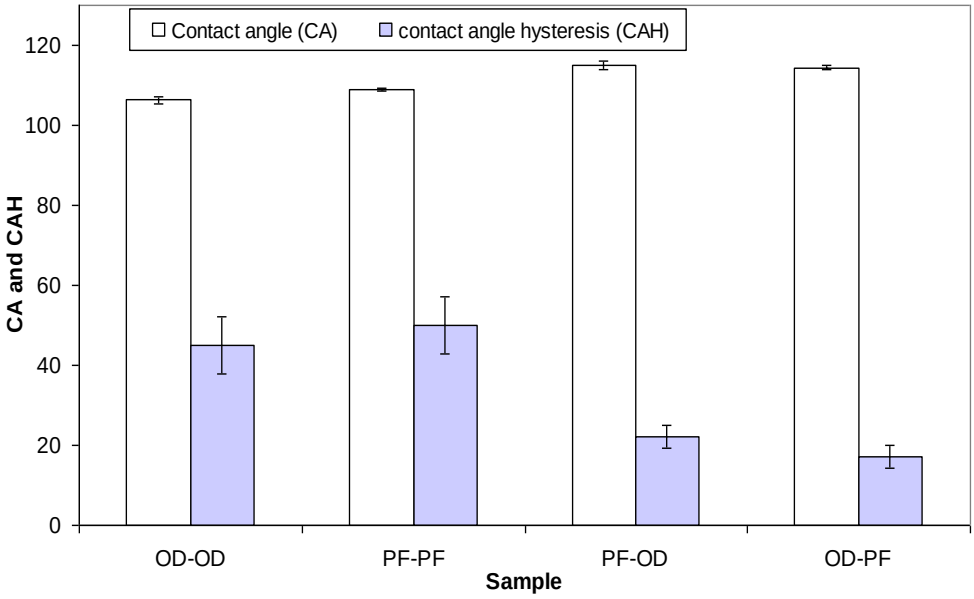

Fig.4. 8. CA and CAH values (deg.) of different glass coated substrates for 12 h ITs.

4.3 Alkyl length effect

To study and better understand the effect of chain length on the wetting characteristic, dissimilar alkylsilanes in terms of chain length have been selected.

Therefore, trichloro (octyl) silane, OT (8 carbon atoms) with a similar chemical component to trichloro (octadecyl) silane, OD (18) and a similar alkyl length of trichloro (1H,1H, 2H, 2H-perfluorooctyl) silane, PF was used.

4.3.1 Immersion time effect

Figures 4.9 and 4.10 illustrate the contact angle and CAH values of surfaces coated with OT-OT, PF-PF, PF-OT; and OT-PF. The concentration of OT in this series of experiments was 1mM OT diluted in toluene. The coating preparation procedures were explained in details in chapter 3. By increasing the immersion time from 6 h to 12 h, the contact angle values of all coated aluminum surfaces were increased. However, CAH values did not change significantly (see Fig. 4.10). In addition, by increasing the IT to 12 hours, the CA values of homo- and HCs prepared from OT are not as large as those of coatings prepared from OD. It is indeed important to mention that when mixed solutions of PF (6 mM) and OT (1 mM) were prepared for both 6 and 12h immersion times, the contact angle and CAH values were $<90^{o}$ and $>60^{o}$, respectively. The CAH values are also not as low as those of the coated samples prepared from OD related to the super-hydrophobic characteristic. This behavior could be explained by the reduction of the molecular reactivity caused by the *steric effect* on a polished Al surface [96]. In chemistry, the *steric effect* has an influence on a reaction's course or rate determined by the fact that all of the atoms within a molecule occupy space, thus certain collision paths are either disfavored or favored, when atoms are brought close [97]. In general, the *steric effect* is classified into several types, namely, steric hindrance, steric shielding, steric

attraction and steric repulsion [98-101]. Among these types, steric attraction was the one present in the self assembly process of OT molecules [100].

Steric attraction occurs when molecules have shapes or geometries that are optimized for interaction with other molecules. In this case, molecules will react with each other most often in specific arrangements and then the contact angle values of homo- and HCs prepared from OT are not as large as those of coatings prepared from OD [100].

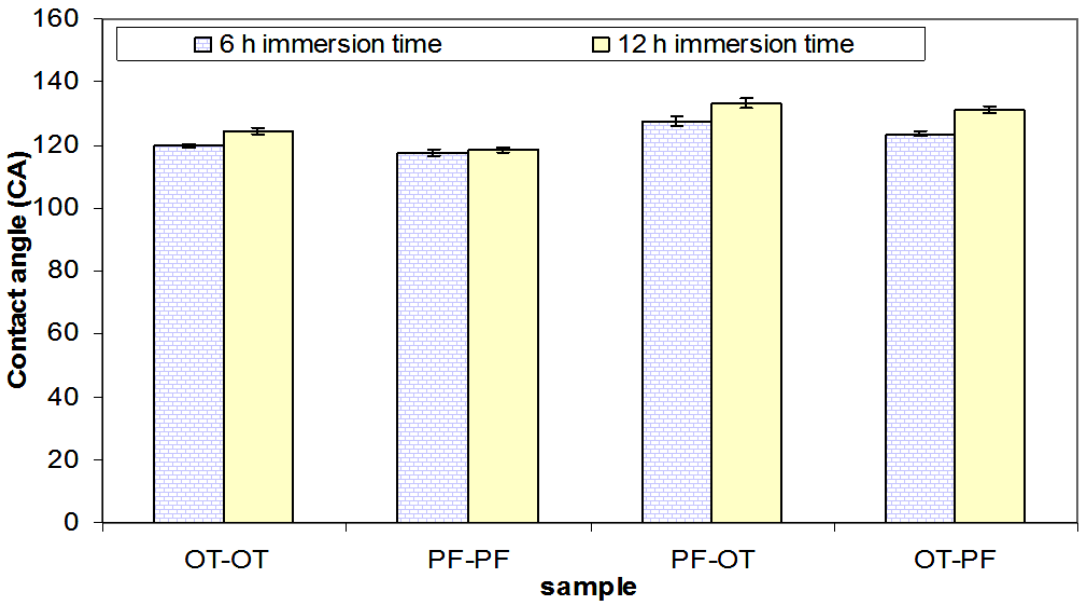

Fig.4. 9. CA values (deg.) of different coated samples with OT (1 mM) for 6 and 12 h ITs.

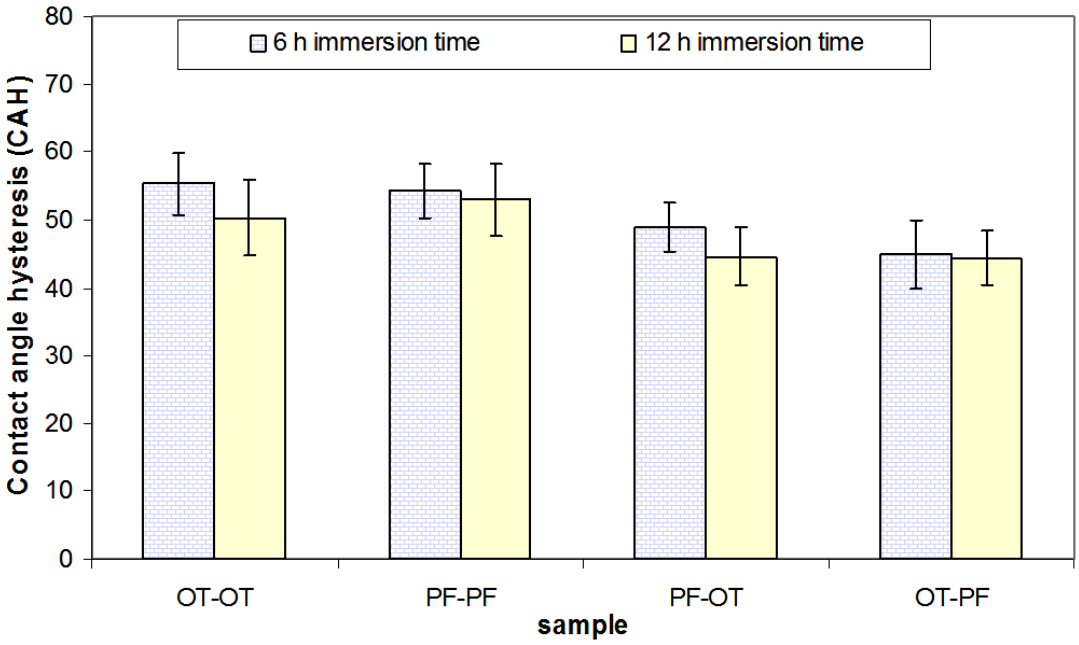

Fig.4. 10. CAH values (deg.) of different coated samples with OT (1 mM) for 6 and 12 h ITs.

To trace any possible effect of solution concentration on surface wettability, the contact angle and CAH of coated samples with 6 mM OT instead of 1mM OT and in the same condition as PF (6 mM) were measured and evaluated as well. As it is clear in Figures 4.11 and 4.12, by increasing the immersion time from 6 h to 12 h, the contact angle values of all aluminum surfaces coated with OT-OT, PF-PF, PF-OT and OT-PF were increased. However, CAH values did not change considerably. For ITs of both 6 and 12 hours, the CA values obtained from either homo- or HCs prepared from 6mM OT were smaller than those obtained from 1mM OT concentration. This observation is probably due to the *steric effect* which in this case prevents the well-ordering of *SAM*s molecular structures on the aluminum oxide layer (see Figs. 4.11 and 4.12) [96]. In other words, the shorter length of an alkyl chain can influence the formation of a network

structure of Si-O-Si instead of a well-ordering of *SAM*s molecular structures on the aluminum oxide layer [96]. To better understand the results obtained from wetting analysis, the scanning electron microscopy (SEM) analysis of homo- and HCs was conducted and the results will be presented in the following sections.

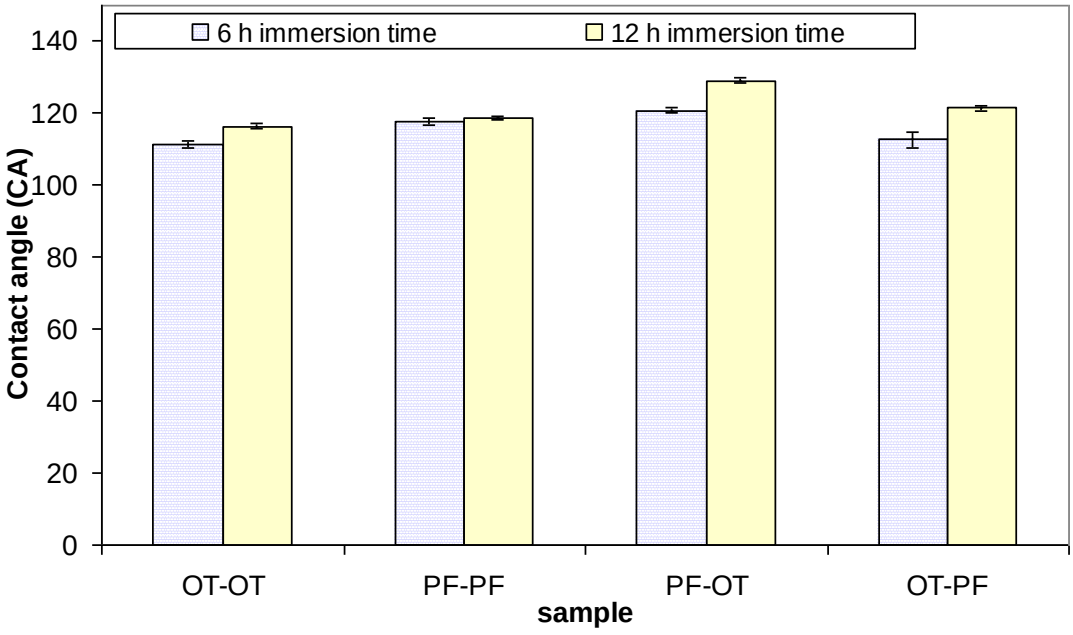

Fig.4. 11. CA values (deg.) of different coated samples with OT (6 mM) for 6 and 12 h ITs.

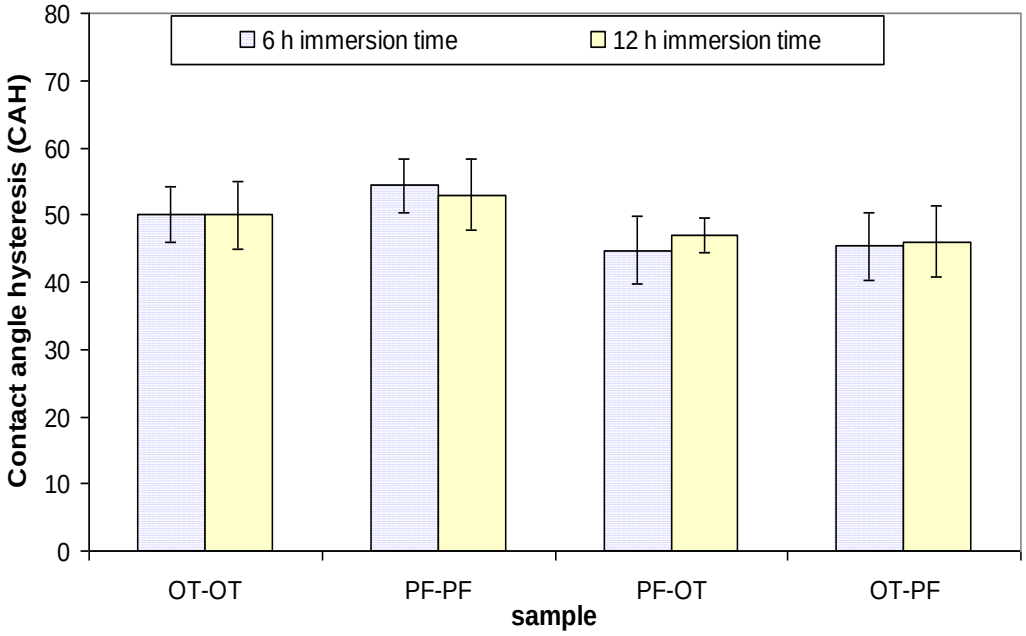

Fig.4. 12. CAH values (deg.) of different coated samples with OT (6 mM) for 6 and 12 h ITs.

4.3.2 Scanning Electron Microscopy (SEM)

The surface morphology of samples coated with OT-OT (1 mM) and PF-OT (12 h ITs) at 2000 and 11000 magnifications can be observed in Figure 4.13 (a) and (b). The SEM images of these series of experiments showed morphology different from that of the experiments prepared with OD. The SEM images of an OT-OT coated surface show the presence of white points at the micrometer scale on the surface, as can be observed in Figure 4.13 (a) and (b). Figure 4.13 (c) illustrates a chemical analysis of the coated surface of OT-OT (8) obtained from energy-dispersive x-ray spectroscopy (EDS) analysis. This series of experiments were conducted to investigate in more details surface morphology and chemical composition of coated surfaces in more details and to find

reasonable explanations for the results obtained. The peaks of Fe, Mn and aluminum refer to the second-phase particles and the aluminum matrix, and the peaks of C and Si are related to alkylsilane molecules coated on aluminum substrates. Since in Al alloys exist other metal additives to improve the strength of the material, these metal additives precipitate during the solidification processes and create second-phase particles in the aluminum matrix.

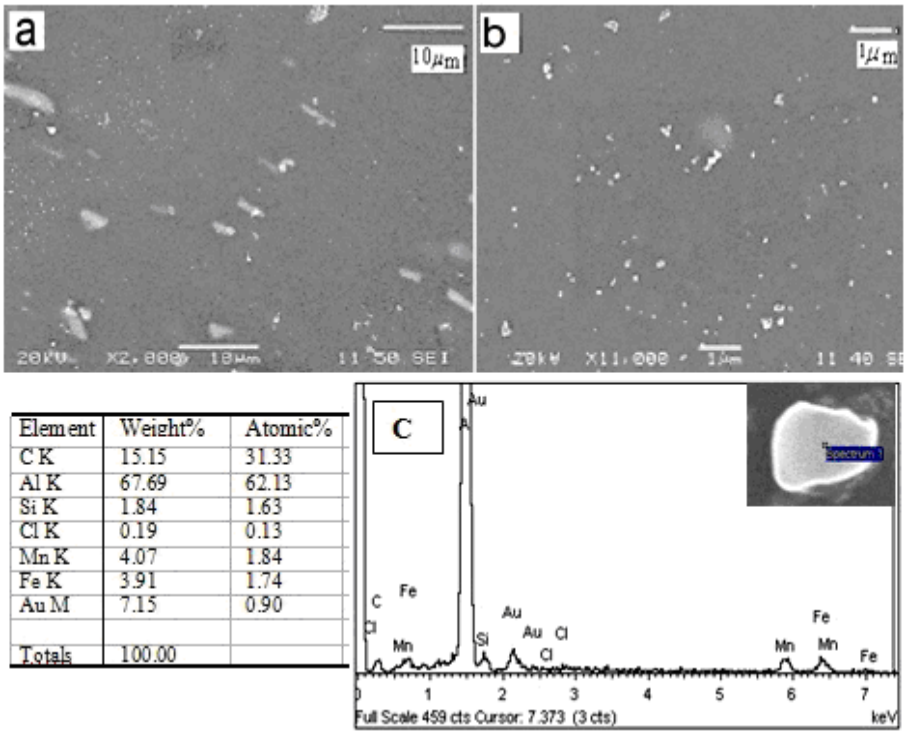

Element	Weight%	Atomic%
C K	15.15	31.33
Al K	67.69	62.13
Si K	1.84	1.63
Cl K	0.19	0.13
Mn K	4.07	1.84
Fe K	3.91	1.74
Au M	7.15	0.90
Totals	100.00	

Fig.4. 13. Scanning electron microscopy (SEM) images of sample coated with OT-OT (1mM) (12 h). Magnification is (a) 2,000 and (b) 11,000. (c) EDS spectrum of Al sample coated with OT-OT(12 h).

This couple, composed of the aluminum matrix and second-phase particles, inevitably leads to increased un-sustainability to electrochemical (or galvanic) corrosion of such alloys, especially of those in close contact with water. Figure 4.14 shows SEM images of a PF-OT heterogeneous coated sample (12 h) at 2000 and 11000

magnifications. The SEM images of a surface coated with PF-OT reveal the propagated branches of organic *SAMs* in several areas. Figure 4.15 shows SEM images of an OT-OT dip coated sample in a solution of OT with a concentration of 6 mM. Compare this to figure 4.13; it is obvious that a sample coated with OT-OT (1mM) has more propagated branches of organic *SAM*s in several areas while increasing the concentration from 1mM to 6mM. It could be due to the increase of the *steric effect* on an aluminum surface by growing more branches up while increasing the OT concentration from 1 mM to 6 mM.

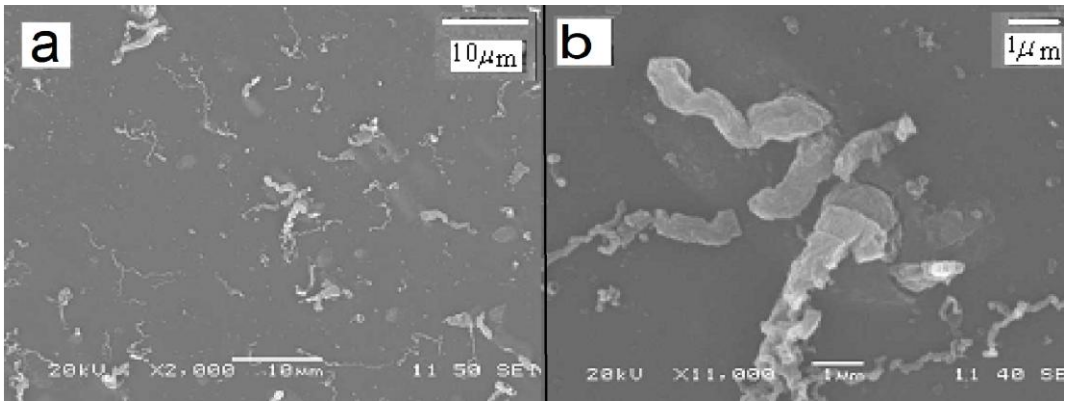

Fig.4. 14. Scanning electron microscopy (SEM) images of sample coated with PF-OT(1mM) (12 h). Magnification is (a) 2,000 and (b) 11,000.

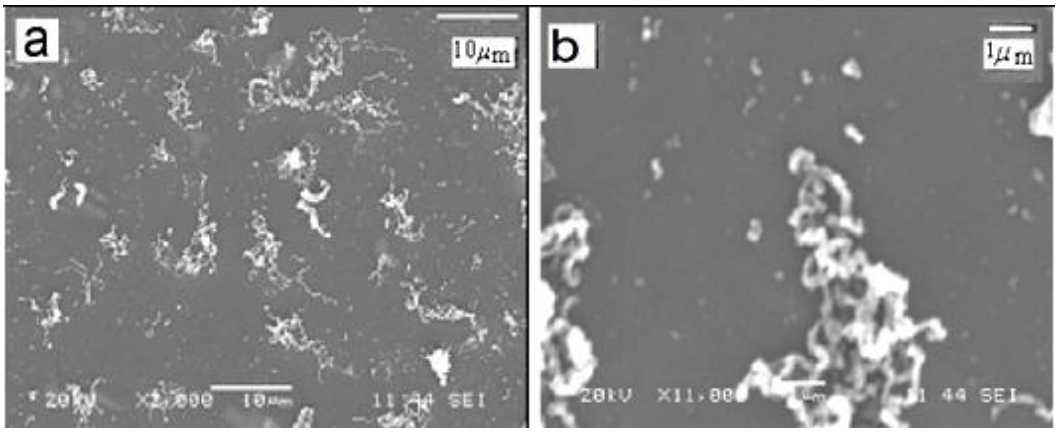

Fig.4. 15. Scanning electron microscopy (SEM) images of sample coated with OT-OT (6mM) (12 h). Magnification is (a) 2,000 and (b) 11,000.

This can act as a factor preventing the well-ordering of *SAM*s molecules on an aluminum oxide layer that consequently leads to the decrease of the contact angle value [96].

4.4 Heterogeneity effect on the interaction energy between coating and water molecules

To better understand and define the heterogeneity effect resulting from dissimilar functions on a coated aluminum surface, the interaction energy between *SAM*s coatings and water molecules was calculated theoretically. To this end, the sliding angle of each coated sample was measured to calculate the interaction energy [25,26,102,103]. A variety of models shows the relation between the sliding angle and the relevant forces [102-110]. All the models discussed in the literature are based on two assumptions. One of them is adhesion of the liquid drop to the solid surface because of the forces developed along the periphery of the liquid drop which is in contact with the solid surface. The other one is the adhesion of a liquid drop to a solid which is the result of intermolecular forces at the interfacial area. The adhesion of the liquid drop to the solid is the result of the forces acting at the contact periphery between the drop and the solid. In this study, the interaction energy was evaluated across the contact periphery between the drop and the solid. Before calculating the interaction energy it is necessary to know some correlations and equations. The radius R that a liquid drop makes with a surface can be calculated from its density ρ, mass m and the contact angle θ of the liquid with the solid (Fig. 4.16). Assuming that the drop is a perfect sphere, the radius of the drop, R, can be expressed according to equation (4.1):

$$R = \left(\frac{3m}{\rho\left(2 - 3\cos\theta + \cos^3\theta\right)} \right)^{1/3} \qquad \textbf{(4.1)}$$

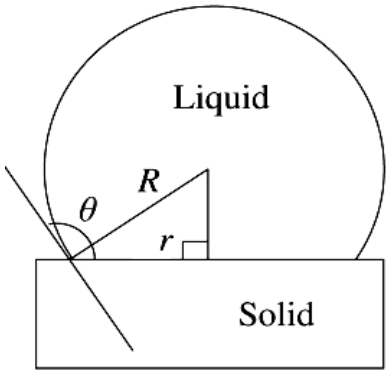

Fig.4. 16. Schematic representation of a water drop on a solid surface.

The radius *r*, of the contact area between the drop and the solid, is given by equation (4.2):

$$r = R\sin\theta \qquad \textbf{(4.2)}$$

Equations (4.1) and (4.2) are valid for hydrophobic surfaces ($\theta > 90^{\circ}$) as in Figure 4.16, as well as for hydrophilic surfaces ($\theta < 90^{\circ}$). When the horizontal plane is tilted, the contact area is assumed to remain circular with a radius *r*, though tilting deforms the drop. At a certain sliding angle the drop is detached from the surface and slides. Equations (4.1) and (4.2) assume that there are no moments and rotational forces acting on the drop, as is shown in Figure (4.17). The driving force for the drop sliding is the gravitational force ($mg \sin \alpha$) and the adhesion force opposing this movement is F_A. At the beginning of

drop motion, the forces acting on the drop will be equilibrium as described by equation (4.3):

$$F_A = mg\sin\alpha \tag{4.3}$$

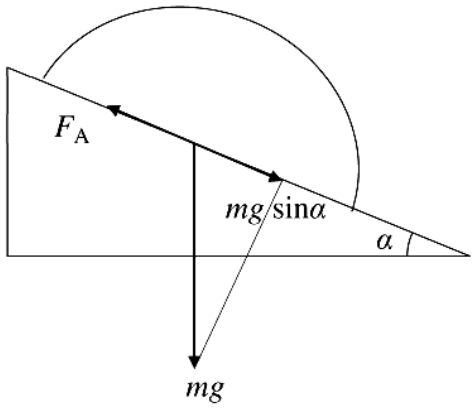

Fig.4. 17. Schematic representation of a water drop on a tilted solid surface.

The adhesion of the liquid drop to the solid is the result of the forces acting at the contact periphery between the drop and the solid [25,26,104,105] as given by equation (4.4):

$$F_A = K_A 2\pi r \tag{4.4}$$

where K_A is a constant with units of surface tension (N/m) or surface energy (J/m^2). K_A represents the energy of adhesion between the two phases. Combining equations (4.3) and (4.4) the equation (5) is obtained [111]:

$$\sin\alpha = \frac{K_A 2\pi r}{mg} \tag{4.5}$$

In addition, substituting r in equation (4.5) from equations (4.1) and (4.2) the following expression is obtained:

$$\sin\alpha = \frac{K_A 2\pi}{g}\left[\frac{3}{\rho\pi\left(2-3\cos\theta+\cos^3\theta\right)}\right]^{1/3} \sin\ \theta m^{\frac{-2}{3}} \tag{4.6}$$

Therefore, for a given liquid and solid (i.e., ρ and θ are constant) sin α depends on the mass of the drop to the −2/3 power. K_A is the interaction energy (invariant for a given surface chemistry) and is expressed by equation (4.7), [102]:

$$K_A = \left[\rho\left(\frac{2-3\cos\theta+\cos^3\theta}{3}\right)\right]^{1/3} \frac{g}{2}\left(\frac{m}{\pi}\right)^{2/3} \frac{\sin\alpha}{\sin\theta} \tag{4.7}$$

For a surface with rough structure the interaction energy between water and the substrate is comparable to the true contact area, which is bf times as large as the apparent contact area. Therefore, the interaction energy k is assumed to be bf times greater than the flat surface [103].

$$K = \frac{g\sin\alpha(r\cos\theta+1)}{2b\sin\theta'(\cos\theta'+1)}\left\{\frac{m^2\rho(2-3\cos\theta'+\cos\theta'^3)}{3\pi^2}\right\}^{1/3} \tag{4.8}$$

where θ' is the equilibrium contact angle on a rough and surface, θ is the equilibrium contact angle on a flat surface and m is a mass of the droplet. Therefore, to calculate the interaction energy of heterogeneous OD-PF and PF-OD coatings with super-hydrophobic properties, equation (4.8) was used. Table 4.2 presents the calculated values of interaction energy for the heterogeneous OD-PF and PF-OD coatings.

Table 4. 2. The values of interaction energy between a water droplet and HC.

Sample	α (deg.)	θ' (deg.)	θ (deg.)	m (mg)	K (mJ/m^2)
OD-PF	1	160.6	114.3	15	3.118
PF-OD	4	154.3	115.1	15	3.113

Similarly, equation (4.7) was applied to calculate the interaction energy of homogeneous OD-OD and PF-PF coatings. Table 4.3 presents the calculated values of interaction energy for the homogeneous OD-OD and PF-PF coatings.

Table 4. 3. The values of interaction energy value between a water droplet and homogeneous coating.

Sample	α (deg.)	θ (deg.)	m (mg)	K (mJ/m^2)
OD-OD	34	123.6	30	15.891
PF-PF	46	106.3	30	16.522

As is obvious in tables 4.2 and 4.3, the interaction energy (K) between a water droplet and HCs is smaller than what was obtained between a water droplet and homogeneous coatings. In other words, when the interaction energy between water droplet and the coating shifts to smaller value, the sliding angle decreases. Consequently,

the water droplet rolls off more easily on that coated sample. So, this heterogeneity effect results in an improved hydrophobicity of those coatings.

Table 4.4 presents the calculated values of interaction energy for the homo- and HCs of different coated samples with OT (1 mM) and PF (6 mM) for 12 hours ITs. As is shown in table 4.4, the interaction energy (*K*) between a water droplet and HCs is smaller than what was obtained between a water droplet and homogeneous coatings. However, in the case of HCs the interaction energy values are also not as low as those of the coated samples prepared from OD related to the super-hydrophobic characteristic. As mentioned before, this behavior highlights the increase of the *steric effect* that prevents well-ordering of *SAM*s molecules on Al substrates [96].

Table 4. 4. The values of interaction energy value between a water droplet and different coated sample.

Sample	α (deg.)	θ (deg.)	m (mg)	K (mJ/m^2)
OT-OT	58	101.1	30	18.472
PF-PF	46	106.3	30	16.522
OT-PF	44	95.2	30	14.307
PF-OT	42	97.6	30	14.092

4.5 Conclusion

Self-assembled mono-/multi-layers (*SAM*s) of three chemically different alkylsilane compounds, i.e. OD (octadecyltrichlorosilane); OT (trichloro(octyl)silane) and PF (1H,1H,2H,2H-perfluorooctyltrichlorosilane) were fabricated on flat aluminum alloy (AA6061) surfaces as homo- and HCs. The wetting behavior of all coated samples

at room temperature after increasing immersion time from 2 to 12 hours showed improved hydrophobic properties, especially in the case of HCs. The surface energy values, SEM/EDS and profilometry confirmed the heterogeneity effect that came from dissimilar functions on coatings. The XPS results of homo- and HCs showed that aluminum surfaces were covered with OD or PF molecules and that in the case of HCs; they were covered by both OD and PF molecules. To further study and analyze the effect of heterogeneity, the glass substrates replaced aluminum samples to avoid any possible effect of surface roughening. This series of glass-substrate coating experiments moreover proved the heterogeneity effect. To study the effect of chain length on coating performance, the same alkyl chain length of PF was selected that was named here as OT. However, it was shown that after 12 h of immersion time, the contact angle values of prepared samples from OT thin layer were not as high as what was obtained from the OD coating. This behavior originates from a decrease in the reactivity caused by the *steric effect* on a polished aluminum surface. By applying the theoretical calculations, the obtained results demonstrated that the interaction energy values decreased when the aluminum substrates were coated with HCs. Accordingly, with all the empirical and theoretical efforts conducted so far, it is possible to definitely conclude that there is a heterogeneity effect on an aluminum surface that uses different functions (HCs).

CHAPTER V

HYDROPHOBIC PROPERTIES OF HOMO- AND HETEROGENEOUS NANOPARTICLESCOATINGS

5. Preparation of HC nanoparticles coatings

5.1Hydrophobic properties of homo- and heterogeneous nanoparticles coatings

5.2 Atomic force microscopy (AFM) analysis

5.3 Effect of type of nanoparticle

5.3.1 CA and CAH measurements

5.3.2 Optical profilometry analysis

5.4 Effect of nanoparticle sizes

5.4.1 CA and CAH measurements

5.4.2 Optical profilometry analysis

5.5 Effect of type of polymers

5.5.1 CA measurements

5.5.2 CAH measurements

5.6 Surface energy

5.7 Scanning electron microscopy (SEM)

5.8 Heterogeneity effect on the interaction energy between coating and water molecules

5.9 Conclusions

5. Introduction

According to our research objectives, the first step in preparing homogeneous and HCs on aluminum alloy substrates was the deposition of self assembled monolayers (*SAM*s) on Al surfaces. Experimental work and theoretical calculations have indeed demonstrated the presence of the heterogeneity effect on an aluminum surface by applying different hydrophobic functions (C-H and C-F). In the following steps, chemically homogeneous and HC nanoparticles coatings of low surface-energy materials on aluminum surface will be studied in more detail. More precisely, different chemical materials such as Polyethylene (PE), Polystyrene (PS), polymethylmethacrylate (PMMA), stearic acid (STA), polytetrafluoroethylene (PTFE), aluminum oxide (Al_2O_3) and zinc oxide (ZnO) were used to prepare the abovementioned coatings. To study the heterogeneity effect in this method, two different approaches are selected. First, homogeneous coatings with similar functions including hydrocarbons or fluorocarbons such as PE, PS, PMMA, STA and PTFE are prepared. HCs with dissimilar functions comprising hydrocarbons and fluorocarbons, *e.g.* PE-PTFE, PS-PTFE, PMMA-PTFE and STA-PTFE are fabricated on aluminum surfaces to study the heterogeneity effect. Moreover, HCs made of hydrophobic and hydrophilic functions (namely PE-ZnO and PE-Al_2O_3) are prepared. These coatings are prepared to better understand the heterogeneity effect, comparing them with heterogeneous PE-PTFE coatings with different hydrophobic functions. For this purpose, the 100 nm-ZnO nanoparticles as well as the 200 nm Al_2O_3 ones (similar in size to the PTFE ones) were used.

5.1 Hydrophobic properties of homo- and heterogeneous nanoparticles coatings

As indicated above, we started by preparing hydrophobic homogeneous coatings with similar functions as well as hydrophobic HCs with dissimilar functions. The homogeneous coatings of PE-spin, PTFE-spin and PTFE-immersion and the HCs of PE+PTFE and PE-PTFE were prepared. The preparation of homogeneous and HCs on an Al surface is described in chapter 3. Figure 5.1 shows the contact angle and CAH for the above-mentioned coatings.

For the homogeneous coatings PE-spin, PTFE-spin and PTFE-immersion on a polished aluminum surface, the contact angle values were ~ 100^{o}, ~ 98^{o} and ~ 133^{o}, respectively. The significant contact angle difference between PTFE-immersion and the two others could be due to surface roughening (see section 5.2 and table 5.1 below). In addition, the large standard deviation displayed by the error bar in Figure 5.1 for PTFE-immersion indicates a non-uniform coating which resulted from the irregular accumulation of PTFE nanoparticles on an aluminum surface.

A significant enhancement of contact angle values (~ 134^{o}) was observed for the HC of PE-PTFE. In the case of HCs, the presence of PTFE nanoparticles on a PE-coated aluminum surface resulted in surface roughening. Therefore, to concentrate only on the heterogeneity effect and to avoid the surface roughening, the PE+PTFE coating on aluminum sample was also prepared. More precisely, the PE+PTFE sample was prepared from the deposition of a mixture of PE and PTFE nanoparticles on an aluminum surface. This sample was only prepared to investigate the effect of the surface roughening and heterogeneity effect. As shown in Figure 5.1, the existence of surface roughening in case

of PE+PTFE coated aluminum sample resulted in a larger contact angle value of ~ 129^{o} compared to homogeneous coatings. This observation is due to surface roughening. However, the CA value of PE-PTFE (~ 134^{o}) was greater than that of PE+PTFE (~ 129^{o}). This may be due to the heterogeneity effect. Moreover, the CAH values are smaller for PE-PTFE (~ 32^{o}) than for homogeneous PE-spin and PTFE-immersion coatings and even the PE+PTFE sample (~ 64^{o}). Therefore, a small value of CAH is the most important factor in the heterogeneity effect.

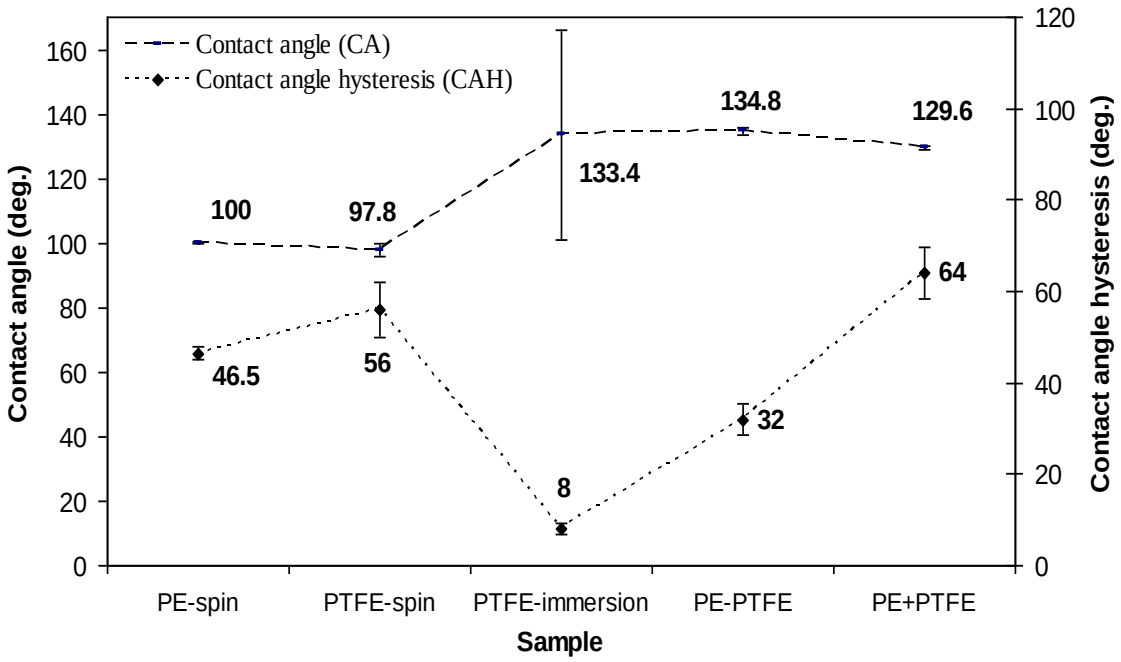

Fig.5. 1. CA and CAH values of homogeneous and HCs made of PE and PTFE on polished Al alloy 6061.

5.2 Atomic force microscopy (AFM) analysis

To evaluate degree of surface roughening on aluminum sample coated with PTFE nanoparticles, an AFM analysis has been conducted. Table 5.1 shows the root mean square (Rms) roughness values for PTFE-spin, PTFE-immersion, PE+PTFE and PE-PTFE coatings. The large Rms value for PTFE-immersion compared to PTFE-spin confirms the much greater surface roughening on the Al surface. This phenomenon also explains the larger contact angle value for PTFE-immersion than for PTFE-spin. It is obvious that the Rms values of PE+PTFE and PE-PTFE are close together, although they are somewhat larger for PE+PTFE than for PE-PTFE. However, the CA value of a PE+PTFE coated aluminum sample was smaller than what was observed in the case of a PE-PTFE coating. Meanwhile, the CAH value for a PE+PTFE coated aluminum sample was much larger than for a PE-PTFE coating. The observed difference in CAH values of such coatings was about 32^{o}. Therefore, it is possible to say that in an AFM analysis, contact angle and contact angle hysteresis measurements confirm again the effect of heterogeneity or dissimilar functions (C-H and C-F) on polished aluminum surfaces.

Table 5. 1. The Rms roughness values (nm) of homogeneous and HCs.

Sample	Root mean square (nm)
PTFE-spin	165.5 ± 68.58
PTFE-immersion	432.27 ± 70.51
PE+PTFE	284.79 **±** 173.14
PE-PTFE	239.85 **±** 145

5.3 Effect of type of nanoparticles

5.3.1 CA and CAH measurements

In the previous section, the HC of PE-PTFE was prepared on aluminum substrates from hydrophobic functions, e.g. hydrocarbon and fluorocarbon. The effect of heterogeneity was proved from contact angle, contact angle hysteresis and AFM results. In this section, different nanoparticles with hydrophilic properties such as ZnO were applied on aluminum surfaces to prepare HCs with hydrophobic and hydrophilic properties, e.g. PE-ZnO, in order to compare with PE-PTFE coatings. This type of HC, in fact, has been prepared on an aluminum substrate to systematically study the heterogeneity effect resulting from dissimilar hydrophobic functions.

Figure 5.2 demonstrates contact angle and CAH values of homogeneous coatings of PE-spin, ZnO-spin and ZnO-immersion and the HCs of PE-ZnO and PE+ZnO. The contact angle values for homogeneous coatings of PE-spin, ZnO-spin and ZnO-immersion on polished aluminum surface were ~ 100^{o}, ~ 84^{o} and ~ 23^{o}, respectively. As shown in Figure 5.2, by changing the method of preparation from spin coating to immersion method the contact angle values decreased from ~ 84^{o} to ~ 23^{o}, respectively. The reason is probably surface roughening which was created by applying different methods.

For heterogeneous nanoparticles coatings, Figure 5.2 shows an increase in the contact angle value for PE-ZnO from ~ 100^{o} to ~ 113^{o} compared to PE-spin. The reason for this slight enhancement of contact angle value for PE-ZnO is probably the roughness effect from ZnO nanoparticles or the heterogeneity effect from applying hydrophobic and

hydrophilic segments. However, the contact angle value for PE-ZnO (~ 113^{o}) was somewhat smaller than for PE-PTFE (~ 134^{o}), whereas the CAH value for PE-ZnO (~ 62^{o}) was much larger than for PE-PTFE (~ 32^{o}). So, it is obvious that applying various hydrophobic functional groups including hydrocarbons and fluorocarbons is the most important factor in the heterogeneity effect. On the other hand, a water molecule interacts with hydrogen (-H) and fluorine (-F) atoms with different lengths and energy bonding at the molecular level, so that, in a HC, these disparities in terms of energy bonding and water molecule orientation lead to a simple slide of a water droplet on HCs [25-28]. As a result, a simple slide of a water droplet on the surface is the most important factor in the heterogeneity effect. Therefore, based on the obtained results, the heterogeneity effect can been seen in the case of PE-PTFE sample having the much larger contact angle value and much smaller CAH value, compared to the PE-ZnO sample. The reason for enhanced contact angle value for PE-ZnO compared to homogeneous samples is the roughness effect from the ZnO nanoparticles. In contrast, the CAH value for PE-ZnO increased compared to homogeneous PE-spin and heterogeneous PE-PTFE. The reason for this observation is the topological nature of the surface roughness which is of prime importance in determining hydrophobicity [114-117]. It is worthy to mention that the CAH values for homogeneous coatings of ZnO-spin and ZnO-immersion were more than 80^{o}.

The difference between the contact angle values for PE+ZnO and PE+PTFE also corresponds probably to the different size of ZnO (100 nm) and PTFE (200 nm) nanoparticles.

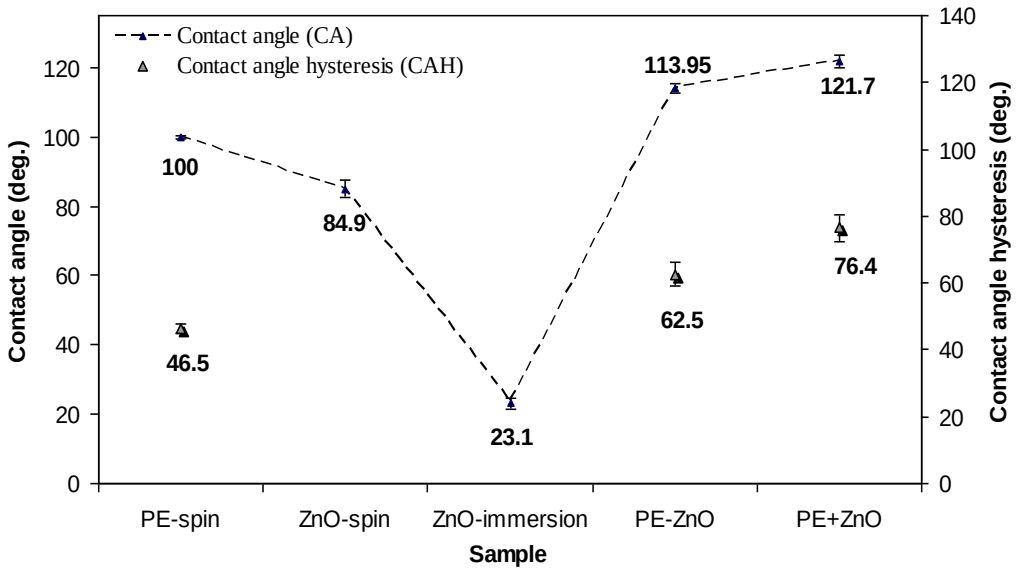

Fig.5. 2. CA and CAH values of homogeneous and HCs made of PE and ZnO.

5.3.2 Optical profilometry analysis

Table 5.2 shows the root mean square roughness values of ZnO-spin and ZnO-immersion samples. By changing the method of preparation from spin coating to immersion the rough structure on Al surface increased from 150.97 ± 58.95 to 494.26 ± 105.33 nm, while the contact angle values decreased from ~ 84^{o} to ~ 23^{o}. This fact is explained very well in the case of hydrophilic surfaces: by increasing the roughness of hydrophilic surface, their wettability properties will increase [117].

Table 5. 2. The Rms roughness values (nm) of homogeneous coatings of ZnO-spin and ZnO-immersion.

Sample	Root mean square (nm)
ZnO-spin	150.97 ± 58.95
ZnO-immersion	494.26 ± 105.33

5.4 Effect of nanoparticles sizes

5.4.1 CA and CAH measurements

In order to better understand the observed results and establish the effect of heterogeneity, another set of experiments was done. The Al_2O_3 nanoparticles with the same size as the PTFE nanoparticles (200 nm) were replaced by the ZnO nanoparticles (100 nm). This replacement was done to ignore any possible effect of surface roughening due to the difference of nanoparticles size. The procedures to prepare coatings were shown in detail in chapter 3. The procedure applied to prepare coatings of PE, PTFE and Al_2O_3 is exactly the same as for homogeneous and HCs made of PE, PTFE and ZnO. Figure 5.3 shows the contact angle and CAH values of the homogeneous and HCs made of PE, PTFE and Al_2O_3 on polished Al substrates. The contact angle values for homogeneous coatings of PE-spin, Al_2O_3-immersion, PTFE-spin and Al_2O_3-spin were ~ 100^o, ~ 11^o, ~ 97^o and ~ 48^o, respectively. Again, a considerable increase of the contact angle value was observed for the HC of PE-PTFE ~ 134^o. An increase in the contact angle also was observed on case of PE-Al_2O_3 from ~ 100^o to ~ 116^o compared to homogeneous PE-spin coating. It is clear that a decrease in the CAH value was also obtained for HC of PE-PTFE (~ 32^o), while the CAH values for homogeneous coatings of PE-spin and PTFE- spin were ~ 46^o and ~ 56^o, respectively. It is indeed important to highlight that the CAH value for HC of PE-Al_2O_3 was larger than those obtained on homogeneous (PE-spin and PTFE-spin) and heterogeneous PE-PTFE coating. This enhanced CAH value for the PE-Al_2O_3 sample is due to the roughness effect from the Al_2O_3 nanoparticles. As discussed earlier in section 5.2 above, the reason for enhanced

contact angle values in the case of the PE-Al_2O_3 sample is the roughness effect from the Al_2O_3 nanoparticles. This fact is obvious from the Kurtosis values (Sku) that for the PE-Al_2O_3 sample was 40.4 and for PE-PTFE sample was 14.1, indicating that the PE-Al_2O_3 sample is spikier. Therefore, the topography and rough structure results give a major reason for the enhancement of contact angle value for the PE-Al_2O_3 sample. The heterogeneity effect was furthermore confirmed by changing the nanoparticles and its corresponding size, *i.e*. from ZnO (100 nm) to Al_2O_3 (200 nm), as it is comparable to the PTFE size (200 nm). Therefore, it is possible to ignore the effect of size within tested limits and consequently the effect of roughness on hydrophobic properties.

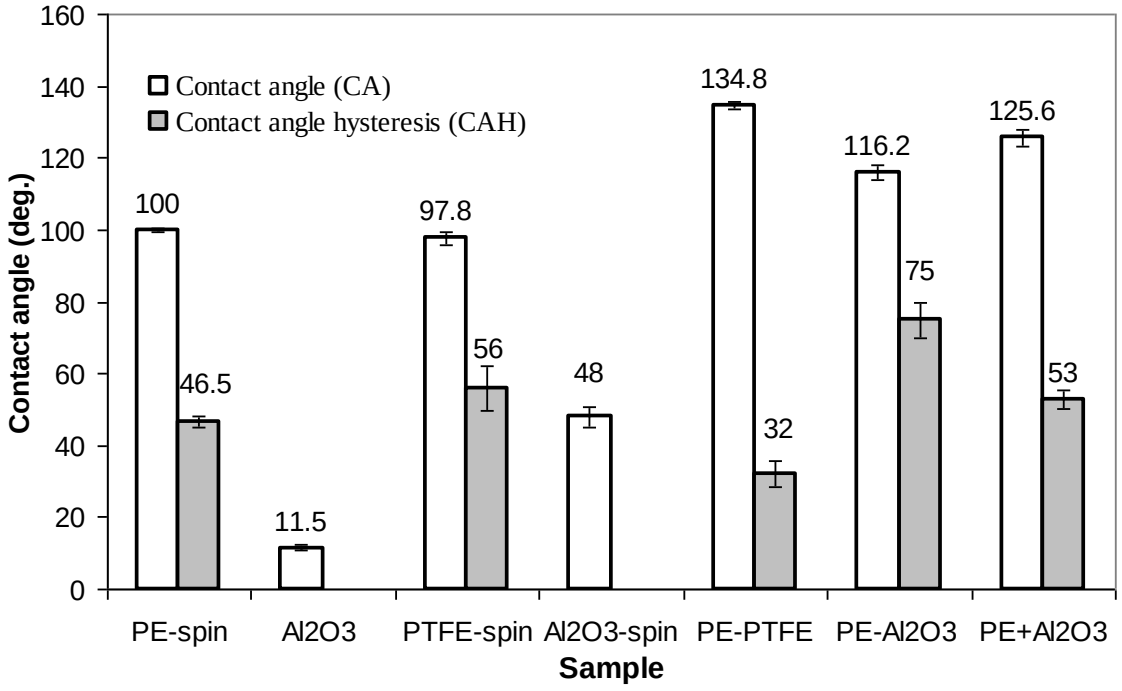

Fig.5. 3. CA and CAH values of homogeneous and HCs made of PE, PTFE and Al_2O_3.

5.4.2 Optical profilometry analysis

Table 5.3 shows the root mean square (Sq) roughness value from three different points on homogeneous and HCs of PE-spin, PE-PTFE and PE-Al_2O_3. One sees that the Sq value of the PE-spin coating is the smallest one compared to PE-PTFE and PE-Al_2O_3 coatings. In addition, the Sq value of the PE-Al_2O_3 coating is larger than that of the PE-PTFE. Figure 5.4 shows the topography and rough structure of the PE-PTFE and PE-Al_2O_3 samples. It is worth mentioning that with a large value of Sq in the case of PE-Al_2O_3 sample, the wetting property, contact angle value, of the sample was not as large as PE-PTFE sample. In other words, the contact angle value of the PE-PTFE sample is much larger than that of coated aluminum with PE-Al_2O_3. The contact angle values of PE-PTFE and PE-Al_2O_3 are ~ 134^o and ~ 116^o, respectively. This observation can be related to the heterogeneity effect that arises from different lengths of hydrogen bonding: -CH_2 (from PE), -CF_3 (from PTFE), and various interaction energies.

Table 5. 3. The Rms of HCs of PE-PTFE and PE-Al_2O_3.

Sample	Root mean square (nm)
PE-spin	108.3 ± 8.6
PE-PTFE	398.85 ± 145
PE-Al_2O_3	522.29 ± 63

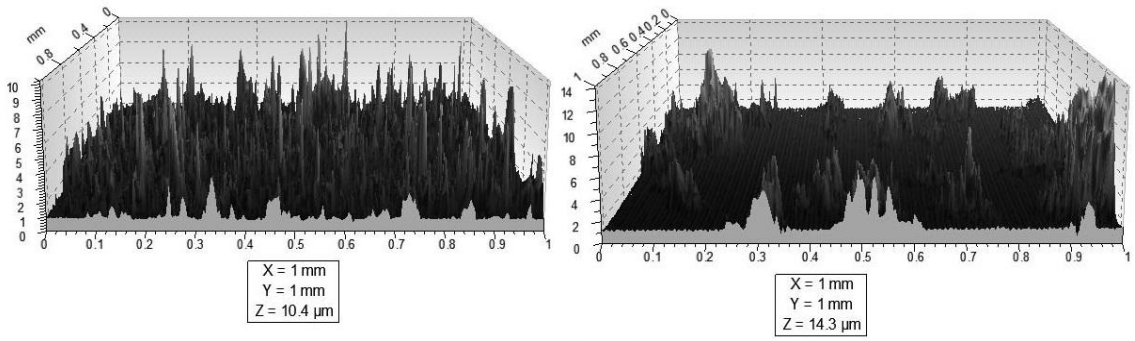

Fig.5. 4. Profilometry images of PE-Al_2O_3 (a) and PE-PTFE (b).

5.5 Effect of various polymers

5.5.1 Contact angle (CA) measurements

To further study the heterogeneity effect on the wetting characteristic, different types of polymer and organic material such as polystyrene (PS), polymethylmethacrylate (PMMA) and stearic acid (STA) were used. These polymers were selected, in fact, to study how different chemical structures affect on the heterogeneity. Before investigating different types of polymer, several nanoparticles were studied. Figures 5.5 to 5.7 show the contact angle values for homogeneous and HCs prepared from PS, PMMA and STA with PTFE and Al_2O_3 nanoparticles. It can be seen that the CA values for homogeneous coatings are smaller than for HCs. The CA values for the homogeneous coating of PS-spin and PMMA-spin were ~ 95^o and ~ 94^o, respectively. Also, the contact angle values for PS-PTFE and PMMA-PTFE (~ 120^o) are larger than for PS-Al_2O_3 and PMMA-Al_2O_3 (~ 109^o). On the other hand, the largest contact angle values were obtained for HCs of PS-PTFE and PMMA-PTFE. Figures 5.5 and 5.6 show that the tendency of variation of contact angle values is the same as for samples made of PE, PTFE and Al_2O_3. Again, the

observed results concerning the hydrophobic properties of HCs are due to dissimilar low surface energy functions that were created by applying different materials.

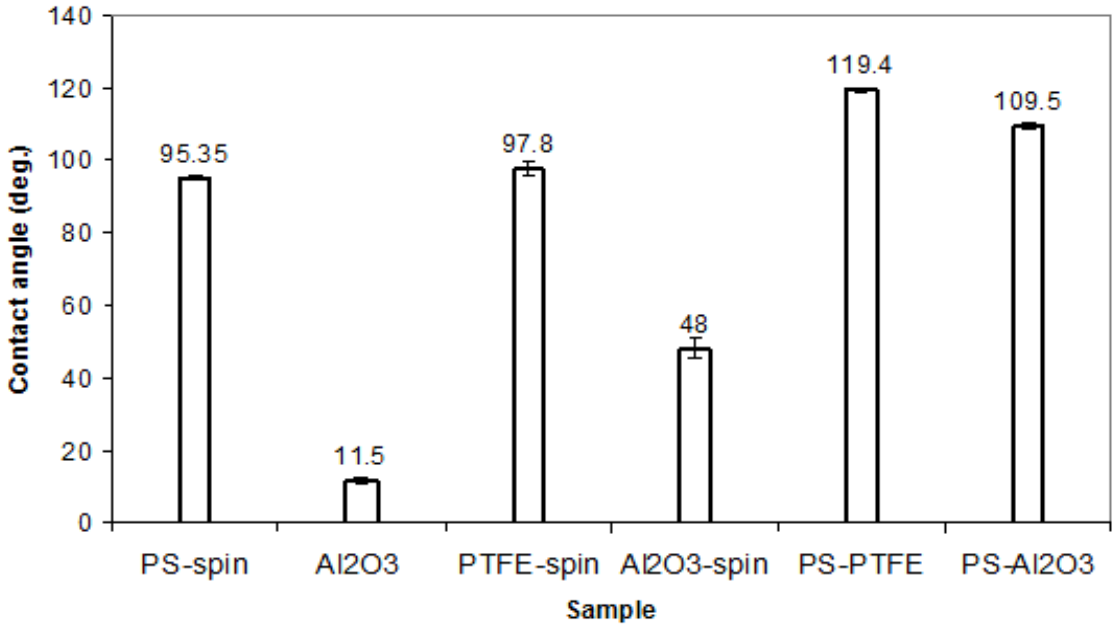

Fig.5. 5. CA values of homogeneous and HCs made of PS, PTFE and Al_2O_3.

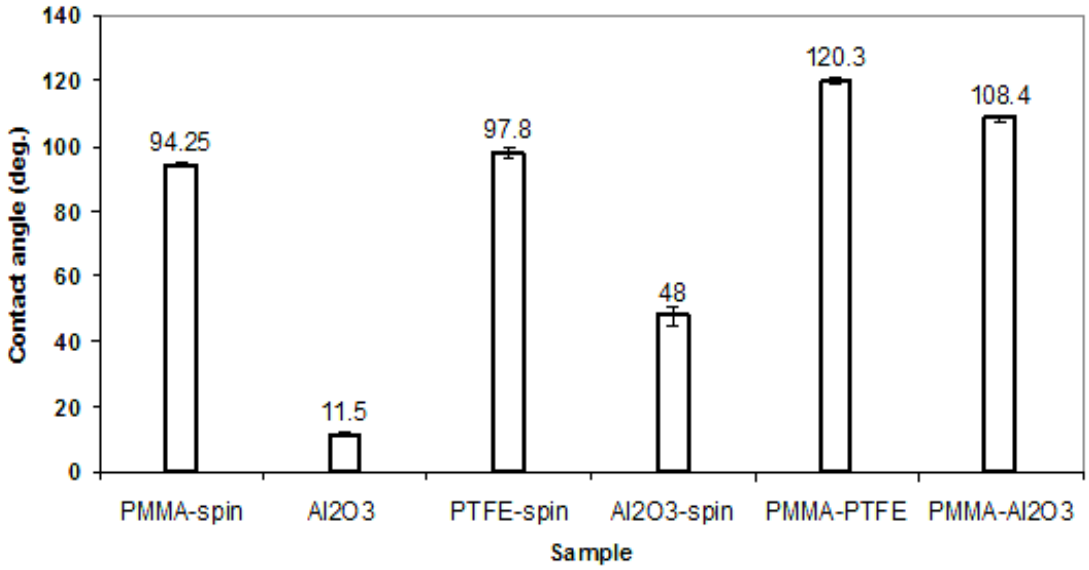

Fig.5. 6. CA values of homogeneous and HCs made of PMMA, PTFE and Al_2O_3.

Different types of polymeric coatings including $-CH_3$ or $-CH_2$ moieties were studied so far. In this case, the $-CH_2$ and $-CH_3$ groups were placed in a horizontal orientation. In order to have a surface with a vertical branch of $-CH_2$ or $-CH_3$ groups in this part at first a self assembled monolayer was fabricated and then a coating of nanoparticles was covered on them. By applying an organic fatty acid such as stearic acid (STA), the CA value of homogeneous coating of STA-spin (~ 107^o) was obtained. The maximum contact angle value was obtained in case of HC of STA-PTFE (~ 125^o) while the CA value for the HC of SAT-Al_2O_3 was ~ 114^o (see Fig.5.8). Therefore, by changing the PE to PS, PMMA and STA, these experiments confirmed accurately the mentioned heterogeneity effect on polished aluminum samples.

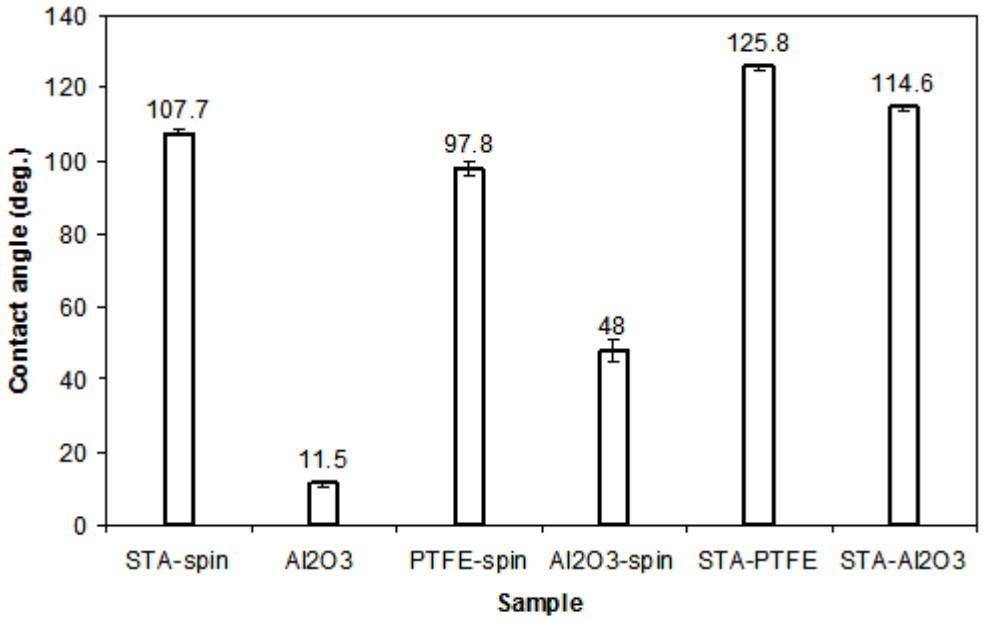

Fig.5. 7. CA values of homogeneous and HCs made of STA, PTFE and Al_2O_3.

5.5.2 Contact angle hysteresis (CAH) measurement

Table 5.4 shows the CAH values of homogeneous and HCs of PS, PMMA and STA materials. It can be seen that the CAH values decreased in case of HCs of PS-PTFE, PMMA-PTFE and STA-PTFE, as it was ~ 37^o to ~ 40^o while the CAH values for homogeneous coatings of PS-Al_2O_3, PMMA-Al_2O_3 and STA-Al_2O_3 were ~ 68^o to ~ 80^o.

Table 5. 4. The CAH values of homogeneous and HCs made of PS, PMMA and STA materials.

Sample	Contact angle hysteresis (CAH) (deg.)
PS	56 ± 2.8
PS-PTFE	**40 ± 2.8**
PS-Al_2O_3	68.5 ± 4.9
PMMA	59 ± 1.41
PMMA-PTFE	**38.5 ± 4.9**
PMMA-Al_2O_3	80.5 ± 3.5
STA	51 ± 1.4
STA-PTFE	**37.5 ± 4.9**
STA-Al_2O_3	71.5 ± 2.1

5.6 Surface energy calculation

Surface energy values of the coatings helps to study more accurately the effect of heterogeneity on the hydrophobic properties of the prepared coatings. Table 5.5 presents the free surface energy values of prepared coatings calculated following contact angle measurements [20]. As it is evident in table 5.5, the HC nanoparticles coatings show minimum values of surface energy compared to what was obtained for homogeneous coatings. Furthermore, the smallest values of surface energy were obtained for HCs including hydrocarbon and fluorocarbon such as PE-PTFE (2.84 ± 0.39 mNm^{-1}) and STA-PTFE (4.17 ± 0.25 mNm^{-1}).

In the case of HCs for instant PE-Al_2O_3 and PE-ZnO, the surface energy value also decreased in comparison with homogeneous coatings, although we did not observe a

significant decrease as what was obtained for HCs such as PE-PTFE. It is worth mentioning that this reduction in surface energy values for HC of PE-Al_2O_3 and PE-ZnO samples is due to surface roughening which resulted from applying nanoparticles. However, for PE-PTFE and STA-PTFE coated aluminum samples, the surface roughening as well as the existence of C-F and C-H functions, spontaneously, caused a further decrease in surface energy. Consequently, it can be concluded that applying different functions of C-F and C-H on aluminum surfaces can definitely affect the hydrophobic properties of samples as their surface energy values decreased further.

Table 5. 5. The surface energy values of homogeneous and heterogeneous nanoparticles coatings.

Sample	Surface energy (mNm^{-1})
PE-spin	13.86 ± 0.46
PTFE-spin	15.6 ± 0.57
ZnO-immersion	67.54 ± 0.70
Al_2O_3-spin	54.92 ± 1.61
Al_2O_3-immersion	71.38 ± 0.17
PE-PTFE	**2.84 ± 0.39**
PE-ZnO	6.98 ± 0.4
PE-Al_2O_3	5.49 ± 0.35
PE+ PTFE	3.89 ± 0.25
PE+ ZnO	4.36 ± 0.34
PE+Al_2O_3	4.15 ± 0.26
PS-spin	16.2 ± 0.39
PS-PTFE	**5.11 ± 0.38**
PS-Al_2O_3	9.68 ± 0.50
PMMA-spin	16.98 ± 0.56
PMMA-PTFE	**4.83 ± 0.48**
PMMA-Al_2O_3	9.38 ± 0.46
STA-spin	9.73 ± 0.59
STA-PTFE	**4.17 ± 0.25**
STA-Al_2O_3	7.1 ± 0.5

5.7 Scanning Electron Microscopy (SEM) analysis

Figures 5.8 and 5.9 show the scanning electron microscopy (SEM) images, at different magnifications, of samples coated with PE-PTFE and PE-Al_2O_3, respectively. These series of characterizations were conducted to investigate sample surface morphology. The SEM images of a coated aluminum surface show a rough structure at the micro-/nano-meter scale on a polished aluminum surface. As is shown in Figures 5.9 and 5.10, the surface morphology of aluminum samples coated with PE-PTFE and PE-Al_2O_3 are similar as they reveal the propagated islands of nanoparticles in several areas and spots. It is possible to conclude from these propagated islands observed in SEM images that the PTFE and Al_2O_3 nanoparticles were agglomerated on the aluminum surface and therefore, they did not cover the surface uniformly.

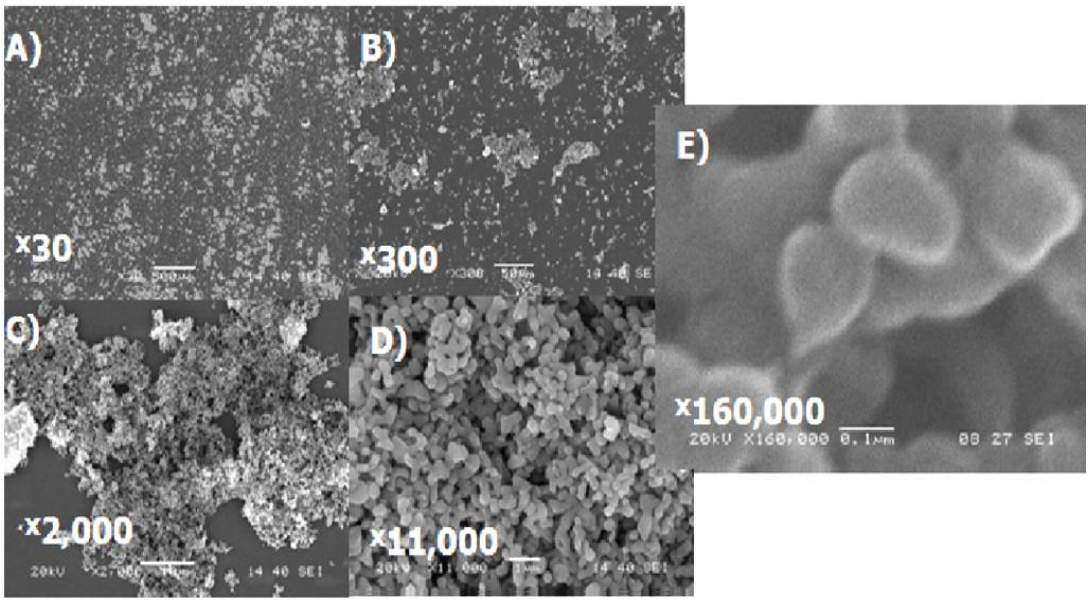

Fig.5. 8. Scanning electron microscopy (SEM) images of surface coated with PE-PTFE, at 30, 300, 2000, 11000 and 160000 magnifications.

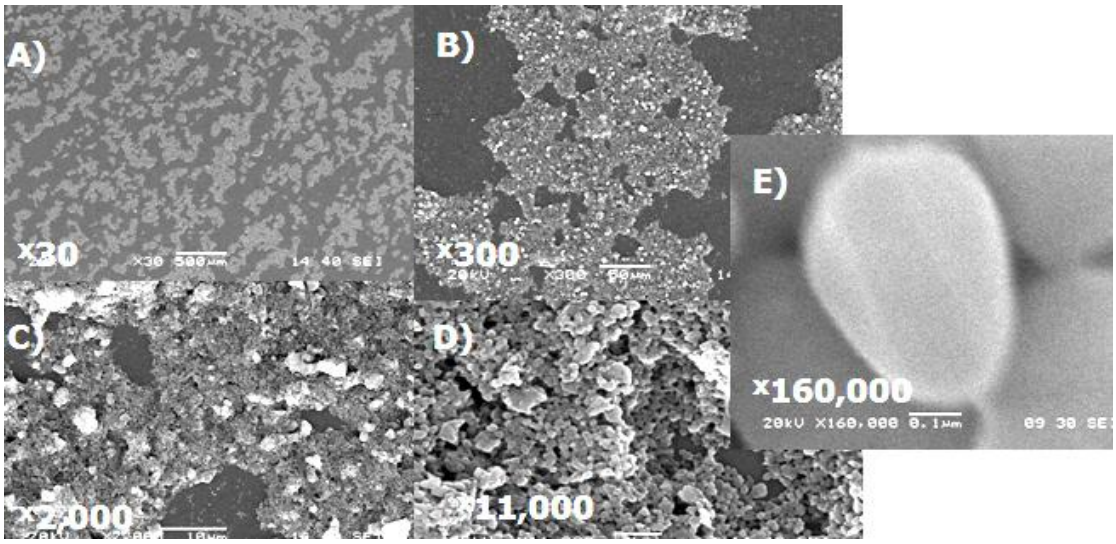

Fig.5. 9. Scanning electron microscopy (SEM) images of surface coated with PE-Al_2O_3, at 30, 300, 2000, 11000 and 160000 magnifications.

Although these series of heterogeneous nanoparticles coatings characterizations proved the presence of the heterogeneity effect on aluminum samples, however, the SEM analysis results showed that the nanoparticles did not cover the aluminum surface uniformly. Therefore, it was decided to study another preparation technique of coating. In fact the heterogeneous plasma coating through masks was selected to produce HCs. In this way there was more control to prepare HCs and thus cover the surface uniformly.

5.8 Heterogeneity effect on the interaction energy between coating and water molecules

As it was discussed previously in chapter 4, the heterogeneity effect can be specified in theory by calculating the interaction energy between homogeneous or heterogeneous *SAM*s coatings and water molecules. Subsequently in this chapter, to estimate the interaction energy, the sliding angle of each coated sample was measured

[102,103]. Table 5.6 illustrates the values of calculated interaction energy of homogeneous and heterogeneous nanoparticles coatings on aluminum surface described by equation (5.1), [102]:

$$K_A = \left[\rho\left(\frac{2-3\cos\theta+\cos^3\theta}{3}\right)\right]^{1/3} \frac{g}{2}\left(\frac{m}{\pi}\right)^{2/3} \frac{\sin\alpha}{\sin\theta} \qquad \textbf{(5.1)}$$

Table 5. 6. The values of interaction energy between a water droplet and a homogeneous or heterogeneous nanoparticles coated surface.

Sample	α (deg.)	θ (deg.)	m (mg)	K (mJ/m^2)
PE-spin	45	97.7	45	19.532
PTFE-spin	55	87	45	20.564
PE-PTFE	28	119	30	12.520
PE-ZnO	52	96.5	45	21.524
PE-Al_2O_3	55	97	45	22.479
PE+ PTFE	50	104.4	30	17.249
PE+ ZnO	53	105.4	45	23.810
PE+Al_2O_3	50	109	45	23.738

According to the results of the calculation of interaction energy between a water droplet and homogeneous and heterogeneous nanoparticles coatings, the smallest value of interaction energy was obtained for PE-PTFE sample that is to say 14.6 mJ/m^2. This small value of the interaction energy indicates a simple slide of a water droplet on HCs prepared from dissimilar hydrophobic functions of C-H and C-F. When the interaction energy between water droplet and the coating shifts to a smaller value, the sliding angle decreases.

5.9 Conclusions

In this research work, homogeneous and HC nanoparticles coatings of low surface-energy materials with hydrophobic properties were prepared by the spin-coating method. The contact angle and contact angle hysteresis measurements, surface energy value calculation, optical profilometry and AFM analysis demonstrated the effect of heterogeneity on aluminum substrates. Among different HCs prepared, the obtained results showed that only the HCs prepared from dissimilar hydrophobic functions of C-H and C-F can affect the hydrophobic characteristic of such coatings. In addition, theoretical calculation of interaction energy between a water droplet and prepared HCs confirmed the heterogeneity effect resulting from different hydrophobic functions. According to the objectives of this research work, subsequently, the second approach in preparing HCs, *i.e.* HC nanoparticles coating, demonstrated the effect of heterogeneity on the improvement of hydrophobic properties of coatings.

CHAPTER VI

HYDROPHOBIC PROPERTIES OF HOMO- AND HETEROGENEOUS PLASMA COATINGS

6. Introduction

In the previous chapters, two approaches were used for preparing the coatings. In this chapter, another method, using plasma sputtering coatings through masks on an aluminum surface, will be studied. To prepare HC plasma coatings, polytetrafluoroethylene (PTFE), were deposited through different copper gauzes as masks of 20 and 60 meshes (corresponding to 0.41 mm and 0.19 mm in wire width) on polyethylene (PE), polystyrene (PS) films. It is also important to mention that the distance between two wires or the opening between each pair of meshes is 0.86 mm. The plasma sputtering system and the process of fabrication of HC plasma coatings through masks on Al surface was explained in detail in chapter 3. In fact, it is decided to study the preparation of HC plasma coatings for two reasons. First, in this way there is more control in the preparation of the coating and second, this method is well-known due to its remarkably significant stability and durability [21,118,119]. To further study and characterize the effect of heterogeneity, the AFM, profilometry, SEM and XPS analyses are done on the surface coatings.

6.1 Hydrophobic properties of homo- and heterogeneous plasma sputtering coatings

6.1.1 Contact angle (CA) measurement

In order to study the effect of heterogeneity on wettability of prepared coatings, the CA and CAH values of a water droplet on the homogeneous and HC plasma sputtered coatings were measured. Figure 6.1 shows the contact angle values of homogeneous and

HC plasma sputtering coatings. The PS and PE coatings were prepared from 1 g PS in 50 ml toluene and 1 g PE in 50 ml toluene solutions (see chapter 3). To prepare the HCs, PTFE as target material was used to deposit coating on a PE and PS coated Al surface through different copper gauzes as masks of 20 and 60 meshes, corresponding to 0.41 mm and 0.19 mm in wire width, respectively. To prepare a homogeneous PTFE sample which is shown in Figure 6.1, PTFE (0.19/0.41 mm), PTFE was deposited on a polished aluminum surface through different copper gauzes as masks of 20 and 60 meshes. The plasma sputtering conditions were explained in detail in chapter 3.

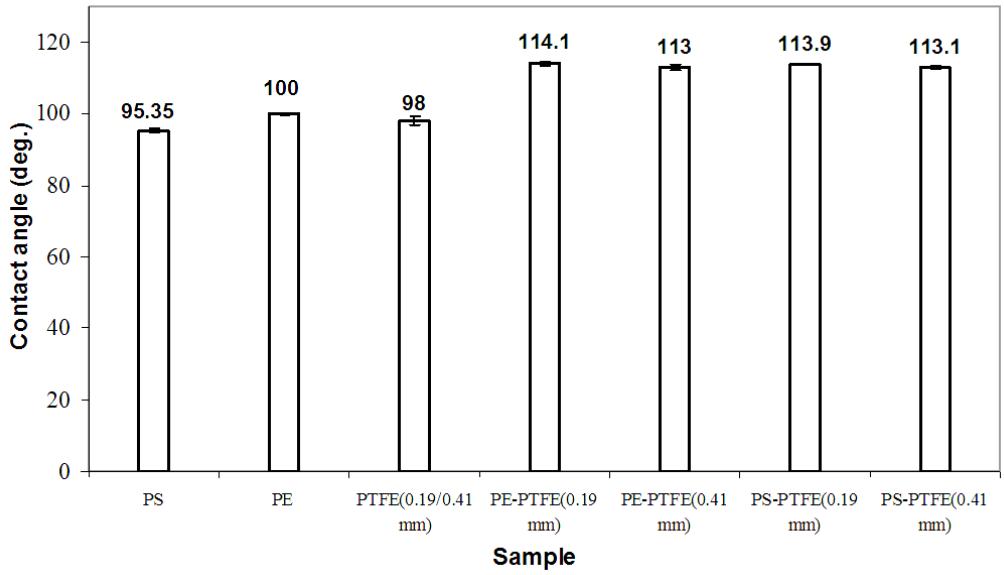

Fig.6. 1. CA values of homogeneous and HC plasma coatings made of PE, PS and PTFE.

As is evident in Figure 6.1 the CA values for homogeneous PE, PS and PTFE coatings were ~ 100^{o}, ~ 95^{o} and ~ 98^{o}, respectively. The contact angle values for both HCs of PE-PTFE and PS-PTFE with both mask mesh sizes were between ~ 113^{o} and ~ 114^{o}. The results obtained in Figure 6.1 show that the contact angle values of HCs are

larger than those obtained in case of homogeneous coatings. To further study the heterogeneity effect the CAH was measured as well.

6.1.2 Contact angle hysteresis (CAH) measurement

Figure 6.2 presents the CAH values of homogeneous and HC coated samples by the plasma coating method. A decrease in CAH values was obtained in the case of HCs of PE-PTFE (0.41 mm), PS-PTFE (0.41 mm), PE-PTFE (0.19 mm) and PS-PTFE (0.41 mm), as they were ~ 24^{o}, ~ 25^{o}, ~ 27^{o} and ~ 32^{o}, respectively, whereas the CAH values for homogeneous coatings were ~ 50-62^{o}.

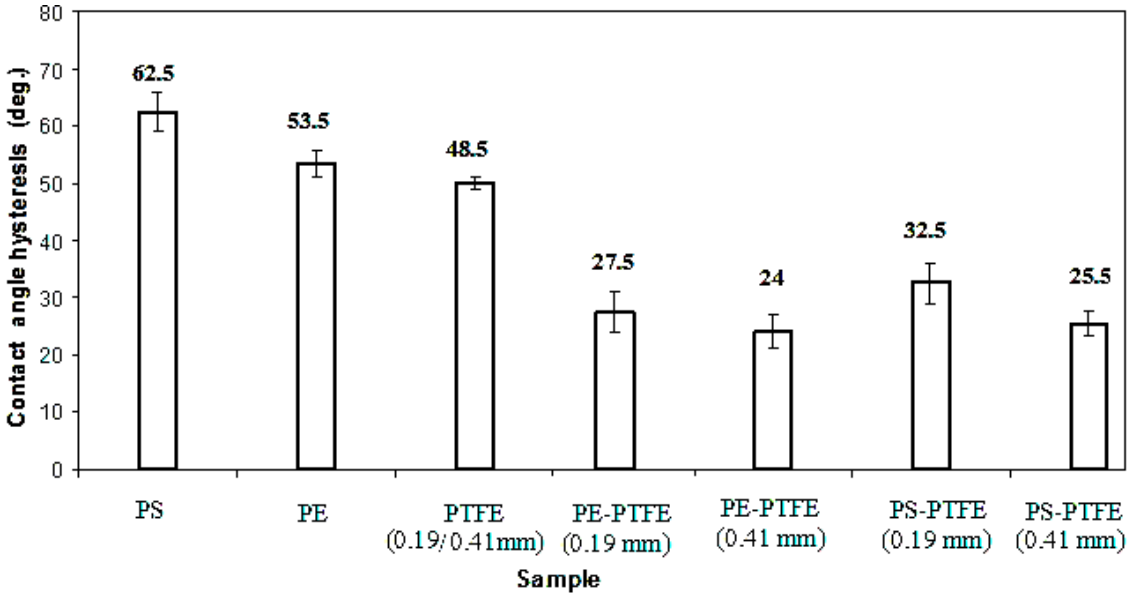

Fig.6. 2. CAH values of homogeneous and HC plasma sputtering coatings.

For an in-depth study of the prepared coatings, in order to be able to interpret the obtained results, the surface characterizations of these coatings have been done and will be presented in the following sections.

6.2 Surface energy calculation

Table 6.1 presents the calculated surface energy values of prepared homogeneous and HC 'masked' plasma coatings, using contact angle measurements. As it is obvious in table 6.1, the HC masked plasma coatings show minimum values of surface energy compared to what was obtained for homogeneous coatings. Since the smallest value of surface energy for heterogeneous plasma coatings including hydrocarbon and fluorocarbon was ~ 6 (mNm^{-1}), it can be concluded that the presence of dissimilar functions of C-F and C-H on aluminum surfaces have an effect on the hydrophobic properties of HCs compared to applying only one of C-F or C-H.

Table 6. 1. The surface energy values of homogeneous and HC 'masked' plasma coatings.

Sample	Surface energy (mNm^{-1})
PE-spin	13.86 ± 0.46
PS-spin	16.2 ± 0.39
PE-PTFE (0.19 mm)	**6.63 ± 0.42**
PE-PTFE (0.41 mm)	**6.78 ± 0.39**
PS-PTFE (0.19 mm)	**6.65 ± 0.16**
PS-PTFE (0.41 mm)	**6.7 ± 0.21**

6.3 Surface characterizations

6.3.1 Scanning Electron Microscopy (SEM) analysis

Figure 6.3 shows the SEM images of a homogeneous PE coating at two different magnifications (300 × and 11000 ×). These images indicate the smooth surface morphology of the PE coating. However, a small number of scattered white points in figure 6.3 (a) are related to contamination.

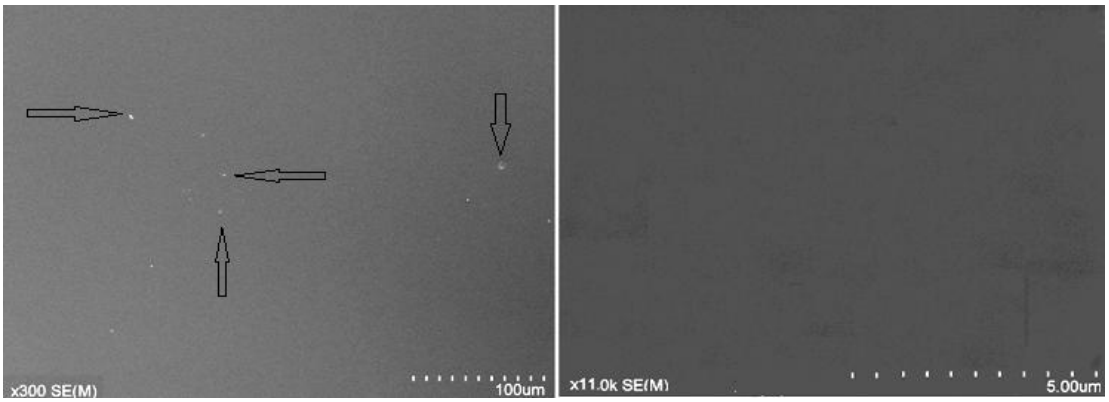

Fig.6. 3. Scanning electron microscopy (SEM) images of PE coating on aluminum alloy at a) 300, b) 11000 magnifications.

After studying and characterizing the homogeneous PE coating, it is logical to compare these results with those obtained for the HC PE-PTFE sample. So, the SEM analysis of PE-PTFE sample was done. Figures 6.4 and 6.5 show the scanning electron microscopy (SEM) and energy-dispersive x-ray spectroscopy (EDS) images of heterogeneous sample coated PS-PTFE (0.41 mm) through a mask by the plasma sputtering method at different magnifications. The SEM images of the coated surface show a distribution of white points at the micrometer scale on the surface (see fig. 6.4). Many attempts have been made by various available vacuum chamber modes here at

CURAL to obtain clear SEM images of PTFE on a flat aluminum surface. However, it was almost impossible to have a clear image due to interaction between the PTFE coating and the electron beam. Finally after keeping the sample overnight at high vacuum with special operating adjustments, a few spots of PTFE (whitish point in Figure 6.5) at 18000 magnifications were detected and observed. This set of experiments was carried out to investigate further the chemical composition of the observed white points existing on the surfaces. As is evident in Figure 6.4, spectra numbers 1 and 2 show the high percentage of F element on the surface which relates to the presence of PTFE. Moreover, this series of experiments confirms the production of a HC by plasma-mask coating.

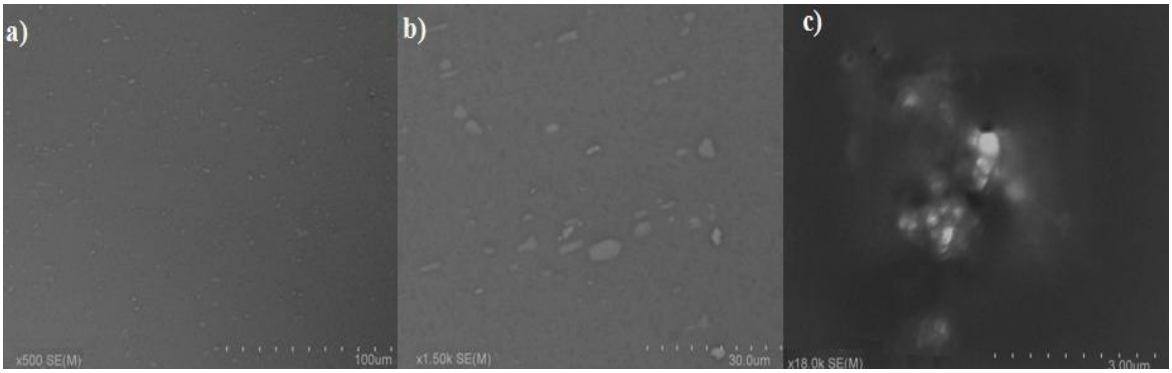

Fig.6. 4. Scanning electron microscopy (SEM) images of plasma-PS-PTFE coating at a) 500, b) 1500 and c) 18000 magnifications.

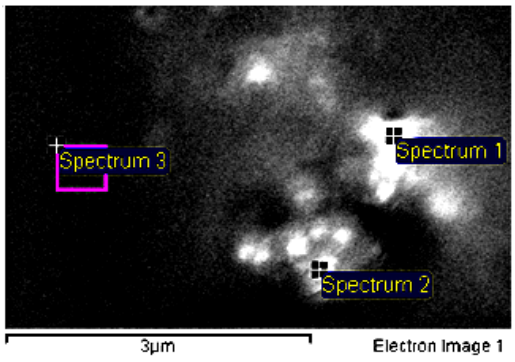

Spectrum	In stats.	C	O	F	Al	Total
Spectrum 1	Yes	40.45	0.78	58.77		100.00
Spectrum 2	Yes	36.47		63.53		100.00
Spectrum 3	Yes	83.93	2.50	9.77	3.80	100.00
Max.				63.53	3.80	
Min.				9.77	3.80	

Fig.6. 5. The SEM image of plasma-PS-PTFE coating at 8000 magnification with EDS spectrum (percentage).

6.3.2 Optical profilometry analysis

Figure 6.6 (a and b) present optical profilometry images of a PS sample and a heterogeneous plasma-coated PS-PTFE (0.41 mm) sample through a mask. The surface morphology of the PS sample obtained by optical profilometry measurements shows some scattered peaks on the surface which could be related to contamination. The heterogeneous PS-PTFE sample demonstrates a rough structure at micro-/nano-meter scale on a polished aluminum surface. This micro-/nano-scale roughness was obtained by deposition of fluoro polymer on PS coating through copper gauzes, used as a mask of 20 meshes, corresponding to 0.41 mm in wire width. If the image (a) is compared with (b), it can be found that the greater number of rough structures on the heterogeneous surface is related to the deposition of a fluoro polymer. The optical profilometry analysis gave an overall Z-axis of about 778.6 nm and 800 nm for PS and PS-PTFE coatings, respectively. Moreover, the value of measured roughness (Sq) by profilometry was 22.8 nm and 50.00

nm, for PS and PS-PTFE coatings, respectively. Parts 1 and 2 in Figure 6.6 (b) will be described in more detail in the next section.

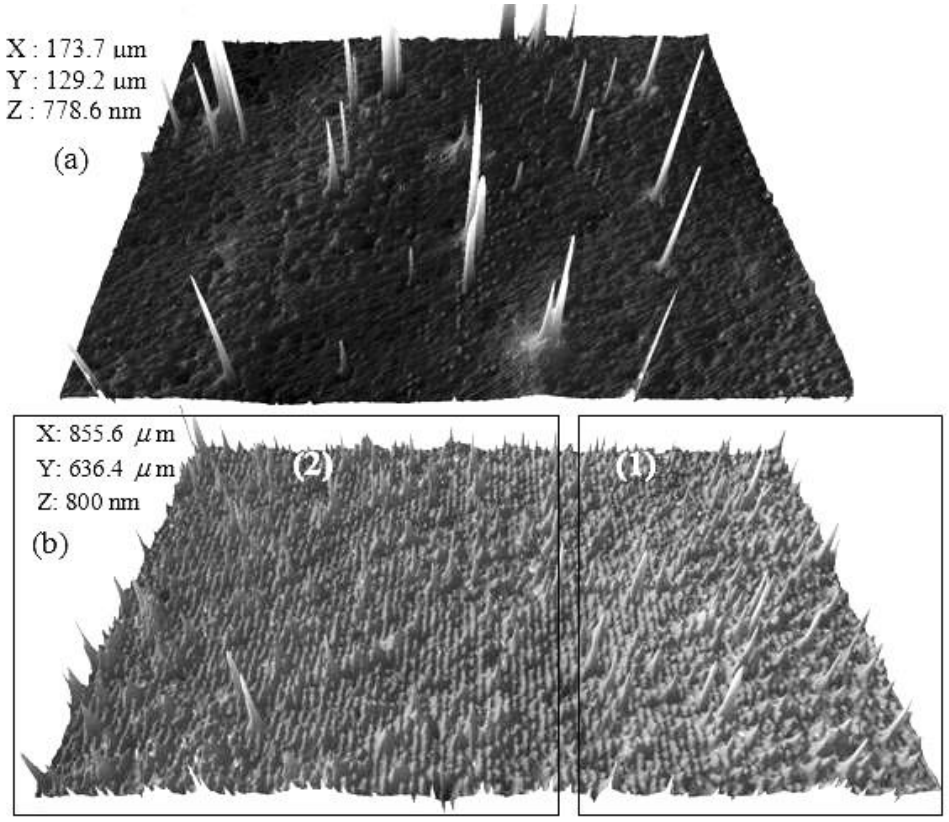

Fig.6. 6. Optical profilometry images of PS sample (a) and heterogeneous PS-PTFE (0.41 mm) coated sample (b) via plasma sputtering method.

6.3.3 Atomic force microscopy (AFM) analysis

Figure 6.7 (a-c) shows the AFM images of plasma-coated PS-PTFE (0.41 mm) through a mask. Figure 6.7 (a) possibly demonstrates the part of surface between each pair of meshes (part 1) and the surface under the wire of meshes (part 2). Figure 6.7 (b) could be related to the surface under the wire of meshes. Figure 6.7 (c) possibly shows the

surface between each pair of meshes. The AFM results are almost consistent with the SEM and profilometry results, since Figure 6.7 (c) probably has the same white points and scattered peaks seen in Figures 6.6 (b) and 6.4 (c). Figure 6.7 (a and b) are in accordance with profilometry images. If Figure 6.6 (b) (see parts 1 and 2) is considered again carefully, it is in agreement with 6.7 (a), since the value of Rms obtained by the AFM machine (53.037 nm) is obviously close to that measured via profilometry technique (50 nm).

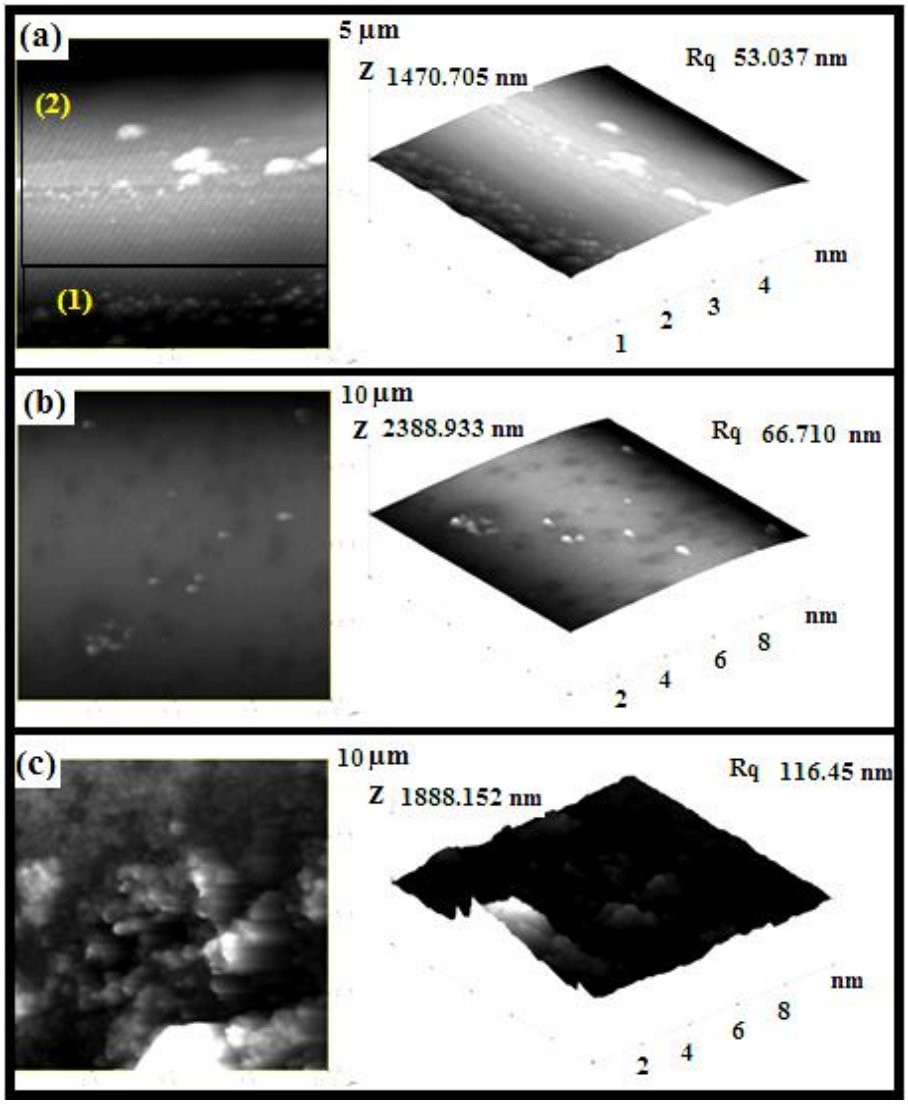

Fig.6. 7. AFM images of three different points of PS-PTFE sample.

6.3.4 X-ray photoelectron spectroscopy (XPS) analysis

Table 6.2 illustrates XPS analysis results of the HC of PS-PTFE (0.41 mm). It is clear from this analysis that the CF_2 and C-CF_x molecules indicate the attendance of fluoropolymer compounds (such as PTFE) on a homogeneous PS coated aluminum substrate. The greater percentage of CF_2 on PS coated aluminum substrate corresponds to the amount of C-F bondings created by plasma deposition which appeared like hills through a mask (See Figure 6.6 (b)). The presence of $(-CF_2CH_2-)_n$ molecules specifies the HC of PS-PTFE on aluminum substrate. The C-C bond and $(CH_2CH_2)_n$ molecules indicate the presence of PS polymer, used as an under layer on aluminum substrate. These XPS results show that the aluminum surfaces were covered with PS and PTFE.

Table 6. 2. XPS results of PS-PTFE (0.41 mm) on Al surface.

Component	**CF_2**	**$(CF_2CH_2)_n$**	**C-CF_x**	**C-C**	**$(CH_2CH_2)_n$**
Percentage	**34.08**	**16.54**	**42.00**	**4.67**	**2.72**

In order to investigate the origin of small value of CAH of HCs and to study if it comes from the variation of roughness due to plasma sputtering coating, we will study the effect of roughness of Teflon sputtering film on the results of contact angle and CAH.

6.4 Investigation of surface roughness effect

To investigate the rough structure of the prepared HCs by the plasma sputtering method, a new series of experiments was conducted. For this study, the following samples were prepared. A Teflon® substrate had two-step plasma PTFE sputtering

coating. The prepared sample after the first step of plasma PTFE sputtering is called Teflon 1 and after the second step of plasma PTFE sputtering, Teflon 2. In the second step Teflon 1 is plasma-sputtered without using masks. It is important to mention that the Teflon sample was used to double check and further study the presence and effect of surface roughening on hydrophobic properties. A PS coated Al surface sample with subsequent (after two steps) PTFE coating was prepared by plasma-sputtering. These prepared samples were either with or without any copper gauze as a mask. The samples of plasma-sputtering on a PS coated aluminum surface without mask are called Sample 1 and Sample 2. In the second step Samples 1 and 2 are plasma-sputtered using masks of mesh sizes of 0.19 and 0.41 mm, respectively, and are then named Sample 3 and Sample 4, respectively. As was described in Chapter 3, the distance between the target (Teflon®) and the substrates (aluminum) was set at 30 cm. After being evacuated to a base pressure of 2.0×10^{-6} Torr, argon gases were admitted into the chamber. The flow rate of the sputtering gas was controlled by an MKS mass flow controller (MFC) and set at 50 standard cubic centimeters per minute (sccm). The aluminum surface was pre-cleaned and pre-activated in 75W plasma argon for 5 min. The sputtering deposition process was carried out under 75W RF power for 20 min at 20mTorr. Figure 6.8 shows the CA and CAH values of Teflon 1 and PS coatings which were coated with plasma-sputtered polytetrafluoroethylene (Samples 1 and 2). The contact angle and CAH values of heterogeneous PS-PTFE coating without mesh were ~ 107^{o} and ~ 41^{o}, respectively. The contact angle and CAH values of Teflon 1 were ~ 111^{o} and ~ 56^{o}, respectively. To study the rough structure on the prepared coatings which probably resulted from the plasma method, Samples 1 and 2 were coated again via plasma method through mask. Figure 6.9

shows the contact angle and CAH values after the second step of plasma-spattering. As mentioned before, Samples 1 and 2 are plasma- sputtered using masks of mesh sizes of 0.19 and 0.41 mm, respectively and are named Sample 3 and Sample 4. As seen in Figure 6.9, the contact angle values of plasma coatings through a mask (Samples 3 and 4) and the Teflon 2 sample were ~ 109.5^{o}, ~ 109.8^{o} and ~ 110^{o}, respectively. The CAH values of Teflon 2, Sample 3 and Sample 4 were ~ 41^{o}, ~ 49^{o} and ~ 41^{o}. If the obtained results are compared to heterogeneous plasma coatings without a mask, the contact angle and CAH values do not change significantly (see Figure 6.8). So, it can be concluded that the rough structure on the surface created by applying the plasma sputtering method did not have any effect on the hydrophobic properties of the prepared HCs.

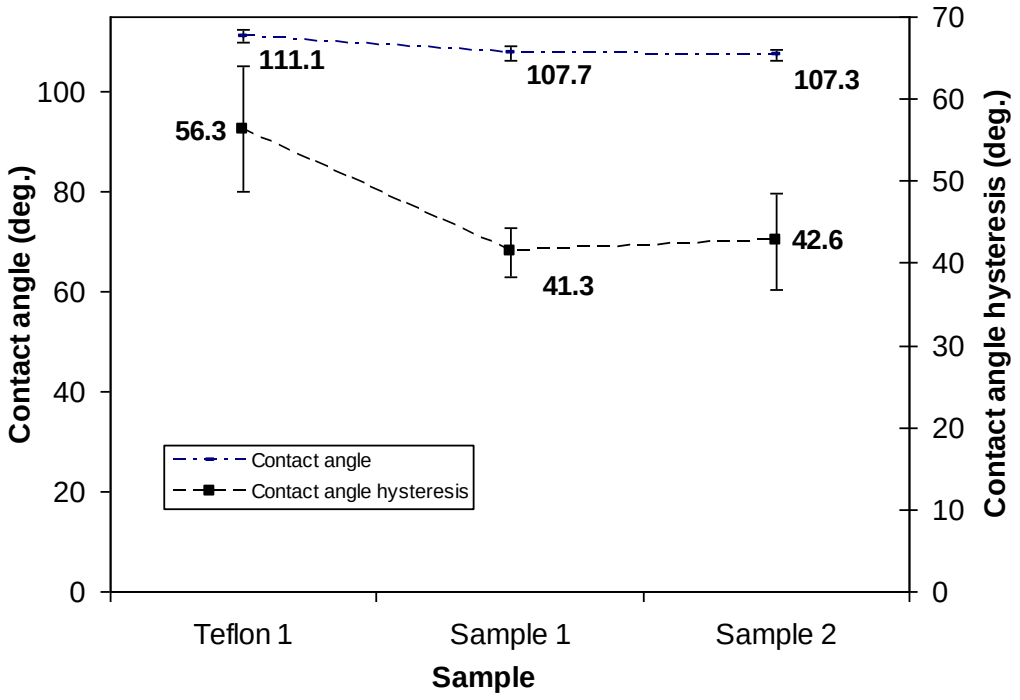

Fig.6. 8. CA and CAH values of plasma-sputtering on Teflon and PS coatings without mesh.

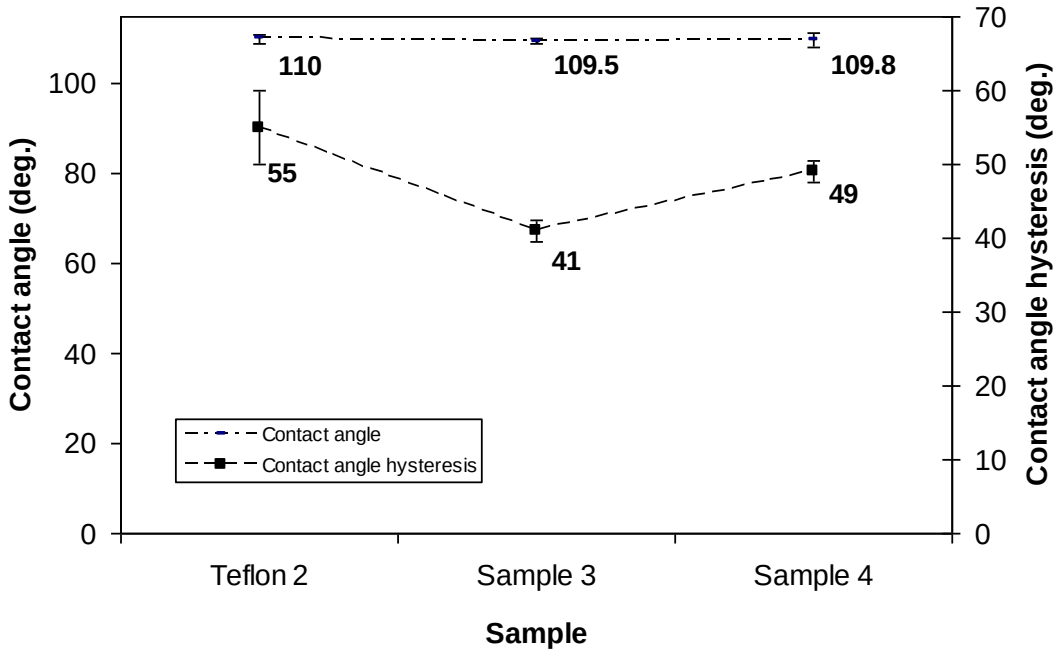

Fig.6. 9. CA and CAH values of plasma-sputtering on Teflon 1 and (Sample 1 and 2 with mesh).

Also, if Figure 6.8 is compared with Figures 6.1 and 6.2, the CA and CAH values of prepared HCs without using a mask were ~ 107^{o} and ~ 41^{o}, respectively, while in the case of prepared HCs using a mask the contact angle values were ~ 113^{o} and ~ 114^{o} and the CAH values were ~ 24^{o}-32^{o}. Therefore, it can be concluded that by using copper gauze as a mask it is possible to have more control preparing a HC and thus covering the surface periodically. In other words, this observation confirms the importance of the method of preparation of HCs. In order to further study the effect of roughness on hydrophobic properties an optical profilometry analysis was performed.

6.4.1 Optical profilometry analysis

Figure 6.10 (a and b) shows the optical profilometry images of Sample 2 (a) and Sample 4 (b). The root mean square (Sq) of Sample 2 showed a value of 24.6 nm, while for Sample 4 the Sq value was 47.6 nm. A difference of Sq value about 23 nm was observed between Sample 2 and Sample 4. However, the value of Sq or created rough structure on the coating did not have any significant effect on hydrophobic properties of HCs, as the contact angle values did not increase and CAH values did not decrease, considerably (see Figures 6.8 and 6.9).

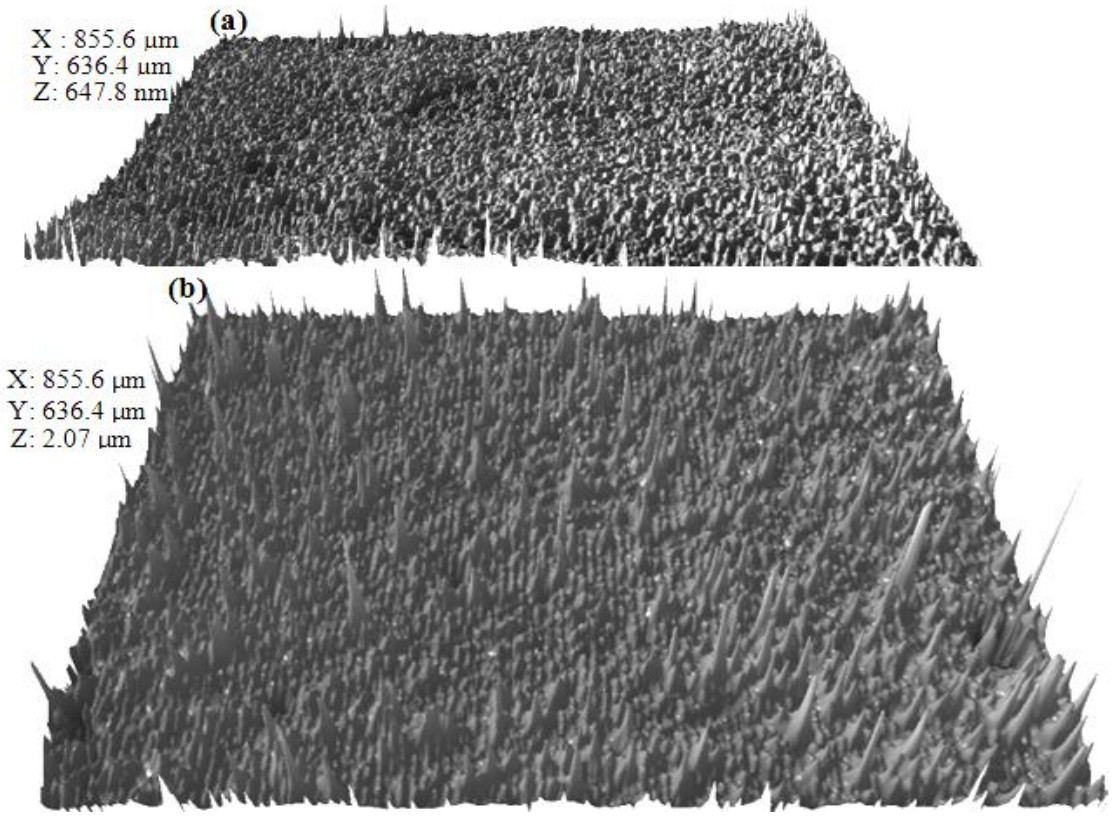

Fig.6. 10. Optical profilometry images of Sample 2 (a) and Sample 4 via plasma method (b).

In addition, the results obtained from the profilometry analysis give a major reason for the enhancement of contact angle values (~ 113^{o} and ~ 114^{o}) and the decrease in CAH values (~ 24^{o}-32^{o}) compared to Figure 6.8; there is a heterogeneity effect created by the plasma method through a mask.

6.5 Heterogeneity effect on the interaction energy between coating and water molecules

To determine the heterogeneity effect the interaction energy between coatings prepared by the plasma sputtering method and water droplet was calculated. As mentioned in chapters 4 and 5 the interaction energy values of homogeneous and HCs on aluminum surface were calculated by the following equation (6.1), [102]:

$$K_A = \left[\rho\left(\frac{2-3\cos\theta+\cos^3\theta}{3}\right)\right]^{1/3} \frac{g}{2}\left(\frac{m}{\pi}\right)^{2/3} \frac{\sin\alpha}{\sin\theta} \qquad \textbf{(6.1)}$$

Table 6. 3. The values of interaction energy between a water droplet and a homogeneous or heterogeneous "masked" plasma coating.

Sample	α (deg.)	θ (deg.)	m (mg)	K (mJ/m^2)
PE-spin	45	95.7	45	19.171
PS-spin	50	91	45	19.908
PTFE	46	90.5	45	18.612
PE-PTFE	18	100	45	**8.726**
PS-PTFE	20	98	45	**9.474**

As is obvious in table 6.2 the smallest value of the interaction energy was obtained for heterogeneous PE-PTFE and PS-PTFE coatings. The interaction energy value for homogeneous coatings of PE-spin and PS-spin were 18.79 and 19.5 mJ/m^2, respectively. A considerable decrease of interaction energy values was observed for the HCs of PE-PTFE and PS-PTFE as 8.3 and 9.2 mJ/m^2, respectively. Therefore, the obtained results from empirical and theoretical efforts in this section definitely confirmed the heterogeneity effect resulting from dissimilar hydrophobic functions of C-H and C-F on the hydrophobicity of such coatings.

6.6 Conclusions

A third method of preparing HCs, by a plasma method through a mask, was used and investigated. This method was chosen with three aims in mind:

(1) To prove the heterogeneity effect, based on the objectives of this research work;

(2) To have more control of the fabrication of HCs, while covering the surface periodically; this aim was achieved by using the copper gauze as a mask on the homogeneous PE and PS coatings before applying the RF-sputtered PTFE coating.

(3) To reduce or even avoid the effect of roughness on the hydrophobic properties of a HC and thus focus only on the heterogeneity effect resulting from dissimilar hydrophobic functions.

To achieve these aims the wetting behavior, surface morphology and chemical characterization of homo- and heterogeneous plasma coatings through a mask were

studied and investigated. All the characterizations proved the heterogeneity effect on the hydrophobic properties of prepared HCs by a plasma sputtering method through a mask. Furthermore, the surface morphology of HCs showed that the roughness of sputtered PTFE coating did not have a significant influence on hydrophobic properties. Therefore, all the three methods of preparing HCs indicated the presence of the heterogeneity effect to improve hydrophobic properties, so far.

In the following chapter, the heterogeneity effect on icephobic properties of prepared HCs via *SAM*s, nanoparticles and plasma through a mask will be studied. The durability of HCs against icing-de-icing cycles, UV exposure, immersion in distilled water and different pH solutions will be investigated.

CHAPTER VII

ICEPHOBIC PROPERTIES AND DURABILITY OF HOMO- AND HETEROGENEOUS COATINGS

7. Introduction

In the present chapter, we study the icephobic properties and the ageing of prepared coatings under UV degradation, in various pH solutions and over successive icing/de-icing cycles. To do this, an attempt is made to reduce the strength of adhesion of ice to the surfaces by applying icephobic coatings. The durability of coated samples under UV degradation and in various pH solutions is evaluated by contact angle measurement. In the meantime, the contact angle values (as a function of the number of icing/de-icing cycles) were measured after each icing/de-icing cycle on the coated samples. The XPS analyses are used to characterize the surface coatings.

7.1 Ice adhesion tests for homo- and HCs

7.1.1 *SAM*s coatings

The ice adhesion tests were carried out on homo- and heterogeneous coated samples under the conditions explained in detail in Section 3.7. Table 7.1 presents the values for the shear stress of ice detachment and the ice adhesion reduction factor (*ARF*) for coated samples of OD-OD, PF-PF, OD-PF and PF-OD.

Table 7. 1. The shear stress of ice detachment and *ARF* values of homo- and heterogeneous *SAM*s coatings with 6 h IT.

Sample	Shear stress of ice detachment (kPa)	*ARF*
Polished Al	226.5 ± 27	1
OD-OD	193.7 ± 20	1.16 ± 0.12
PF-PF	211.2 ± 19	1.07 ± 0.09
OD-PF	145.9 ± 13	1.55 ± 0.13
PF-OD	152.2 ± 16	1.48 ± 0.15

This table shows that the initial shear stress values of ice detachment for the heterogeneous coated samples (OD-PF and PF-OD) are lower than those for the homogeneous ones (OD-OD and PF-PF). Also, the ice adhesion reduction factor (*ARF*) for all samples demonstrates that the ice adhesion strength values are ~ 1.1 (homogeneous case) and ~ 1.5 times (heterogeneous case) lower than those obtained on a polished aluminum sample. That is, the *ARF* values for HCs are larger than for homogeneous coatings. This observation is another proof of the heterogeneity effect.

As was mentioned in Chapter 4, by increasing the immersion time (IT), the efficiency of formation of *SAM*s on a surface can be described in terms of order degree of self assemble monolayer and thus the surface coverage [91-93]. It was also observed in Chapter 4, that by increasing the IT from 6h to 12h, the aluminum surfaces coated with PF-OD and OD-PF became super-hydrophobic. Now, it is well-known that super-hydrophobic surfaces with low wetting hysteresis (CAH) are in fact icephobic surfaces [15]. Therefore, in this chapter, to study the effect of IT on icephobic properties, the ice adhesion tests were done on prepared homo- and heterogeneous *SAM*s coatings for 12 h IT. Table 7.2 shows the values for the shear stress of ice detachment and the ice adhesion reduction factor (*ARF*) of homo- and heterogeneous coated samples of OD-OD, PF-PF, OD-PF and PF-OD for 12 h IT. The *ARF* values for homo- and HCs show that the ice adhesion strength is ~ 1.5 and ~ 3 times lower than that obtained on a polished Al sample, respectively. In addition, these results for 12 h IT showed a greater reduction of ice adhesion compared to all prepared samples for 6 h IT. This reduced ice adhesion strength can be resulted from well ordered *SAM*s fabrications on the aluminum oxide layer as well as more rougher aluminum substrate compared to a shorter immersion time [61,91-93,95].

Table 7. 2. The shear stress of ice detachment and *ARF* values of homo- and heterogeneous *SAM*s coatings with 12 h IT.

Sample	Shear stress of ice detachment (kPa)	*ARF*
Polished Al	226.5 ± 27	1
OD-OD	177.2 ± 15	1.53 ± 0.1
PF-PF	195.2 ± 16	1.43 ± 0.09
OD-PF	71.5 ± 15	3.1 ± 0.7
PF-OD	95.6 ± 13	2.37 ± 0.32

As was described in Chapter 4, to further study wetting and icephobic properties of HCs, trichloro(octyl)silane (OT) with 8 carbons as a different alkyl chain length has been chosen. The icephobic properties of all coated samples prepared from OT (1 mM) and PF (6 mM) for 12 h immersion time are shown in table 7.3. This table shows that the shear stress of ice detachment values of heterogeneous samples (OT-PF and PF-OT) are lower than those of homogeneous coated samples of OT-OT and PF-PF. The ice adhesion reduction factor (*ARF*) of all homo- and heterogeneous samples also show the ice adhesion strength to be ~ 1.1 and ~ 1.2 times lower than those obtained on the polished bare aluminum sample, respectively.

Table 7. 3. The shear stress of ice detachment values and *ARF* values of homo- and HCs prepared from OT (1mM) and PF (6 mM) for 12 h IT.

Sample	Shear stress of ice detachment (kPa)	*ARF*
Polished Al	226.5 ± 27	1
OT-OT	213.1 ± 12	1.04 ± 0.06
PF-PF	195.2 ± 16	1.11 ± 0.09
OT-PF	169.5 ± 15	1.22 ± 0.11
PF-OT	182.1 ± 13	1.18 ± 0.08

However, the shear stress of ice detachment values were not observed to be as small as those obtained in the case of coated samples prepared from OD for 12 h IT. This behavior highlights the increase of the *steric effect* that prevents well-ordering of *SAM*s molecules on aluminum substrates, as explained in chapter 4 [96].

Since the project aims in studying and developing HCs on aluminum alloy substrates which would reduce ice accumulation, therefore, their durability in terms of repeated icing/de-icing conditions similar to real conditions was considered as well. In order to study the durability of prepared coated samples, the shear stress of ice detachment of homo- and heterogeneous *SAM*s coatings as a function of the number of icing/de-icing cycles is presented in the following section.

7.1.2 Durability of *SAM*s coatings

In order to evaluate the durability of homo- and heterogeneous *SAM*s coatings for 6h IT, one sample was subjected to 9 successive icing/de-icing cycles. It can be seen in Figure 7.1 that the ice-releasing performance of the coated samples somewhat deteriorated over 9 icing/de-icing cycles. After 9 cycles the values of shear stress of ice detachment are close to those obtained on polished aluminum surface. This can be explained by some damage to the coatings caused by icing/de-icing. The hydrophobic properties of those surfaces were evaluated after each icing/de-icing cycle (see Fig. 7.2).

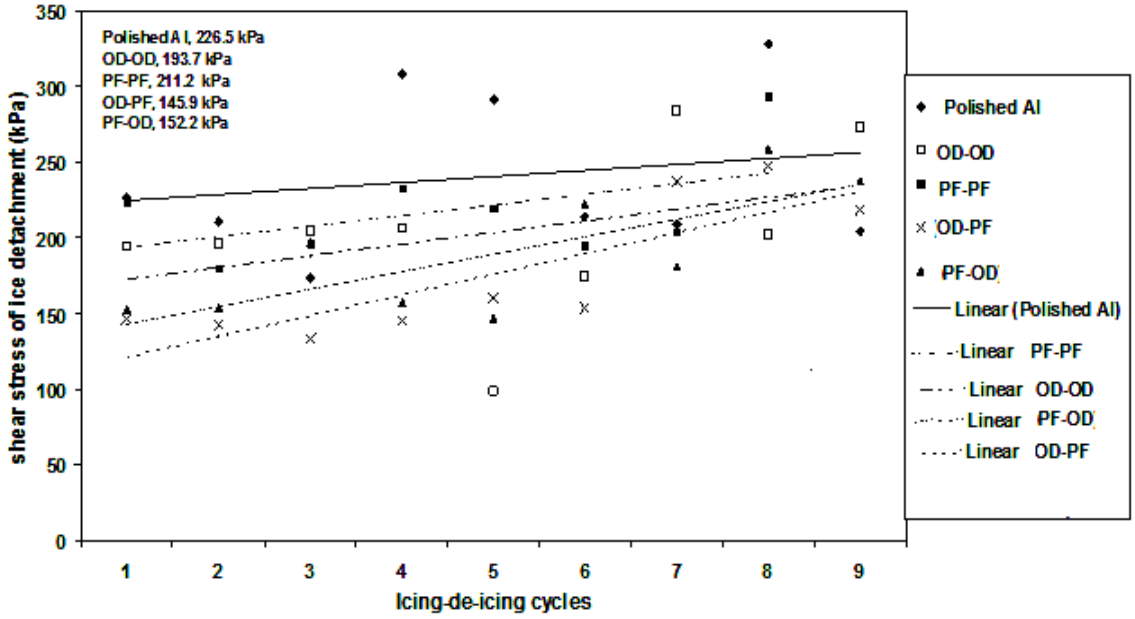

Fig.7. 1. Shear stress of ice detachment *vs.* number of icing/de-icing cycles for different prepared samples with 6h IT. The numbers mentioned are the first values of shear stress of ice detachment.

Figure 7.2 shows the contact angle and CAH values of homo- and heterogeneous *SAM*s coatings for 6 h IT after a number of icing/de-icing cycles. After 9 cycles, the contact angle values of the homogeneous coated samples of OD-OD decreased from ~ 141^{o} to ~ 112^{o} and in the case of PF-PF decreased from ~ 121^{o} to ~ 99^{o}. The contact angle values of the heterogeneous samples of OD-PF and PF-OD decreased from ~ 150^{o} to ~ 114^{o} and the CAH values in the case of all coated samples increased to ~ 50-70^{o}. Therefore, all coated samples showed a reduction in contact angle values after a certain number of icing/de-icing cycles. This observation confirms that the coated surfaces were partially damaged and removed during icing/de-icing experiments.

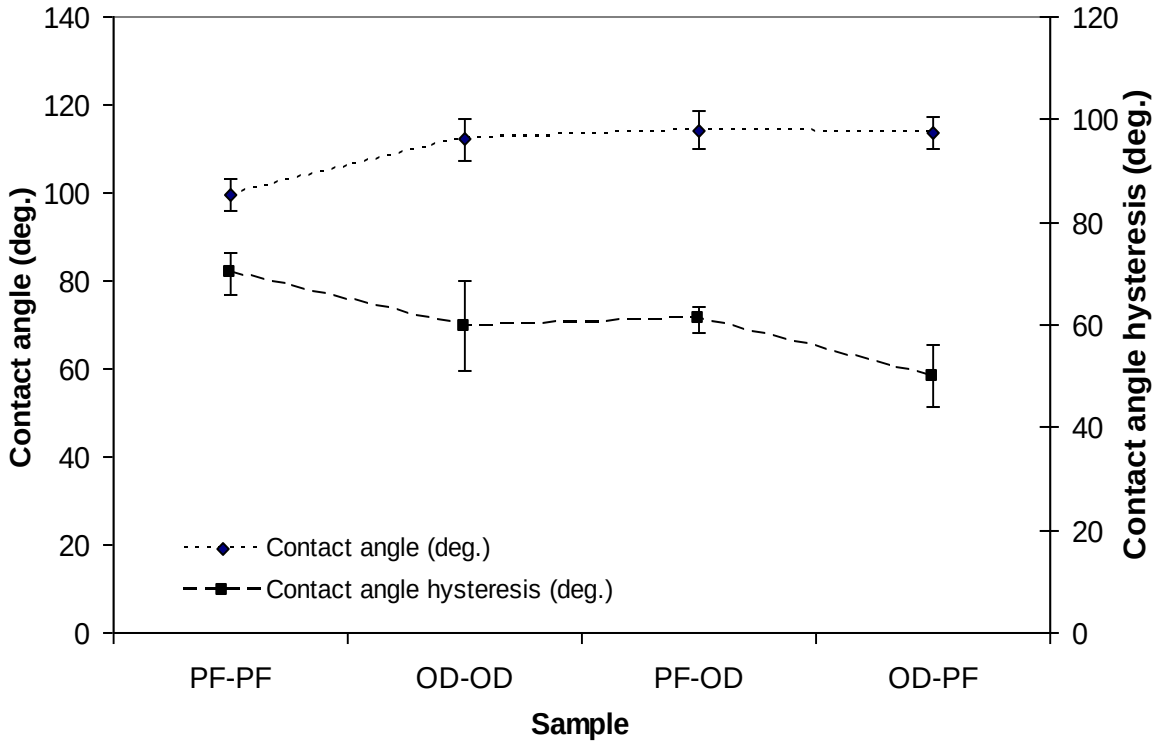

Fig.7. 2. CA and CAH values of coated samples for 6h IT after 9 icing/de-icing cycles.

Figure 7.3 presents the shear stress of ice detachment values of homo- and heterogeneous coated samples with 12h IT as a function of icing/de-icing cycles, in order to study the durability of coated samples. For each coating in question, one sample was subjected to 12 consecutive icing/de-icing cycles. It is evident from Figure 7.3 that the anti-ice performance of the coated samples slightly degraded after 12 icing/de-icing cycles. This can be explained by partial damage to the coatings caused by the icing/de-icing experiment and ice-removal step. Moreover, it can be seen in Figure 7.3 that after 12 cycles the values of shear stress of ice detachment of homogeneous samples are close to those obtained on polished aluminum surface. However, the shear stress of ice detachment

values of HCs compared to homogeneous samples after 12 cycles are close to those obtained on polished aluminum surface.

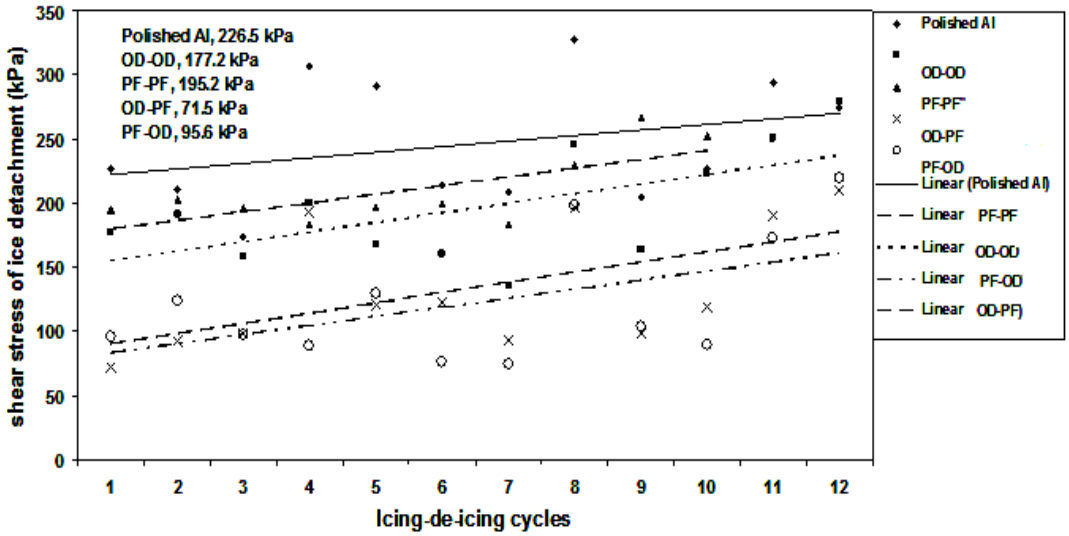

Fig.7. 3. Shear stress of ice detachment *vs.* icing/de-icing cycle number of different prepared samples, OD (1mM) and PF (6mM) for 12 h IT. The numbers mentioned are the first values of shear stress of ice detachment.

The hydrophobic properties of homo- and HCs after 12 cycles of icing/de-icing are presented in Figure 7.4. The contact angle values of OD-OD and PF-PF samples (12 h immersion time) decreased from ~ 141^{o} and ~ 121^{o}, respectively, to ~ 109^{o}, and the contact angle values of HCs of OD-PF and PF-OD decreased from ~ 160^{o} and ~ 154 ^{o} to ~ 122 ^{o}. The CAH values of homo- and HCs for the 12 h IT increased to ~ 40-70^{o}.

This reduction in contact angle values after 12 icing/de-icing cycles confirms the partial deterioration and damage of coated surfaces during icing/de-icing experiments.

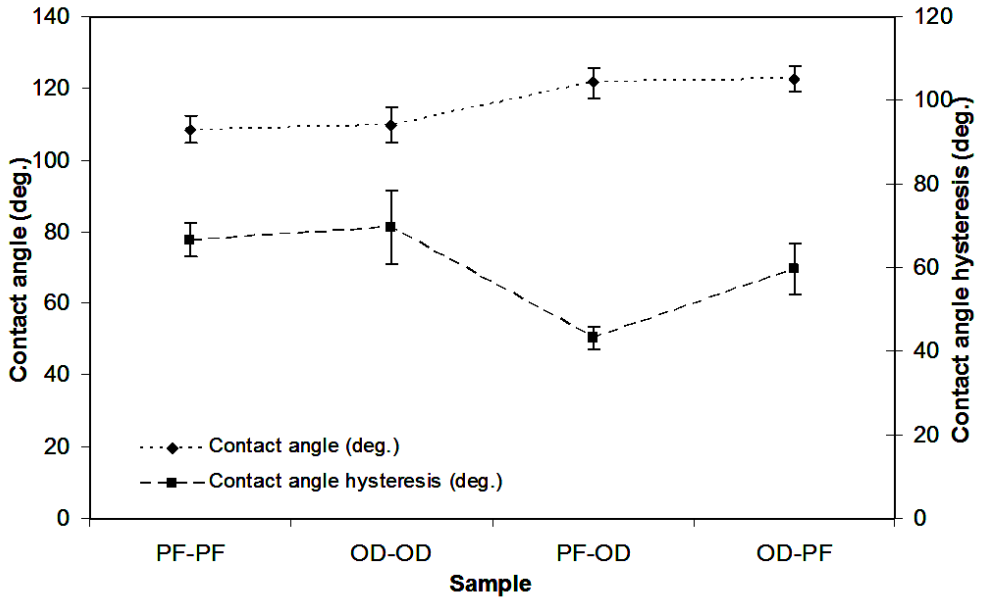

Fig.7. 4. CA and CAH values for coated samples for 12 h ITs after 12 icing/de-icing cycles.

Figure 7.5 illustrates shear stress values of ice detachment after 7 icing/de-icing cycles for homo- and heterogeneous coated samples of OT (1mM) and PF (6mM) for 12 h IT.

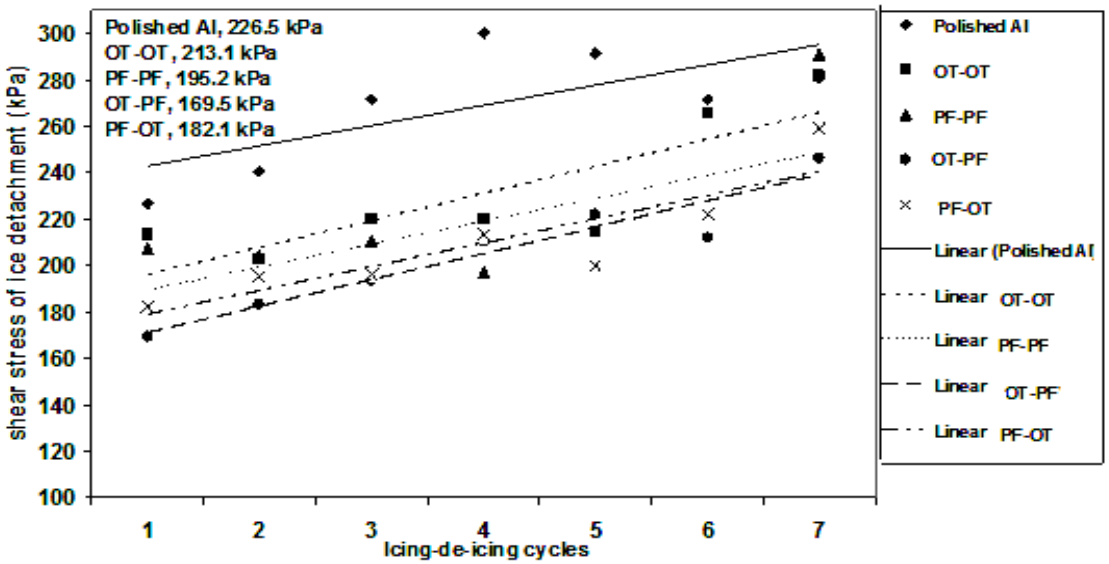

Fig.7. 5. Shear stress of ice detachment *vs.* number of icing/de-icing cycles for different prepared samples, OT (1mM) and PF (6mM) for 12 IT. The numbers mentioned are the first values of shear stress of ice detachment.

As is shown in Figure 7.5 the anti-ice performance of the coated samples deteriorated after 7 icing/de-icing cycles. If it is compared to homo- and heterogeneous samples prepared from OD (1mM) and PF (6mM) for 6 and 12 h IT, their durability is lowest. The reason is again the increase of the *steric effect* that happens by applying OT molecules instead of OD molecules [96].

Figure 7.6 shows the contact angle values after 7 icing/de-icing cycles for homo- and HCs of OT (1mM) and PF (6 mM) with 12 h IT. The CA values of OD-OD and PF-PF samples (12 h IT) decreased from ~ 124^{o} and ~ 118^{o} to ~ 100^{o} and ~ 105^{o}, respectively. Meanwhile, the CAH values of all coated samples increased to more than 60^{o}.

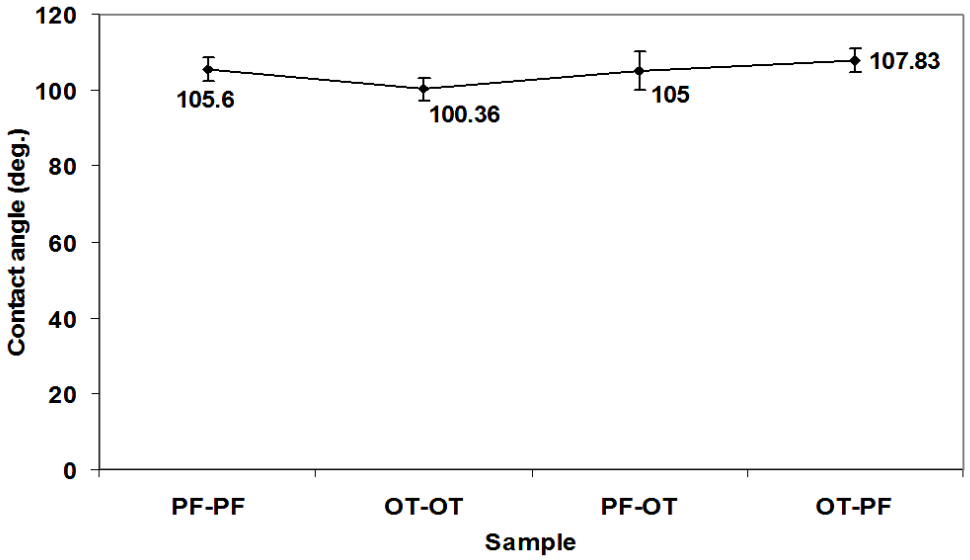

Fig.7. 6. CA values for samples with 12 h ITs after 7 icing/de-icing cycles.

7.1.3 Nanoparticles coatings

Ice adhesion tests were carried out on homo- and HC nanoparticles coatings. Table 7.4 shows the values of shear stress of ice detachment and the ice adhesion

reduction factor (*ARF*) of homogeneous PE, PS and PMMA and HCs made of PE, PS and PMMA coated with nanoparticles of PTFE and Al_2O_3, separately.

Table 7. 4. The shear stress of ice detachment and *ARF* values of homo- and HCs prepared with PE, PS, PMMA, PTFE and Al_2O_3.

Sample	Shear stress of ice detachment (kPa)	*ARF*
Polished Al	251.5 ± 27	1
PE-spin	220.8 ± 19.3	1.14 ± 0.1
PE-PTFE	190.7 ± 34	1.32 ± 0.24
PE-Al_2O_3	235 ± 19	1.06 ± 0.087
PS-spin	232.3 ± 14.9	1.08 ± 0.069
PS-PTFE	199.3 ± 31.2	1.26 ± 0.2
PS-Al_2O_3	243.7 ± 11.4	1.03 ± 0.04
PMMA-spin	228.2 ± 12.9	1.1 ± 0.06
PMMA-PTFE	189.3 ± 44.4	1.32 ± 0.33
PMMA-Al_2O_3	237.1 ± 14.49	1.05 ± 0.065

The table above shows that the shear stress values of ice detachment for HCs of PE-PTFE, PS-PTFE and PMMA-PTFE are smaller than for homogeneous (PE, PS, and PMMA) and HC coated samples of PE-Al_2O_3, PS-Al_2O_3 and PMMA-Al_2O_3. Also, the ice adhesion reduction factor (*ARF*) of all homo- and heterogeneous samples shows that the ice adhesion strength values are at least ~ 1.03 and ~ 1.3 times lower than those obtained on polished aluminum samples, respectively. It is indeed evident in Table 7.4 that the values for the shear stress of ice detachment for the PE-Al_2O_3, PS-Al_2O_3 and PMMA-Al_2O_3 are greater than those for the homogeneous coatings PE, PS, and PMMA. It is

worthy to mention that the shear stress values of ice detachment for the PE+Al_2O_3 and PE+PTFE samples were generally greater than those obtained on polished aluminum samples. This fact is obvious from the CAH values of homo- and HCs made with PE, PTFE and Al_2O_3. Thus, the CAH values for the HCs of PE-Al_2O_3, PE+Al_2O_3 and PE+PTFE samples were greater than for the homo- and HCs of PE-spin and PE-PTFE, respectively. This is therefore in agreement with the values of the shear stress of ice detachment [15]. As was mentioned in Chapter 5, the reason for the enhanced CAH values in the case of the PE-Al_2O_3, PE+Al_2O_3 and PE+PTFE compared to homogeneous samples is the topological nature of the surface roughness which is of prime importance in determining hydrophobicity [112-116].

Chapter 5 mentioned several types of polymeric coatings including -CH_3 or -CH_2 moieties which were placed in a horizontal orientation. In order to have a surface with a vertical branch of -CH_2 or -CH_3 groups, self assembled monolayers (*SAM*s) were used and then a layer of nanoparticles were placed on them. Therefore, the STA was chosen to have different positions of the -CH_2 or -CH_3 groups, in order to see any influence on the heterogeneity effect. Table 7.5 shows values for the shear stress of ice detachment and the ice adhesion reduction factor (*ARF*) of homogeneous and HCs made of STA, STA-PTFE and STA- Al_2O_3. The ice adhesion reduction factor (*ARF*) of all homo- and HCs shows that the ice adhesion strength values are at least ~ 1.1 and ~ 1.7 times lower than those obtained on a polished aluminum sample, respectively. The shear stress of ice detachment of the STA-PTFE sample is lower than the homogeneous coating STA-spin and the STA-Al_2O_3 sample. The ice adhesion strength of the STA-Al_2O_3 sample is greater than that of the homogeneous STA coating. This behavior was explained earlier [15].

Therefore, by changing the coating including a horizontal orientation of $-CH_2$ or $-CH_3$ moieties with a coating including vertical branch of $-CH_2$ or $-CH_3$ groups, the heterogeneity effect was observed.

Table 7. 5. The shear stress of ice detachment and *ARF* values of prepared samples from STA, PTFE and Al_2O_3.

Sample	Shear stress of ice detachment (kPa)	*ARF*
Polished Al	251.5 ± 27	1
STA-spin	185.5 ± 17.1	1.35 ± 0.12
STA-PTFE	141.5 ± 15.6	1.78 ± 0.19
STA-Al_2O_3	218.6 ± 10.1	1.15 ± 0.05

7.1.4 Durability of nanoparticles coatings

In order to study the durability of prepared homo- and heterogeneous nanoparticles coatings, the shear stress of ice detachment of homo- and HCs as a function of icing/de-icing cycles was evaluated. However, the durability of HCs in terms of anti-ice performance over time is very short, because the coated samples deteriorated after 2 icing/de-icing cycles in the case of prepared samples of PE, PS and PMMA. Table 7.6 and Figure 7.7 show the XPS analysis results of the PE-PTFE sample before and after 2 icing/de-icing cycles. The table shows that the percentage of spectrum F1s is 26.4% before icing/de-icing but only 10.10% after two icing/de-icing cycles. This means that after icing/de-icing twice, the PTFE nanoparticles were partially removed during the experiments (see Fig. 7.8).

Table 7. 6. XPS results of PE-PTFE sample before and after two icing/de-icing cycles.

Element	C 1s %	F 1s %	O 1s %	Si 2p %
Before icing/de-icing	68.30	26.41	2.86	2.18
After 2 times icing/de-icing	83.37	10.10	5.26	1.28

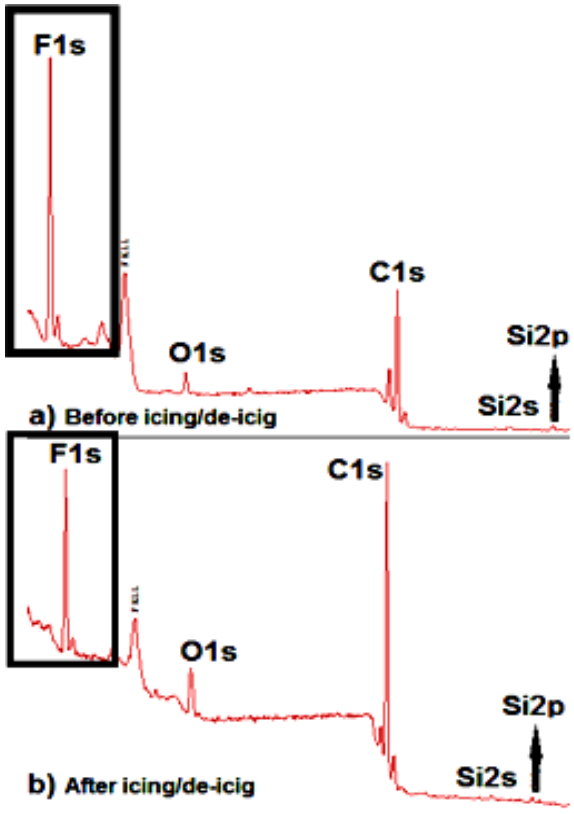

Fig.7. 7. Survey XPS spectra of PE-PTFE sample before and after icing/de-icing.

Figure 7.7 also confirms that in case of HC the PTFE nanoparticles were removed during icing/de-icing experiments. As is evident in Figure 7.7, the intensity of the F1s peak for PE-PTFE sample before icing/de-icing tests (Fig. 7.7a) is more than the intensity of the F1s peak after icing/de-icing tests (Fig. 7.7b).

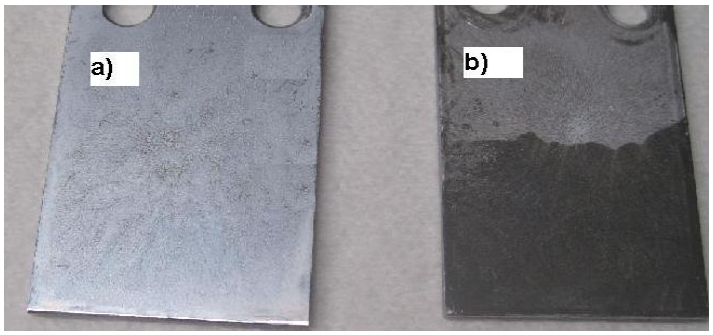

Fig.7. 8. Image of heterogeneous PE-PTFE sample before (a), and after two icing/de-icing cycles (b).

Figure 7.9 shows shear stress values of ice detachment of homo- and HCs prepared with STA, PTFE and Al_2O_3. For each coating studied, one sample was subjected to 4 successive icing/de-icing cycles. It can be seen in Figure 7.9 that the anti-ice performance of the coated samples was destroyed after 4 icing/de-icing cycles. This can be explained by some damage to the coatings caused by several icing/de-icing cycles.

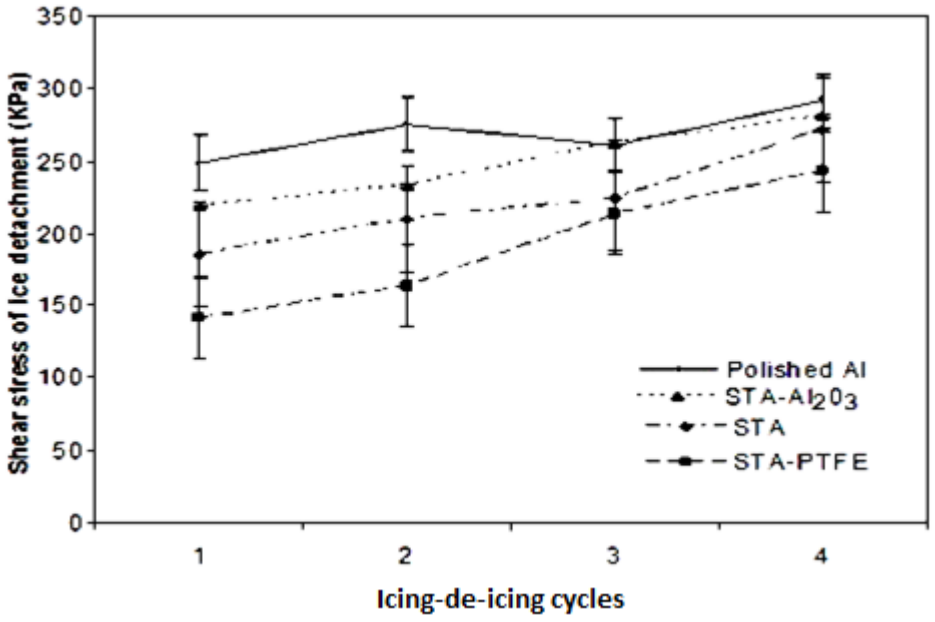

Fig.7. 9. Shear stress of ice detachment *vs.* number of icing/de-icing cycles for various prepared samples (STA, STA-PTFE and STA- Al_2O_3).

Table 7.7 shows the CA values of prepared homogeneous and HC samples of PE, PS, PMMA and STA before and after the icing/de-icing test. However, the durability of HCs in terms of anti-ice performance over time is very short, because the coated samples deteriorated after 2 icing/de-icing cycles in the case of prepared samples of PE, PS and PMMA. The contact angle values of homo- and HCs prepared with STA, PTFE and Al_2O_3 decreased to ~ 95^o-100^o after four icing/de-icing cycles. This reduction in CA values after two icing/de-icing cycles confirms that in the case of HCs the PTFE and Al_2O_3 nanoparticles were removed during the icing/de-icing experiments. This was observed visually (see Fig. 7.8) as well.

Table 7. 7. CA values of homo- and HC samples of PE, PS, PMMA before and after icing/de-icing twice and STA before and after four icing/de-icing tests.

Sample	CA value (deg.) before icing/de-icing	CA value (deg.) after icing/de-icing
PE-spin	100 ± 0.36	97.1 ±1.85
PE-PTFE	129.6 ± 0.6	96 ± 1.67
PE-Al_2O_3	116.2 ± 2.1	95.7 ± 1.2
PS-spin	95.3 ± 0.6	90.2 ± 2.4
PS-PTFE	119.4 ± 0.7	96.5 ± 3.8
PS-Al_2O_3	109.5 ± 0.8	88.7 ± 1.7
PMMA-spin	94.2 ± 0.91	88.2 ± 2.5
PMMA-PTFE	120.3 ± 0.94	89.7 ± 4.5
PMMA-Al_2O_3	108.4 ± 0.95	88.8 ± 1.9
STA-spin	107.7 ± 1.4	95.9 ± 2.6
STA-PTFE	125.8 ± 1.2	100.6 ± 1.6
STA-Al_2O_3	114.6 ± 1.6	99.2 ± 1

7.1.5 Plasma sputtering coatings

Table 7.8 shows the values of the shear stress of ice detachment and the ice adhesion reduction factor (*ARF*) of homogeneous (PE and PS) and HC (PE-PTFE and PS-PTFE at 0.41 mm) coatings prepared by plasma sputtering through a mask (see section 5.2). The table shows that the ice adhesion strength values for the above HCs are smaller than those for the homogeneous ones. In addition, the ice adhesion reduction factor of all homogeneous and heterogeneous samples shows that the ice adhesion strength values are at least ~ 1.11 and ~ 1.37 times lower than those obtained on a polished Al sample, respectively.

Table 7. 8. The shear stress values of ice detachment and *ARF* values of coatings made by plasma sputtering.

Sample	Shear stress of ice detachment (kPa)	*ARF*
Polished Al	251.5 ± 27	1
PE	226.61 ± 11.9	1.11 ± 0.05
PS	222.89 ± 6.45	1.13 ± 0.03
PE-PTFE	183.18 ± 14.2	1.37 ± 0.1
PS-PTFE	200.33 ± 10.2	1.25 ± 0.06

7.1.6 Durability of plasma sputtering coatings

For each coating in question, one sample was subjected to 10 consecutive icing/de-icing cycles. It is evident from Figure 7.10 that the anti-ice performance of the coated samples slightly degraded after 10 icing/de-icing cycles.

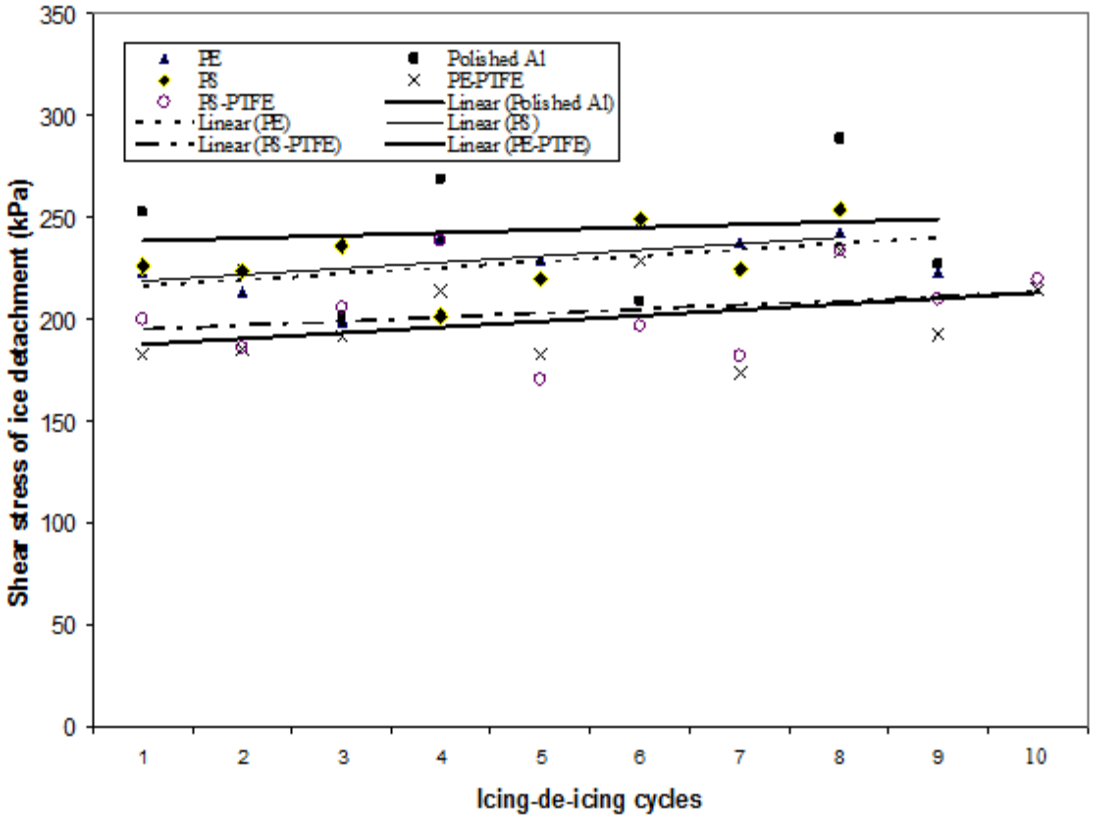

Fig.7. 10. Shear stress of ice detachment *vs.* number of icing/de-icing cycles for samples prepared by the plasma sputtering method.

Therefore, it is obvious from these results that the durability and stability of prepared HC samples coated by the plasma sputtering method are definitely higher than those obtained from other methods. The hydrophobic properties of those homo- and HCs after 10 cycles of icing/de-icing are shown in Figure 7.11. The contact angle values of homogeneous coatings of PS and PE decreased from ~ 95^{o} to ~ 90^{o} and from ~ 86^{o} to ~ 84^{o}, respectively. The contact angle values of HCs of PE-PTFE and PS-PTFE diminished from ~ 113^{o} to ~ 109^{o}. This minor reduction in contact angle values after 10 icing/de-icing cycles demonstrates the stability and durability of the coatings prepared by the

plasma sputtering method. In other words, the HC coated surfaces were only slightly damaged during the aforementioned icing/de-icing experiments.

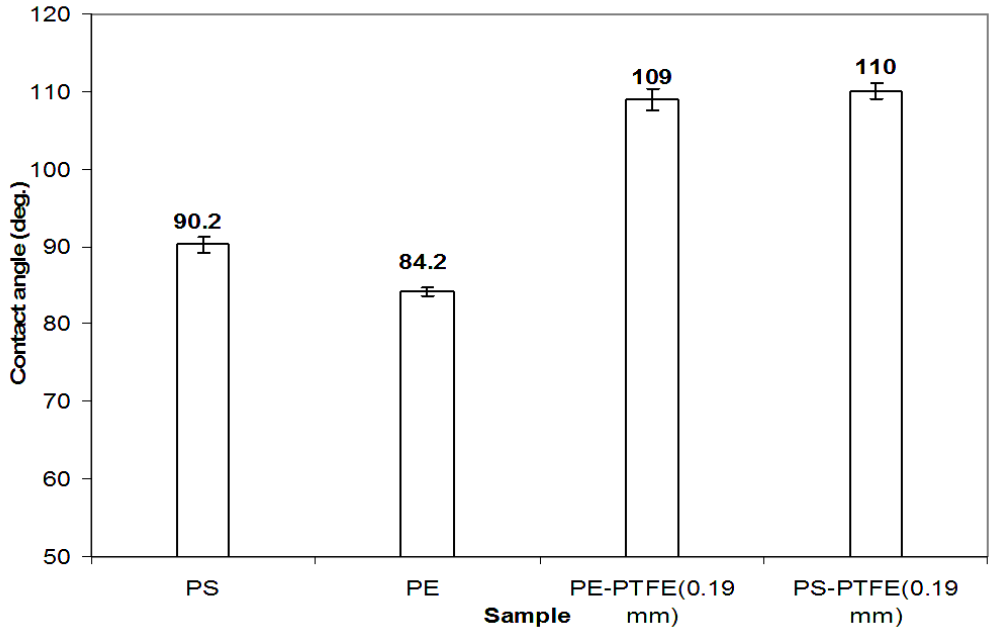

Fig.7. 11. CA values on a polished Al 6061 alloy coated by the plasma sputtering method, after 10 icing/de-icing cycles.

7.2 Effect of different pH solutions on hydro- and ice- phobic properties of homo- and HCs

These icephobic coatings must necessarily accomplish both of the following requirements: first, they must efficiently reduce snow or ice adhesion force, and second, they must have a reasonably long service-life or durability. The first requirement was studied in the above sections. For the second requirement, the homo- and heterogeneous *SAM*s, nanoparticles and plasma sputtering coatings were examined under different conditions, in various pH solutions and UV degradation. The long service-life or

durability of the coatings is important factor in the lifetime of a coating under extreme environmental conditions.

7.2.1 *SAM*s coatings

In order to study the durability of the coating in different conditions which are similar to those happening in real situations, the coatings were immersed in different pH (4, 7 and 10) solutions.

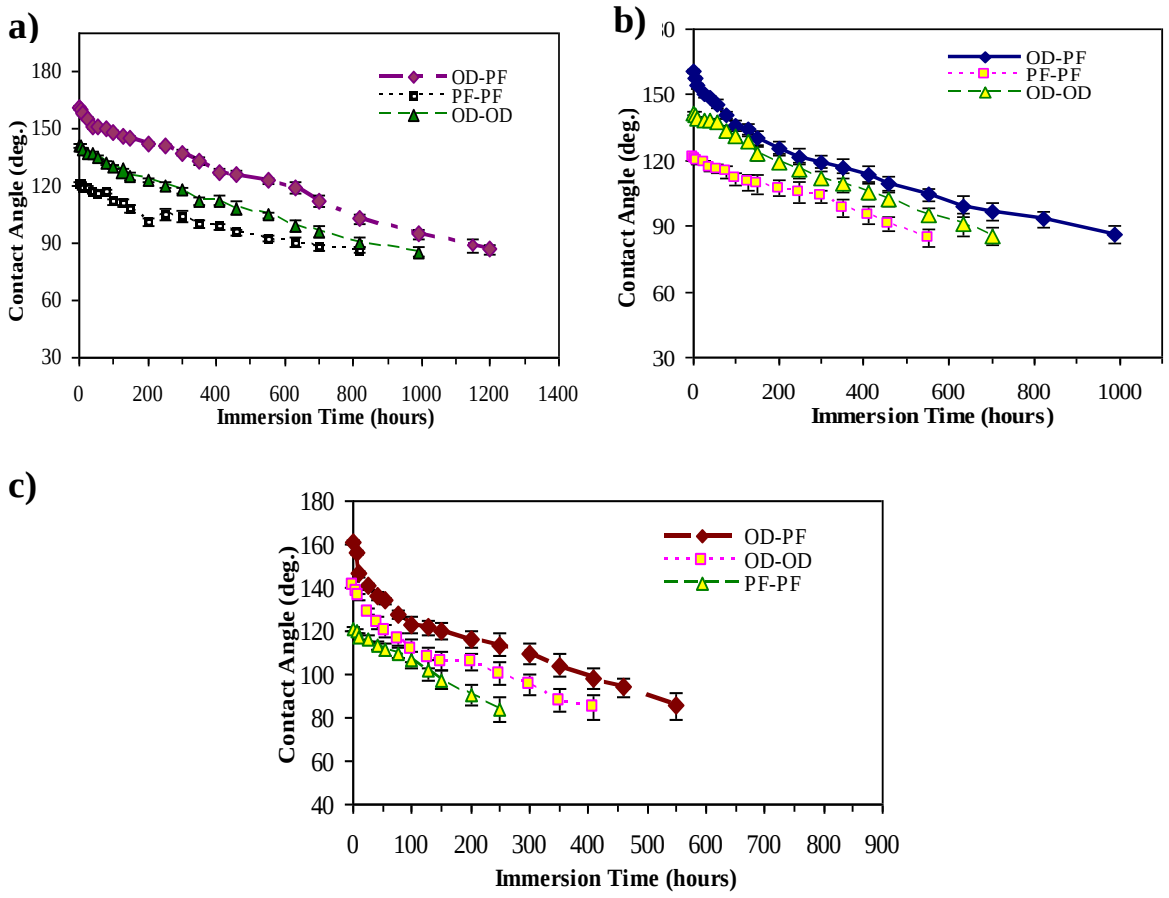

Fig.7. 12. CA values for homo- and heterogeneous *SAM*s coatings as a function of IT in a) distilled water (pH=7), b) acidic (pH=4) and c) basic (pH=10) solutions.

Figure 7.12 (a, b and c) shows the contact angle values for aluminum samples coated with homogeneous (OD-OD and PF-PF) and heterogeneous (OD-PF) coatings as a function of immersion time (IT), in distilled water as well as basic and acidic media. A heterogeneous (OD-PF) coating was used as the best coating for having high static contact angle and low contact angle hysteresis.

As it is obvious in Figure 7.12, the coated samples immersed in distilled water (pH= 7), were found to gradually lose their hydrophobic properties after ~ 800h, which was associated with the decrease of contact angle values from ~ 121 ^{o}, ~ 141 ^{o} and ~ 160 ^{o} to ~ 85-87^{o}, respectively, for PF-PF, OD-OD and OD-PF, (Fig.7.12a). This reduction was slower for the heterogeneous OD-PF coating. By immersing the coated samples in acidic media, the CA values decreased to ~ 84-86^{o} after ~ 550h (Fig.7.12b). More precisely, for the OD-PF sample the contact angle values decreased after ~ 990 h. This tendency to lose hydrophobicity is most likely due to hydrolysis of the Al-O-Si-R bonds, leading to formation of Al-OH and RSi-OH components (-OH groups), a rather hydrophilic functional group on aluminum samples [62]. The contact angle values of homogeneous OD-OD and PF-PF and heterogeneous OD-PF samples as a function of immersion time in basic media are shown in Figure 7.12c. It can be seen that the contact angle values decreased faster, from ~ 121 ^{o}, ~ 141 ^{o} and ~ 160 ^{o} to ~ 84-85^{o}, respectively, for PF-PF, OD-OD and OD-PF compared to distilled water (pH=7) and acidic (pH=4) solutions. In other words, the results showed that the coating is more stable in acidic and neutral than in basic media. This observation can be attributed to the influence of basic conditions on aluminum oxide layer stability and therefore, the rate of corrosion increases [120]. This difference in stability leads to accelerated coating deterioration.

7.2.2 Nanoparticles coatings

Figure 7.13 (a, b and c) shows the contact angle values of homo- and heterogeneous nanoparticles coatings as a function of immersion time in distilled water, acidic and basic media.

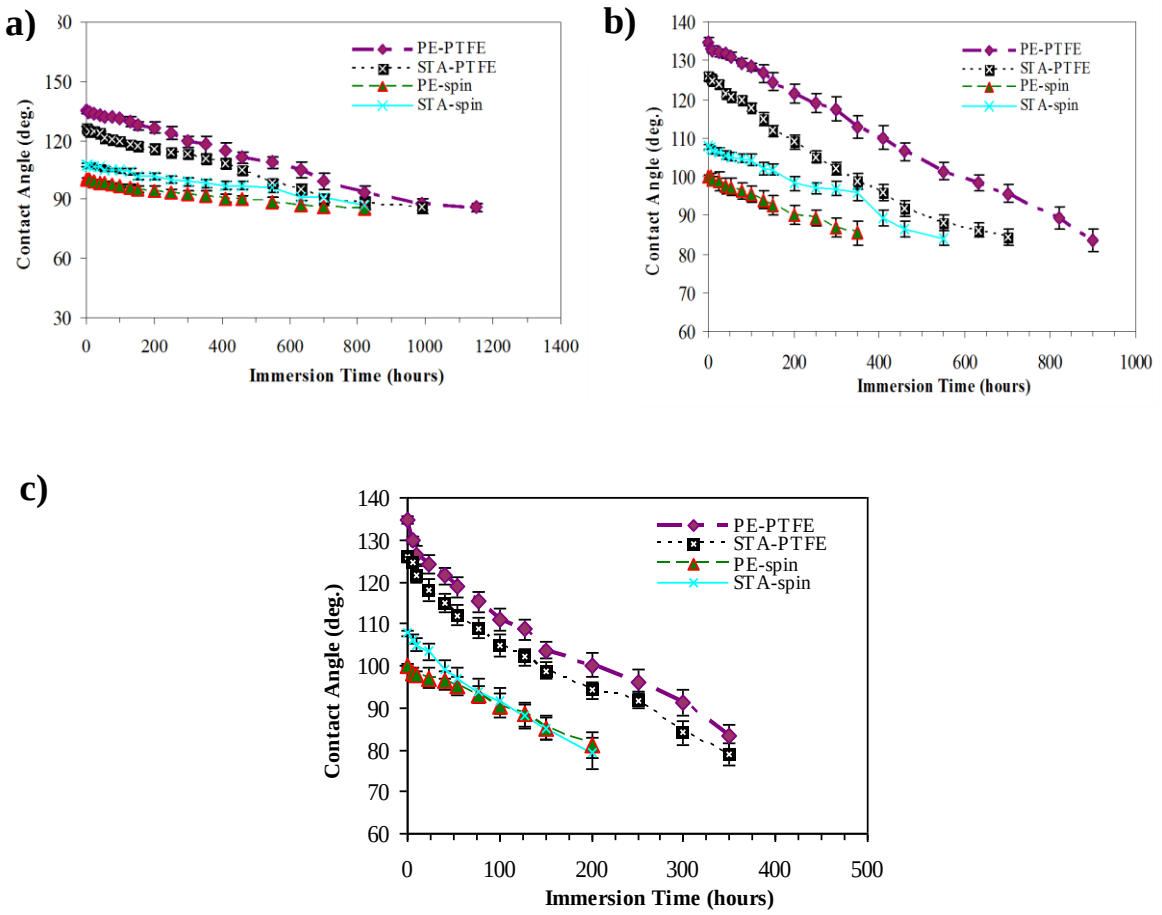

Fig.7. 13. CA values for homo- and heterogeneous nanoparticles coatings as a function of immersion time in a) distilled water (pH=7), b) acidic (pH=4) and c) basic (pH=10) solutions.

These contact angle values of nanoparticles coatings immersed in distilled water decreased from ~ 100-134 ^{o} to ~ 85-87^{o} after 800 h. For the samples immersed in an acidic condition the CA values were reduced to ~ 83-85^{o} after ~ 350 h. while in basic

media, the contact angle values decreased to ~ 78-83^{o} after ~ 200 h. As is evident in Figure 7.13 (a, b and c), the durability of HCs of PE-PTFE and STA-PTFE is more than homogeneous PE-spin and STA-spin coatings. The obtained results also showed that the structure of the chemical composition of the coating can be affected by different pH values. For example, the STA is faintly acidic and would be more unstable under a basic condition [121]. In the case of homo- and heterogeneous nanoparticles coatings, the reduction of CA values in different pH solutions probably is due to the dissolving and then corrosion of the samples. Therefore, the coatings degrade, in fact, within several days of immersion in aggressive media.

7.2.3 Plasma sputtering coatings

Figure 7.14 (a, b and c) shows the contact angle values of Al samples coated with homo- and heterogeneous plasma coatings through masks as a function of immersion time (IT) in solutions with different pH values (4, 7 and 10). The contact angle values for PE-spin and PE-PTFE coatings as a function of IT in distilled water (pH=7) are shown in Figure 7.14a. It can be seen that the CA values for homogeneous PE-spin and heterogeneous PE-PTFE coatings decreased respectively, from ~ 100° and ~ 114º to ~ 86º and ~ 85º, after 820 and 1200 h, respectively. By immersing the coated samples in pH=4 or acidic media, the contact angle values of PE-spin and PE-PTFE coatings decreased to ~ 85º after 350 and 820 hours, respectively, while in basic media, the contact angle values of PE-spin and PE-PTFE decreased to ~ 81^{o} after ~ 200 h and ~ 410 h, respectively. As is evident in the case of immersion in a pH=10 or basic solution, the

contact angle values decreased sharply.

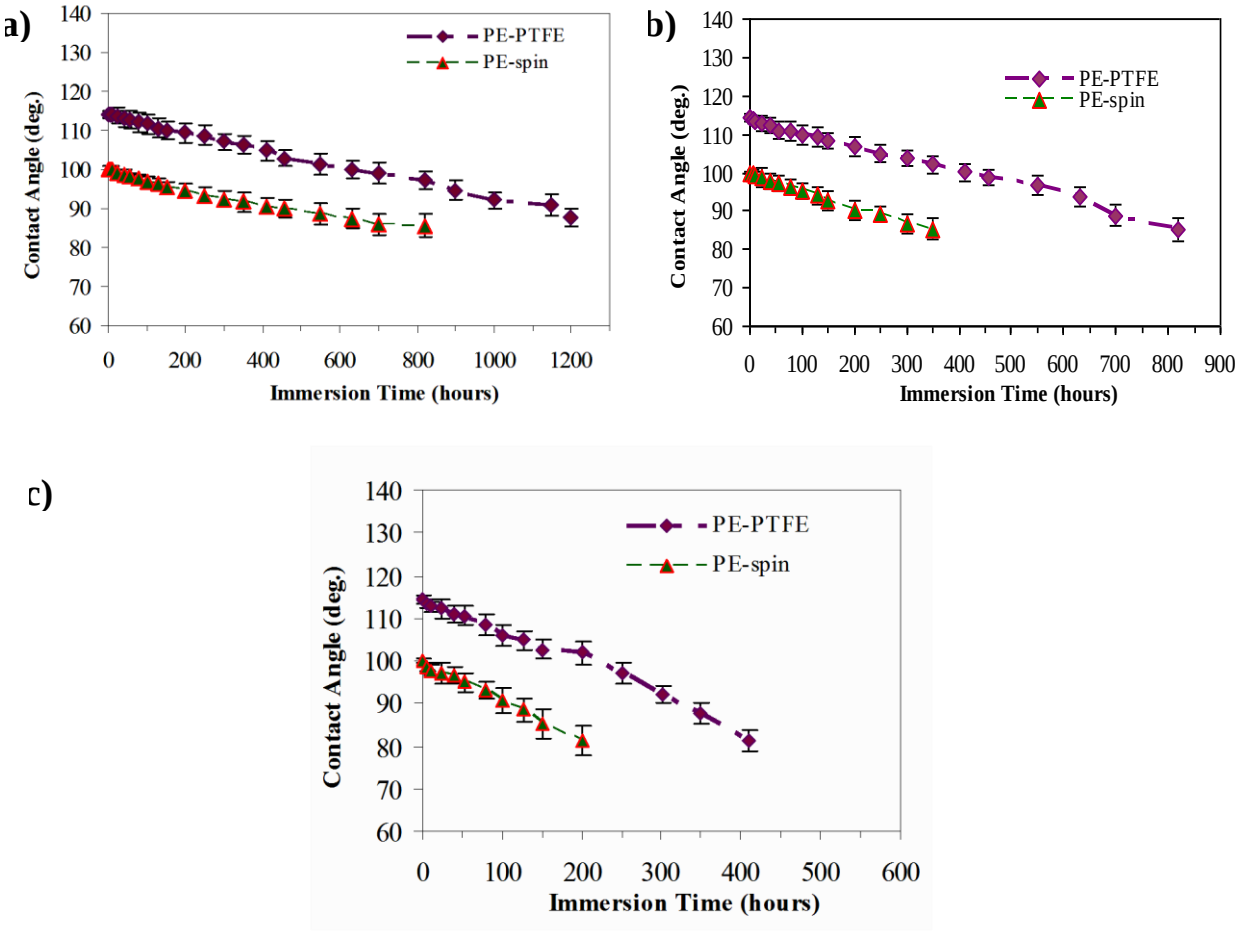

Fig.7. 14. CA values for homo- and heterogeneous plasma coatings through masks as a function of immersion time in a) distilled water (pH=7), b) acidic (pH=4) and c) basic (pH=10) solutions.

After a study on durability of homo- and HCs in solutions with different pH, it can be concluded that the HCs are more stable than the homogeneous coatings over time. These results in addition showed greater durability of homo- and HC in neutral and acidic solutions than in a basic solution [120].

7.3 Effect of UV radiation on hydro- and ice- phobic properties of homo- and HCs

In order to study the durability of homo- and HCs, the coated samples are exposed to a UVA-340 fluorescent lamp according to ASTM G154. The contact angle values are measured after each eight-hour cycle of exposure. It is worthy to highlight the fact that almost each 537 hours of artificial UV exposure is equal to one year of sunlight exposure [85]. This section focuses on the durability of homo- and heterogeneous *SAM*s, nanoparticles and plasma sputtering coatings against UV degradation.

7.3.1 *SAM*s coatings

Figure 7.15 shows the wettability of homo- OD-OD and PF-PF and heterogeneous OD-PF *SAM*s coatings following UV exposure. The CA values of OD-OD and PF-PF decreased from ~ 141.4 ^{o} and ~ 121.1^{o} to ~ 87^{o}, after 86 and 77 cycles, respectively. For the heterogeneous OD-PF coating the contact angle values decreased from ~ 160.66^{o} to ~ 88^{o} after 107 cycles. It is worthy to mention that when the contact angle measurements reached to a value of ~ 87^{o}, close to those obtained on a polished Al surface, the UV exposure test was stopped. Therefore, the coated samples lost their hydrophobic properties while UV cycles increased. A decrease of CA values is due to the gradual loss of the deposited coating after UV exposure. In other words, the hydroxyl groups adsorbed on defective sites can be replaced gradually by O atoms when samples are UV-irradiated [122]. A realistic durability was observed for the heterogeneous OD-PF sample over almost one year and six months of natural sunlight exposure. However, for the homo-

OD-OD and PF-PF samples, a realistic durability was almost one year of natural sunlight exposure. The result show that the heterogeneous OD-PF sample is more stable compared to the homogeneous OD-OD and PF-PF samples following UV exposure. It is evident in Figure 7.15 that loss of hydrophobicity takes longer for the OD-PF sample, as its initial contact angle value (~ 160^{o}) is greater than for the homogeneous samples (~ 140^{o} and ~ 120^{o}). However, in case of homo- OD-OD and PF-PF samples, a realistic durability was almost one year of natural sunlight exposure.

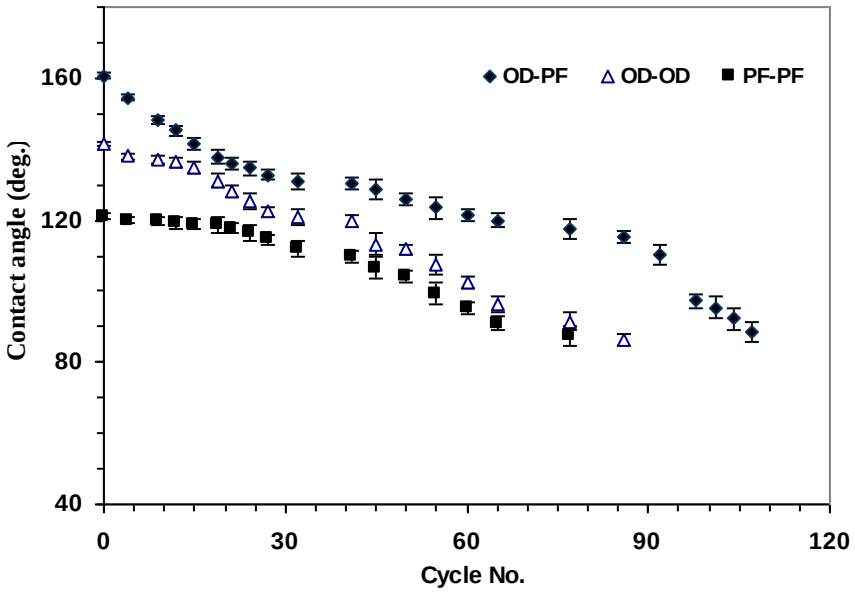

Fig.7. 15. Durability of homo- and heterogeneous *SAM*s coatings *vs.* exposure time of UV radiation.

7.3.2 Nanoparticles coatings

The durability of homo- and heterogeneous nanoparticles coatings was also studied after UV exposure by measuring the CA values (Figure 7.16). The contact angle values of heterogeneous PE-PTFE and STA-PTFE decreased from ~ 134° and ~ 125° to ~

89° and ~ 85°, respectively, after 53 cycles of UV exposure. The heterogeneous (PE-PTFE) coating was used as the best coating, because it has the highest static contact angle and lowest contact angle hysteresis among the polymeric coatings including $-CH_3$ or $-CH_2$ moieties with a horizontal orientation. Another heterogeneous (STA-PTFE) coating in addition was used with a vertical branch of $-CH_2$ or $-CH_3$ groups to compare their results with the heterogeneous PE-PTFE coating and homogeneous STA-spin coating. For homogeneous PE-spin and STA-spin coatings the contact angle values decreased to ~ 87º and ~ 88.5º after 35 and 38 cycles, respectively. The durability of heterogeneous PE-PTFE and STA-PTFE coatings was found to be almost one year of natural sunlight exposure. However, for PE-spin and STA-spin coatings, the durability was almost six months of natural sunlight exposure.

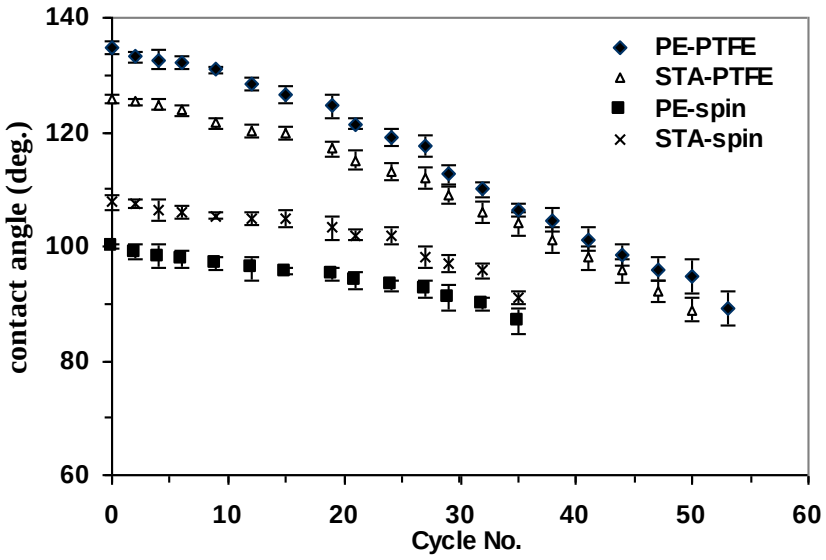

Fig.7. 16. Durability of homo- and heterogeneous nanoparticles coatings *vs*. exposure time of UV radiations.

7.3.3 Plasma sputtering coatings

Figure 7.17 shows the hydrophobic properties of homo- and heterogeneous PE-spin and PE-PTFE coatings, respectively, following UV exposure. The contact angle values of PE-spin decreased from ~ 100 to ~ 87^{o}, after 35 cycles. For the heterogeneous PE-PTFE coating the contact angle values decreased from ~ 114^{o} to ~ 87^{o} after 98 cycles. The durability of the PE-PTFE was found to be about one year and a half; however, for the homogeneous PE-spin coating it was about 6 months.

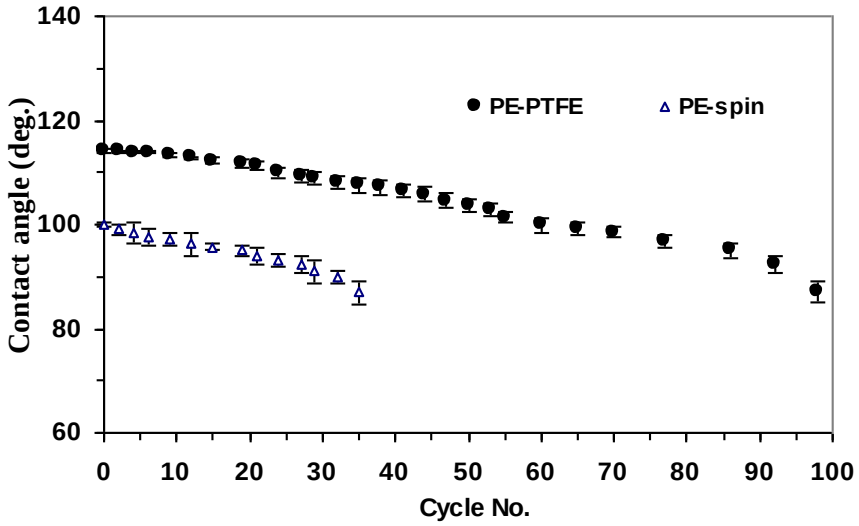

Fig.7. 17. Durability of homo- and heterogeneous plasma coatings *vs*. exposure time of UV radiations.

7.4 Conclusion

In this chapter, the icephobic properties of homo- and HCs prepared from three different methods were studied. The anti-ice performance of HCs, confirmed the

heterogeneity effect on aluminum surfaces, as the icephobic properties of HCs improved upon those of homogeneous coatings. The durability and stability of homogeneous and HC plasma sputtering coatings and *SAM*s coatings, in terms of the number of icing/de-icing cycles was considerable and significant compared to those obtained on HC nanoparticles coatings. The CA values of prepared HCs by *SAM*s and the plasma method showed a small decrease, after several icing/de-icing cycles. The durability results showed that the prepared coatings had a low resistance in basic solutions, although they had a good durability in distilled water (~ 1200 h) and acidic media (~ 900 hours). The durability results against UV radiations showed that the HCs had a good resistance to UV degradation. In fact the durability of HCs prepared with *SAM*s, nanoparticles and plasma methods were 856, 424 and 784 hours, respectively, which were longer time periods than for the homogeneous coatings.

CHAPTER VIII

CONCLUSION AND RECOMMENDATION

8.1 Conclusions
8.2 Recommendations for Future Work

8. 1 Conclusions

This study focused on the preparation of HCs with icephobic properties presenting a number of advantages, such as easy application, time-saving and low cost. A few studies on the preparation of HCs with icephobic properties showed a significant reduction of the ice adhesion force. These studies focused on heterogeneous polymer coatings or copolymers including hydrocarbons and fluorocarbons. However, the purpose of this research work is the preparation of HCs using different techniques other than those applied and reported in the literature. This helps further study and confirms the heterogeneity effect on the icephobicity of coatings. Indeed, the HCs introduced in this study were cheap, simply prepared and easy to apply when compared to the HCs studied previously.

The current research, therefore, mainly dealt with developing the HCs as an anti-icing agent. In this study, hydro- and icephobic properties of heterogeneous self assembled monolayers (*SAM*s), nanoparticles and "masked" plasma sputtering coatings were studied and compared with that of homogeneous coatings. Various homo- and HCs were therefore prepared by three different methods.

- It was shown that the hydro- and icephobic properties of HCs were influenced by applying different functions including the low surface energy of hydrocarbons and fluorocarbons. It should be noted that the water molecule orientations at the surfaces of the fluorocarbon and hydrocarbon groups were completely different. As a result, by inducing and creating various disparities (hydrocarbons and fluorocarbons) in terms of

energy bonding and water molecule orientation at the molecular level, the ice-solid interface is weakened.

- In general, HCs showed higher water contact angle values and smaller water CAH values. This observation was observed by applying different functions of hydrocarbons and fluorocarbons. The superhydrophobicity achieved by the *SAM*s was shown to have two causes: a low surface energy layer resulting from applying hydrocarbons and fluorocarbons, and micro-/nano roughness on an aluminum surface. This roughness was generated by releasing hydrochloric acid in the hydrolysis step of the *SAM*s configuration process.

- To better understand the heterogeneity effect, the aluminum samples were replaced by glass substrates to avoid any possible effect of surface roughening on alkylsilane-based materials. This series of glass substrate coating experiments confirmed the heterogeneity effect in reducing the CAH and increasing the contact angle on aluminum samples.

- Applying hydrocarbons and fluorocarbons together to an aluminum surface was found to lead to coatings with improved hydro- and icephobicity. The enhanced icephobic performance of HCs, compared to those of homogeneous coatings, was explained by the disruption of the hydrogen bond between ice and the coated surface. This disruption led to reducing the ability of the ice to adhere to the surface.

- The *ARF* values of all HCs showed that in optimal conditions the ice adhesion strength was smaller than those obtained on an aluminum surface by factors of ~ 3, ~ 1.7 and ~ 1.3 times for *SAM*s, nanoparticles and "masked" plasma sputtering, respectively.

This decrease in ice adhesion strength can lead to easier removal of accumulated ice from these coated surfaces.

- The icephobic performance of these HCs somewhat degraded during successive icing/de-icing cycles, implying the occurrence of some damage to the coatings. In optimal conditions the icephobic performance of the coatings of *SAM*s, nanoparticles and "masked" plasma showed damage after 12, 4 and more than 10 icing/de-icing cycles, respectively. The durability of heterogeneous nanoparticles coatings in terms of anti-ice performance over time was very short. In contrast to the heterogeneous nanoparticles coatings, the "masked" plasma HCs produced a significant stability and durability (even more than 10 times) versus icing/de-icing.

- All HCs studied showed a gradual loss of their hydrophobic properties after ~ 1200 h of immersion in de-ionized water (pH=7). In acidic conditions the HCs lost their hydrophobicity after ~ 900-1000 h of immersion in a pH=4 solution. Therefore, after a study on durability of homo- and HCs in solutions with different pH, it was concluded that the HCs are more stable than homogeneous coatings over time. Meanwhile, the durability of homo- and HCs immersed in neutral and acidic solutions were higher than in a basic solution. This observation can be attributed to the influence of basic conditions on aluminum oxide layer durability and therefore, the rate of corrosion.

- The durability of heterogeneous *SAM*s coatings was found to be almost one year and seven months of natural sunlight exposure. For heterogeneous nanoparticles coatings, it was approximately one year and for "masked" plasma HCs, one year and a half of natural sunlight exposure. In addition, if the results of the durability of HCs are compared

to homogeneous ones, they showed a greater durability following UV exposure. It is worthy to mention that when the contact angle measurements reached to a value of ~ 87^{o}, close to those obtained on a polished aluminum surface, the UV exposure test was stopped. A decrease of contact angle values returns to the gradual loss of the deposited coating after UV exposure. In other words, the hydroxyl groups adsorbed on defective sites can be replaced gradually by O atoms when samples are UV-irradiated. The results show that the heterogeneous samples are more stable than the homogeneous ones following UV exposure.

- As a general conclusion, all the prepared HCs showed that the effect of heterogeneity came from applying hydrocarbons and fluorocarbons compared to only hydrocarbons or only fluorocarbons as a homogeneous coating. It was shown by applying different functions, for example both C-F and C-H, the surface energy is decreased more compared to applying only one function (C-F or C-H alone).

- The (theoretical) calculations in addition confirmed the effect of heterogeneity on the coatings.

8.2 Recommendations for Future Work

By this research work, the effect of heterogeneity on hydro- and icephobicity was confirmed. In this light the following work can be recommended for further study:

(i) Different types of *SAM*s molecules such as long alkyl chains should be carefully studied on aluminum substrates, and optimal parameters for enhanced hydro- and icephobicity should be sought. In this study a fluoro-alkylsilane with short fluoro-alkyl chains, an alkylsilane with long alkyl chains, and also an alkylsilane and a fluoro-alkylsilane, both with short alkyl chains, were studied. They confirmed the effect of heterogeneity on hydro- and icephobicity. However, it was not possible to expand our study to alkylsilane and fluoro-alkylsilane, both with long alkyl chains, due to a time limitation. In future work it would be good to consider the heterogeneity effect for alkylsilane and fluoro-alkylsilane with long alkyl chains.

(ii) For heterogeneous nanoparticles coatings, to increase the stability and adhesion to the coatings, the nanoparticles can be doped to solution before spin-coating and creation of the coatings. Then with an instantaneous surface polishing, a very thin layer of coating is removed to release the nanoparticles and modify the mechanical properties of HCs.

(iii) Some tests could be performed under natural conditions to observe their hydro- and ice-hydrophobicity in the real world.

Reference

[1] M. Farzaneh, J. Zhang and C. Volat, "Effect of Insulator Diameter on AC Flashover Voltage of an Ice-covered Insulator String", IEEE Trans. Diel. El. Ins., 13 (2006)264.

[2] M. Farzaneh, I. Fofana, I. Ndiaye, and K.D. Srivastava, "Experimental studies of ice surface discharde inception and development", J. of Power and Energy Systems., 26 (2006) 34.

[3] M. Farzaneh (Chair), "IEEE standard 1783 – guide for test methods and procedures to evaluate the electrical performance of insulators in freezing conditions". IEEE Press, New York, October 2009.

[4] M. Farzaneh, "Ice accretion on H.V. conductors and insulators and related phenomena", Philos. Trans. R. Soc. London, Ser. A. 358 (2000) 1.

[5] M. Farzaneh, W.A. Chisholm, "Insulators for icing and polluted environments", IEEE Press series on Power Engineering, IEEE/John Wiley, New York, ISBN 9780470282342, 680 p, October 2009.

[6] M. Farzaneh, Ed., "Atmospheric Icing of Power Networks", Springer, Berlin, ISBN 9781402085307, August 2008, 381 p.

[7] 'Minimizing Effects from Highway Deicing', EPA 832-F-99-016 (1999).

[8] 'Airplane Deicing Fluid Recovery Systems', EPA 832-F-99-043 (1999).

[9] V. F. Petrenko and S. Qi, "Reduction of ice adhesion to stainless steel by ice electrolysis", J. Appl. Phys. 86(1999)5450.

[10] C. Laforte, J. L. Laforte, J. C. Carrier, "How a solid coating can reduce the adhesion of ice on a structure", Proceedings of the International Workshop on Atmospheric Icing of Structures (IWAIS), 2002 p. 1-5.

[11] R. Menini and M. Farzaneh, "Elaboration of Al_2O_3/PTFE icephobic coatings for protecting aluminium surfaces". Surf. Coat. Technol. 203 (2009) 1941.

[12] V. F. Petrenko and S. Peng, "Reduction of ice adhesion to metal by using self-assembling monolayers (*SAMs*)", Can. J. Phys. 81 (2003) 387.

[13] J. L. Laforte, M. A. Allaire and J. Laflamme, "State-of-the-art on power line de-icing", Atm. Res. 46 (1998) 143.

[14] V. K. Croutch and R. A. Hartley, “Adhesion of ice to coatings and the performance of ice release coatings”, J. Coat. Technol. 64 (1992)41.

[15] S.A. Kulinich, M. Farzaneh, “How wetting hysteresis influences ice adhesion strength on superhydrophobic surfaces”, Langmuir 25 (2009) 8854.

[16] F. Arianpour, M. Farzaneh, S. Kulinich, “Hydrophobic and ice-retarding properties of doped silicone rubber coatings”, Appl. Surf. Sci. 265 (2013) 546.

[17] S. Farhadi, M. Farzaneh, S.A. Kulinich, “Anti-icing performance of superhydrophobic surfaces”, Surf. Sci., 257 (2011) 6264.

[18] R. Jafari, R. Menini, M. Farzaneh, “Superhydrophobic and icephobic surfacesprepared by RF-sputtered polytetrafluoroetylene”, Appl. Surf. Sci. 257 (2010)1540.

[19] R. Menini, Z. Ghalmi, M. Farzaneh, “Highly resistant ice-phobic coatings on aluminum alloys”, Cold Reg. Sci. Technol. 65 (2011) 65.

[20] G. Momen, M. Farzaneh, “Facile approach in the development of icephobic hierarchicallytextured coatings as corrosion barrier”, Appl. Surf. Sci. 299 (2014) 41.

[21] Safaee A., 2008, "Nanostructured Metal Surfaces and Their Passivation For Superhydrophobic and Antiicing Applications," University of Quebec at Chicoutimi.

[22] Z. Ghalmi, R. Menini, and M. Farzaneh, 2009, "Theoritical Studies and Quantification of Ice Adhesion Mechanisms," Proceeding of the 13th International workshop on Atmospheric icing of structures, IWAIS, Andermatt.

[23] P. Tourkine, M. Le Merrer, D. Quéré, “Delayed freezing on water repellent materials”, Langmuir 25 (2009) 7214.

[24] S. Jung, M. Dorrestijn, D. Raps, A. Das, C. M. Megaridis, and D. Poulikakos, “Are Superhydrophobic Surfaces Best for Icephobicity?”, Surf. Colloids, (2011) 3059.

[25] H. Murase, and T. Fujibayashi, “characterization of molecular interfaces in hydrophobic systems”, Prog. Org. Coat., 31 (1997) 97.

[26] H. Murase, K. Nanishi, H. Kogure, T. Fujibayashi, K. Tamura, N. Haruta, “Intraction between heterogeneous surfaces of polymers and water”, J. Appl. Polym. Sci., 54 (1994) 2051.

[27] N.R. Byrd, “Polysiloxane (Amide-ureide) anti-ice coating”, US 6,797,795 (2004).

[28] R. Menini and M. Farzaneh “Advanced Icephobic Coatings”. J. Adhes. Sci. Tech.25 (2011) 971.

[29] M. Amin, M. Akbar and S. Amin, “Hydrophobicity of silicone rubber used for out door insulation”, Rev. Adv. Mater. Sci. 16 (2007) 10.

[30] V. K. Croutch and R. A. Hartley, “Adhesion of ice to coatings and the performance of ice release coatings”, J. Coat. Technol., 64 (1992) 41.

[31] T. Young, “An Essay on the Cohesion of Fluids,” Phil. Trans. R. Soc. Lond., 95, (1805) 609–612.

[32] T. S. Lin, C. F. Wu, C. T. Hsieh, “Enhancement of water-repellent performance on functional coating by using the Taguchi method”, Surf. Coat. Technol. 200 (2006) 5253.

[33] A. Nakajima, K. Hashimoto and T. Watanabe, “Invited review recent studies on super-hydrophobic films’’, Monatsh. Chem., 132 (2001) 31.

[34] B. Bhushan “Biomimetics: lessons from nature–an overview”, Phil. Trans. R. Soc. A. 367 (2009) 86.

[35] B. Bhushan, Y. C. Jung and K. Koch, “Micro-, nano- and hierarchical structures for super-hydrophobicity, self-cleaning and low adhesion”, Phil. Trans. R. Soc. A. 367 (2009) 72.

[36] K. Koch, B. Bhushan, Y. C. Jung and W. Barthlott, “Fabrication of artificial lotus leaves and significance of hierarchical structure for super-hydrophobicity and low adhesion”, Soft. Matter. 5 (2009) 93.

[37] C. Neinhuis and W. Barthlott, “Characterization and distribution of water-repellent, self-cleaning plant surfaces”, Ann. Bot. 79 (1997) 77.

[38] W. Barthlott and C. Neinhuis, “Purity of the sacred lotus, or escape from contamination in biological surfaces”, Planta. 202 (1997) 1.

[39] P. Wagner, R. Furstner, W. Barthlott and C. Neinhuis, “Quantitative assessment to the structural basis of water repellency innatural and technical surfaces”, J. Exp. Bot. 54 (2003) 303.

[40] Z. Burton and B. Bhushan, “Surface characterization and adhesion and friction properties of hydrophobic leaf surfaces”, Ultramicroscopy. 106 (2006) 19.

[41] B. Bhushan and Y. C. Jung, “Micro and nanoscale characterization of hydrophobic and hydrophilic leaf surface”, Nanotechnolgy. 17 (2006) 72.

[42] K. Koch, B. Bhushan and W. Barthlott, “Diversity of structure, morphology, and wetting of plant surfaces (invited)”, Soft. Matter. 4 (2008) 63.

[43] K. Koch, B. Bhushan and W. Barthlott, "Multifunctional surface structures of plants: an inspiration for biomimetics (invited)", Prog. Mater. Sci. 54 (2009) 78.

[44] X. F. Gao and L. Jiang, "Biophysics: water-repellent legs of water striders", Nature. 432 (2004) 36.

[45] B. Bhushan and Y. C. Jung, "Natural and biomimetic artificial surfaces for superhydrophobicity, self-cleaning, low adhesion, and drag reduction", Pro. Mater, Sci., 56 (2010) 1-108.

[46] R. N. Wenzel, "Resistance of solid surfaces to wetting by water", Indust. Eng. Chem. 28 (1936) 94.

[47] Zisman, W. A, "Relation of the equilibrium contact angle to liquid and solid constitution", Am.Chem.Soc. 43 (1964).

[48] A. Cassie, S. Baxter, "Wettability of porous surfaces", Trans. Faraday. Soc. 40 (1944) 51.

[49] K. Tadanaga, N. Katata, and T. Minami, "Super-water-repellent Al_2O_3 coating films with high transparency", J. Am. Ceram. Soc., 80 (1997) 1040.

[50] R. Colin, C. P. Parkin and I. P. Parkin, "Preparation and characterisation of super-hydrophobic surfaces",Chem. Eur. J. 16 (2010) 3568 – 3588.

[51] K. Geunjae, L. Mikyung, S. Karuppanan and Y. Kijung, "Wettability control and water droplet dynamics on SiC−SiO_2 core−shell nanowires", Langmuir, 26 (2010) 12273.

[52] D. Kuroiwa, "Icing and snow accretion on electric wires", CRREL Res. Report 123 (1965).

[53] R. Cattin, S. Kunz, A. Heimo, R. Oechslin, M. Russi, "An improved approach for the determination of in-cloud icing at wind turbine sites", Federal Office of Meteorology and Climatology Meteo-Swiss COST Action 727.

[54] W. D. Macklin, "The density and structure of ice formed by accretion", Q. J. Roy. Meteorol. Soc. 88(375) (1962) 30.

[55] E. R. LaChapelle, "Field guide to snow crystals", Seattle, Wash.: University of Washington Press. 101 (1969).

[56] N. D. Mulherin, "Atmospheric icing on communication masts in New England", CRREL Res. Report , 86-17 (1986) 46.

[57] D. Kuroiwa, "Icing and snow accretion on electric wires", U.S. Army Cold Regions Research and Engineering Laboratory, Res. Report, 123 (1965) 10.

[58] L. Makkonen and K. Ahti, “The effect of meteorological parameters on rime formation in Finland”, U.S. Army Cold Regions Re-search and Engineering Laboratory Special Report, 83-17 (1983) 167-174.

[59] S. A. Kulinich and M. Farzaneh, “Hydrophobic properties of surfaces coated with fluoroalkylsiloxane and alkylsiloxane monolayers ’’, Surf. Sci., 573 (2004) 379.

[60] R. Menini, Z. Ghalmi, M. Farzaneh, “Effect of different aluminium surface treatments on ice adhesion strength”, Cold Reg. Sci. Technol. 65 (2011) 65.

[61] A. Franquet, J. De Laet, T. Schram, H. Terryn, V. Subramanian, W.J. van Ooij, J. Vereecken, “Determination of the thickness of thin silane films on aluminium surfaces by means of spectroscopic ellipsometry” , Thin Solid Films., 384 (2001) 37.

[62] D. Wanga, Y. Nia, Q. Huo, D. E. Tallman , “Self-assembled monolayer and multilayer thin films on aluminum 2024-T3 substrates and their corrosion resistance study” , Thin Solid Films., 471 (2005) 177.

[63] D. Quéré, “Non-sticking drops”, Rep. Prog. Phys., 68 (2005) 2495.

[64] S. Farhadi, M. Farzaneh, S.A. Kulinich, “Anti-icing performance of superhydrophobic surfaces”, Surf. Sci., 257 (2011) 6264.

[65] V. Subramanian, and W. J. van Ooij, “Silane based metal pretreatments as alternatives to choromating” , Surface Eng., 15 (1999) 168.

[66] B. Somlo, and V. Gupta, “A hydrophobic self-assembled monolayer with improved adhesion to aluminum for deicing application” , Mech. Mater., 33 (2001) 471.

[67] M. Maccarini, M. Himmelhaus, S. Stoycheva, M. Grunze, “Characterisation and stability of hydrophobic surfaces in water”, J. Appl. Surf. Sci., 252 (2005) 1941.

[68] A. Kanta, R. Sedev, J. Ralston, “The formation and stability of self-assembled monolayers of octadecylphosphonic acid on titania”, Colloids Surf., A., 291 (2006) 51.

[69] N. N. Khusnatdinov and V. F. Petrenko, “Experimental study of ice electrolysis under UV irradiation”, J. Phys. Chem. 101 (1997) 6208.

[70] V.F. Petrenko and C.R. Sullivan,“Methods and systems for removing ice from surfaces,” U.S. Patent 6653598, 2003.

[71] Z. Guan, K. Niu, G. Peng, F. Zhang, L. Wang, B. Lutz, “ Hydrophobicity transfer property of silicone rubber material”, Int. J. Elec. Eng. Educ., 4 (2012) 261.

[72] F. Arianpour and M. Farzaneh, “On hydrophobic and icephobic properties of TiO_2-doped silicon rubber coatings”, IJTAN.1 (2012) 79.

[73] R. Jafari and M. Farzaneh, “A simple method to create superhydrophobic aluminium surfaces”, Mater. Sci. Forum., 706 (2012) 2874.

[74] D. Sarkar and M. Farzaneh,"Superhydrophobic coatings with reduced ice adhesion," J. Adhes. Sci. Technol., 23 (2009) 1215.

[75] A. Safaee, D.K. Sarkar, M. Farzaneh, “Superhydrophobic properties of silver-coated films on copper surface by galvanic exchange reaction”, Appl. Surf. Sci., 254 (2008) 2493.

[76] S. Farhadi and M. Farzaneh, “On stability and ice-releasing performance of nanostructured fluoro-alkylsilane-based superhydrophobic Al alloy2024 Surfaces”, IJTAN.1 (2012) 38.

[77] M. Aromaa, A. Arffman, H. Suhonen, “Atmospheric synthesis of superhydrophobic TiO_2 nanoparticle deposits in a single step using liquid flame spray”, J. Aerosol. Sci., (2012).04.009.

[78] A. K. Gnanappa, C. O. Murchu, O. Slattery, F. Peters, B. Aszalo, S. A.M. Tofail, “Effect of annealing on hydrophobic stability of plasma deposited fluoropolymer coatings” , Poly. Deg. Stab. 93 (2008) 2119.

[79] L. F. Mobarakeh, R. Jafari, M. Farzaneh, “Superhydrophobic surface elaboration using plasma polymerization of hexamethyldisiloxane (HMDSO)”, Adv. Mater. Res., 409 (2012) 783.

[80] K. Teshima, H. Sugimura, Y. Inoue, O. Takai, A. Takano, “Transparent ultra water-repellent poly(ethylene terephthalate) substrates fabricated by oxygen plasma treatment and subsequent hydrophobic coating”, J. Appl. Surf. Sci. 244 (2005) 619.

[81] R. Jafari, M. Farzaneh, “Fabrication of superhydrophobic nanostructured surface on aluminum alloy”, Appl. Phys. A, 102 (2011) 195.

[82] J. Shiu, C. Kuo, P. Chen, C. Mou, “Fabrication of tunable superhydrophobic surfaces by nanosphere lithography”, Chem. Mater. 16 (2004) 561.

[83] K. Teshima, H. Sugimura, Y. Inoue, O. Takai, A. Takano, “Transparent ultra water-repellent poly(ethylene terephthalate) substrates fabricated by oxygen plasma treatment and subsequent hydrophobic coating”, Appl. Surf. Sci., 244 (2005) 619.

[84] QUV /Accelerated Weathering Tester catalogue.

[85] Mission T. A., 2001, "What is the network of weathering?" Weathering Testing 152 Guidebook, p. 108.

[86] S. Suzuki, A. Nakajima, T. Kouichi, S. Munetoshi, H. Ayako, Y. Naoya, K. Yoshikazu and O. Kiyoshi, "Sliding behavior of water droplets on line-patterned hydrophobic surfaces" , Appl. Surf. Sci., 254 (2008)1797

[87] M. Sakai, J. H. Song, N. Yoshida, S. Suzuki, Y. Kameshima and A. Nakajima, " Direct Observation of Internal Fluidity in a Water Droplet during Sliding on Hydrophobic Surfaces" , Langmuir, 22 (2006) 4906

[88] L. E. Kollar and M. Farzaneh, "Wind-tunnel Investigation of icing of an inclined cylinder", Int. J. Heat. Mass. Tran., 53 (2010) 849.

[89] L. Kollar and M. Farzaneh, "Spray Characteristics of Artificial Aerosol Clouds in a Low- Speed Icing Wind Tunnel", Atomization Spray, 19 (2009) 389.

[90] L. Kollar, M. Farzaneh and A. Karev, "Modeling Droplet-Size Distribution near a Nozzle Outlet in an Icing Wind Tunnel", Atomization Spray, 16 (2006) 673.

[91] M. J. Pellerite, T. D. Dunbar, L. D. Boardman *et al.*, "Effects of Fluorination on Self-Assembled Monolayer Formation from Alkanephosphonic Acids on Aluminum: Kinetics and Structure", J. Phys. Chem., 107 (2003)11726.

[92] W. Limbut, P. Kanatharana, B. Mattiasson *et al.*, "A comparative study of capacitive immunosensors based on self-assembled monolayers formed from thiourea, thioctic acid, and 3-mercaptopropionic acid" , J. Biosens. Bioelectron., 22 (2006) 233.

[93] V. Lakshminarayanan, and U. K. Sur, "Hydrophobicity-induced drying transition in alkanethiol self-assembled monolayer–water interface", J. Phys., 61 (2003) 361.

[94] F. Schreiber, "Structure and growth of self-assembling monolayers", Prog. Surf. Sci., 65 (2000) 151.

[95] C. R. Kessel and S. Granick, "Formation and Characterization of a Highly Ordered and Well- Anchored Alkylsilane Monolayer on Mica by Self –Assembly", Langmuir., 7 (1991) 532.

[96] M. Jin, S. Li, J. Wanga, *et al.*, "Controllable fabrication of organosilane nano-architectured surfaces with tunable wettability" , Appl. Surf. Sci., 258 (2012) 7552.

[97] V. Pophristic and L. Goodman, "Hyperconjugation not steric repulsion leads to the staggered structure of ethane", L. Nature, 411 (2001) 565.

[98] Z. Cao and Z. Zhang, "Steric-hide-Deactivation of photocatalytically active ZnO nanoparticle and enhancement of its compatibility with organic compounds by surface-capping with organically modified silica", Appl. Surf. Sci., 257 (2011) 4151.

[99] Y. Xiao, M. R. Wiesner, "Characterization of surface hydrophobicity of engineered nanoparticles", J. Hazardous Mater., 215– 216 (2012) 146.

[100] R. R. Sauers, "Steric attraction: The far side", J. Chem. Education, 73 (1996) 114.

[101] D. Kleshchanok , P. Lang, "Steric repulsion by adsorbed polymer layers studied with total internal reflection microscopy", Langumuir, 23(8) (2007) 4332.

[102] P. F. Rios, H. Dodiuk, S. Kenig, *et al.*, "The effect of polymer surface on the wetting and adhesion of liquid systems", J. Adhesion Sci. Technol., 21 (2007) 227.

[103] M. Miwa, A. Nakajima, A. Fujishima, *et al.* "Effects of the Surface Roughness on Sliding Angles of Water Droplets on Superhydrophobic Surfaces" , Langmuir 16 (2000) 5754.

[104] C. G. L. Furmidge, "Studies at phase interfaces", J. Colloid Sci., 309 (1962) 17.

[105] E. B. Dussan and R. T. P. Chow, "On the ability of drops or bubbles to stick to non-horizontal surfaces of solides", J. Fluid Mech., 137 (1983) 1.

[106] E. B. Dussan, "On the ability of drops or bubbles to stick to non-horizontal surfaces of solides", J. Fluid Mech., 151 (1985) 1.

[107] B. J. Briscoe and K. P. Galvin, "The sliding of sessile and pendent droplets: the critical condition", Colloids Surf., 52 (1991) 219.

[108] C. W. Extrand and Y. Kumagai, "Liquid drops on an inclined plane: The relation between contact angles, drop shape and retentive force", J. Colloid Interface Sci., 170 (1995) 515.

[109] A. Carre and M. E. R. Shanahan, "Drop motion on an inclined plane and evaluation of hydrophobic treatments to glass", J. Adhesion 49 (1995) 177.

[110] O. Albenge, C. Lacabanne, J. D. Beguin, A. Koënen and C. Evo, Langmuir 18, 8929 (2002).

[111] A. Von Buzágh and E. Wolfram, "Bestimmung der Haftfähigkeit von Flüssigkeiten an festen Körpern mit der Abreißwinkelmethode", Kolloid Z. 149 (1956) 125.

[112] S. A. Kulinich and M. Farzaneh, "Hydrophobic properties of surfaces coated with fluoroalkylsiloxane and alkylsiloxane monolayers", Appl. Surf. Sci., 573 (2004) 379–390

[113] S. A. Kulinich and M. Farzaneh, "On ice-releasing properties of rough hydrophobic coatings", Cold Regions Science and Technology, 65 (2011) 60–64.

[114] M. Miwa, A. Nakajima, A. Fujishima, K. Hashimoto, T. Watanabe, "Effects of surface roughness on sliding angles of water droplets on superhydrophobic surfaces", Langmuir 16 (2000) 5754.

[115] W. Chen, A.Y. Fadeev, M.C. Hsieh, D. Oner, J. Youngblood, T.J. McCarthy, "Ultrahydrophilic and ultrahydrophobic surfaces: Some comments and examples", Langmuir 15 (1999) 3395.

[116] H. Nakae, R. Inui, Y. Hirata, H. Saito, "Effects of surface roughness on wettability", Acta Mater. 46 (1998) 2313.

[117] Zisman, W. A, "Relation of the equilibrium contact angle to liquid and solid constitution , Am.Chem.Soc. 43 (1964).

[118] B. Arora, A. Narayanasamy, J. Nirmala *et al.*, "Development and validation of a LC–MS/MS method for homocysteinethiolactone in plasma and evaluation of its stability in plasma samples", J. Chrom. 944 (2014) 49.

[119] M. Touzin, P. Chevallier, F. Lewis, S. Turgeon, S. Holvoet, G. Laroche, and D. Mantovani, 2008, "Study on the stability of plasma-polymerized fluorocarbon ultra-thin coatings on stainless steel in water," Surface and Coatings Technology, 202 (2008) 4884.

[120] C. Vargel and M. P. Schmidt, "Corrosion of aluminum", Elsevier , ISBN0080444954, (2004).

[121] T. Wu, Y. Pan, L. Li, "Study on superhydrophobic hybrids fabricated from multiwalled carbon nanotubes and stearic acid", J. Colloid and Interface Sci., 348 (2010) 265.

[122] M. Ma, R. M. Hill, "Superhydrophobic surfaces", J. Colloid & Interface Sci., 11 (2006) 193.